Characterization of the geological and geo-chemical footprint of the Koolhoven gold deposit, Suriname.

By: L.C.F. Carlier.

Abstract

IAMGold operates Rosebel N.V. Gold Mines in Suriname, South America. The producing deposits are characterized to be Archaen greenstone hosted quartz-carbonate vein deposits. Regional exploration projects are located in rainforest environment. Geologists are therefore confronted with difficult access, few outcrops and deep weathering. Efficient exploration is crucial and for this reason a profound understanding of the local geology, gold depositional mechanism and signature is required.

There is a hypothesis that a temperature gradient resulting from the flow of hydrothermal fluids through the shear and tension veins will have caused alteration halos to be formed around the gold deposit. Specific element enrichment and depletion are also expected near the gold deposition as a result of changing pressure/temperature regime and fluid characteristics. Recognizing and understanding alteration halos will increase the target area in an exploration campaign.

To test this hypothesis 28 boreholes with a maximum downhole depth of 230 meters were sampled across the producing Koolhoven pit on the Rosebel concession. 85 Samples were analysed for trace element and major element content in a laboratory. 904 Samples were analysed using an X-50 Mobile XRF device for element content. 1573 Spectral measurements were obtained using a Hi-Res Terraspec and 40 thin sections were analysed using a conventional polarization microscope and electron microprobe.

The petrographic analysis reveals the presence of quartz, carbonate, chlorite, pyrite, chalcopyrite, magnetite, hematite, rutile, clay mineral and feldspar including plagioclase. Bleached veins selvages are associated with high concentrations of carbonate and sericite, pyrite porphyroblasts and are devoid of chlorite. The sulfide mineral content does not exceed 5%. The conglomerate clasts are identified to be of volcanic origin mainly, hereby supporting the major element results. The veins contain quartz, carbonate, chlorite and the accessory minerals white-mica and tourmaline. Due to the low degree of deformation the veins are concluded to be of late timing compared to the main deformation.

The use of major element analysis has resulted in the effective differentiation of lithologies present in the Koolhoven pit. Siltstone/mudstone, two types of greywacke (A and B), sandstone, conglomerate and volcanic rock ranging from mafic to felsic have been recognized. Greywacke B and conglomerate are spatially related and their major-element content resembles that of the volcanic rock.

The use of log-ratios to analyse the trace element data suggests the presence of correlations between specific element ratios and gold concentrations. The best results were obtained by analysing one borehole a time. Different correlations are suggested in the different boreholes. It therefore remains uncertain to use the presented results for the entire deposit.

The visible and near infrared spectral analysis reveals that paragonite, Fe-chlorite and carbonate are the dominant minerals encountered. No direct link has been found between specific minerals, mineral crystallinity and relative mineral proportions to gold concentrations. Volcanic rock is devoid of muscovite.

The presented results of the identified lithologies are in accordance with the regional geological evolution. The alteration characteristics determined are to be considered as the proximal alteration

zone of the Koolhoven deposit. Up to a distance of 500 to 1 km away from the gold mineralization no alteration halo has been found except from the small scale bleaching near veins. Since the characteristics described in this report represent the proximal alteration, they may be used in exploration campaigns to define if hydrothermal fluids have been flowing in the area and hence there is a chance of gold deposition.

Acknowledgements

The last step towards obtaining my MSc degree has brought me to discover new places and meet a variety of new people along the way. This research project would not have been possible without the help and dedication of some to organise the logistics and share their knowledge. I would therefore like to thank a few persons in particular.

I owe much gratitude to my supervisors Mike Buxton, Jack Voncken and Marinus Dalm for sharing their knowledge and supporting me throughout the project. I very much appreciated the offer from Mike Buxton to send me the "short course on the geology of gold deposits" organized by the Society of Economic Geologists. I would like to thank Jack Voncken for performing the electron microprobe analysis and Marinus Dalm for discussing the various possibilities of spectral interpretation as well as the application of partial least squares regression.

Advice given by Gert Jan Weltje and Menno Bloemsma on the calibration methods of XRF data has been valuable for the progress of this project.

My special thanks to Hans the Ruiter for having the first contact with IAMGold which would eventually lead me to do my MSc thesis partially in Suriname.

I would like to thank Sasha Pontual not only for organising a crucial course on spectra interpretation but also for taking to time to give her opinion on part of the gathered spectral dataset.

I would like to thank Marie-France Bugnon for her great help to organize my arrival in Suriname and at last but not least a new group of friends who have made my time in Suriname enjoyable and fun. I would like to thank the Suriname Exploration team for their enthusiasm and help during the months that I was in Suriname.

Table of Contents

List of figures

List of tables

Equation

Nomenclature

3-beam setup	Is a specific setup of the X-50 Mobile XRF.
ASD	Analytical spectral device.
Crystallinity	Refers to the level of order in a solid.
ICP-AES	Inductively coupled plasma- atomic emission spectrometry.
ICP-MS	Inductively coupled plasma- mass spectrometry.
Electron microprobe	Is an analytical tool used to determine the chemical composition of solids without destroying them.
Four-acid	Refers to the dissolution method used for the preparation of samples before being analysed for geochemistry. Four-acid digestion uses: hydrochloric, nitric, per-chloric and hydrofluoric acids.
Fresh rock	Non-weathered rock.
Fusion	Refers to the method used for the preparation of samples before being analysed for geochemistry. In this case fusion refers to Lithium Borate fusion.
I_{ij}	Represents the net intensity of element j in sample i.
Kaolinite PX	Low crystalline kaolinite
Kaolinite WX	High crystalline kaolinite
K_j	Is the calibration constant for element j specific to the device. This represents the sensitivity of the device
LOD	Limit of detection.
Major element	Element present in a rock with concentrations above 1 w%.
Minor element	Element present in a rock with concentrations between 0.1 and 1w%.
M_{ij}	Is the matrix effect which corrects for scattering, absorption and enhancement effects in I_{ij}.
n	Is the number of samples
ND	Not detected
Qualitative data	Is the result of a qualitative analysis. A qualitative analysis reports the presence or absence of an element but does not give accurate quantities in which the element is present.
Quantitative data	Is the result of quantitative analysis. The quantitative analysis gives accurate concentrations in which the element is present in a rock.

r	A dimensionless index that ranges from -1 to 1. The number indicates the extend of linear relationship between two datasets. 1 being the highest attainable positive correlations and -1 the highest attainable negative (inverse) correlation.
R^2 %	Statistical measure to indicate how well a regression line fits a set of data. In this report the value will be indicated in percentages ranging from -100% to +100%
RGM	Rosebel Gold Mines.
Rock	Refers to fresh un-weathered rock in plots.
Sap	Refers to saprolite in plots.
Saprolite	Chemically weathered rock.
S_i	Represents the homogeneity and variations in measurement geometry compared to the standard measurement configuration.
SWIR	Short wave infrared. Includes the wavelength from 1400 to 2500 nm.
t	Referrers to the t-value which is used to determine if a correlation is significant or not depending on the size of the sample space.
Trace element	Element present in a rock with concentrations below 0.1 w%.
Tran	Refers to transitional rock in plots.
TTG	Tonalite-trondhjemite-grandiorite.
Transitional rock	Refers to the rock between saprolite and fresh rock.
Vein selvage	Area of altered wallrock surrounding a vein.
VNIR	Visible and near infrared. Includes the wavelengths from 400 to 1400 nm.
W_{ij}	Is the concentrations of element j in sample i

1 Introduction

1.1 Motivation

The easily detectable gold deposits all have long been discovered. Nowadays, exploration geologists are confronted with more complex gold deposits. Greater depths, lower grades and complicated geology all contribute to the difficulty to detect the remaining gold deposits. Another non-negligible factor is access to the exploration sites. Deposits with easy access are more easily investigated and most have been found. This forces the exploration geologist to search in regions of difficult access such as rainforest and oceans.

The motivation for this research project comes from the desire from IAMGold to expand their operations. At this stage Rosebel Gold Mines NV is the largest mine operated by IAMGold and located in Suriname on the transition from savannah to rainforest environment. Exploration is split into two different parts. Mine exploration (reserves development) is directed towards the extension of existing mines and new deposits at close range of known deposits. Regional exploration is directed towards totally new areas. The Regional Exploration department currently directs several exploration campaigns in rainforest environment.

To solve these issues among others, exploration has to be performed more efficiently. A better understanding of gold occurrence and indicators is therefore required. Not only will this allow to be more selective when selecting the new exploration area but it may allow to make faster conclusions and to adapt exploration campaigns on the go. To gain this crucial knowledge the Regional Exploration department decided to investigate a producing pit from the Rosebel concession where a denser dataset would be available. Drillholes from the Koolhoven pit on the Northern trend of the Rosebel concession were selected to obtain geochemical data, Visible and near infrared (VNIR) spectral data and thin sections (for petrographic study).

1.2 Research question

To which extend is it possible to characterise the Koolhoven gold deposit and its surrounding volume on the basis of alteration mineralogy, geochemistry and petrography using boreholes with a maximum down length of 230 meters at an average angle of 45 degrees.?

The research question is further subdivided into three questions to more specifically determine the subject of this research project.

RQ 1: Is it possible to differentiate the different lithologies in the Koolhoven deposit on the basis of element content?

RQ 2: Are specific elements related to the gold mineralization?

RQ 3: Are alteration mineral halo's detectable in and around the Koolhoven gold deposit?

1.3 Aim and objective

The proposed research aims to define the geological and geochemical footprints of the Koolhoven deposit at Rosebel. The research project includes data on: alteration mineralogy, major and trace element litho-chemistry and petrography using:

- Petrography, performed at Delft University of technology using a conventional polarisation microscope (transmitted and reflected light) and electron microprobe.
- Multi element geochemistry:
    1) Desktop X-ray fluorescence (XRF) performed at mine site using a X-50 Mobile XRF.
    2) Fusion XRF, performed by ALS laboratory in Lima.
    3) Four acids inductive coupled plasma-mass spectrometry (ICP-MS) and inductive coupled plasma- atomic emission spectrometry (ICP-AES), performed by ALS laboratory in Lima.
- Visible and near infrared spectral data, performed at mine site using a Terraspec Hi-Res manufactured by ASD.Inc

The samples for the analysis mentioned above are selected from drillholes with a maximum downhole depth of 230 meters (average angle 45 degrees). An existing database containing information on: gold content, lithology, alteration, mineralogy, texture, weathering and pictures of all the cores will first be used in the process of selecting the samples. At a later stage the same database will be used to put the acquired data in a geological context.

1.4 Hypotheses

It is hypothesised that the different lithologies should lead to different chemical compositions. Furthermore due to the flow of hydrothermal fluids specific elements will have enriched the deposit while others will have been depleted leading to a characteristic element assemblage specific to the deposit (path-finder elements). Heat from the hydrothermal fluids is expected to lead to specific combinations of alteration minerals forming halos around the gold deposit as a result of a decreasing temperature gradient away from where the hydrothermal fluid passed through.

1.5 Research scope

This research is directed towards characterization of the Koolhoven deposit using the methods listed in 1.3. All methods used in the course of this research project have been used as tools to gather information and by no means are a subject of research themselves.

1.6 Thesis outline

The research project has been subdivided into three major parts. The first stage consists of data gathering on-site in Suriname. The first stage is followed by data treatment and analysis at Delft University of Technology (the Netherlands). The last part combines all the result and data to define whether it can be concluded that gold deposits can or cannot be identified on the regional scale on the basis of alteration mineralogy and geochemistry.

2 Background

2.1 IAMGold – Rosebel Gold Mine NV

IAMGold is a leading mid-tier gold mining company producing roughly one million ounces of gold each year from five gold mines. Besides gold more than 4500 tonnes of niobium are produced annually through Niobec Inc which is operated by IAMGold.

The Rosebel Gold Mine NV (RGM) is the largest mine owned by IAMGold. IAMGold owns a 95% share of RGM and the remaining 5% are owned by the Surinamese government. The concession is located in Brokopondo district in Suriname. The total Rosebel concession covers an area of 170 km^2 situated between the Suriname River and the Saramaca River (Figure 2-1). The concession includes 8 deposits (Figure 2-4).

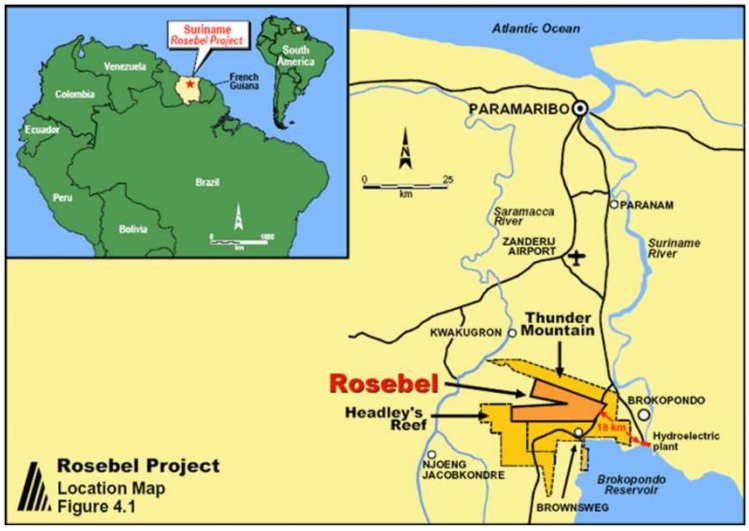

Figure 2-1, Location of the Rosebel concession South of Paramaribo.

The very beginning of the Rosebel concession dates to 1879 when small scale artisanal miners discovered gold. Since then the concession has been worked both by small scale miners as well as multinational companies. In 2004 commercial production started with Cambior as operator. By acquiring Cambior in 2006, IAMGold became owner of Rosebel Gold Mines NV. Approximately half of the recorded gold production of Suriname originates from this district. The milestones of the concession together with general information are depicted in Appendix Figure 10-1 and Figure 10-2.

2.2 Geology

2.2.1 Regional geology

Suriname is located on the Amazonian craton which hosts the oldest rock formations of the South American continent. More specifically Suriname is on the Northern part of the Amazonian craton named Guiana Shield. With a total area of 900,000 km^2 the Guiana shield also includes the countries: Venezuela, Guiana, French Guiana and Northern Brazil. Geological features on the scale of the Koolhoven pit as well as Suriname can be related back to geological events that affected the Guiana shield.

The evolution of the Guiana Shield can be subdivided into four stages (Delor, et al., 2003):

- Archean basement.
- Main transamazonian orogeny including two phases namely: D1 and D2a (Rhyacian evolution 2.26-2.08 GA).
- Late- transamazonian orogeny including phase D2b (Late-Rhyacian to Orosirian evolution (2.07-1.93GA).
- Proterozoic events and Paleozoic events.

Evidence of the Achaean basement is present in the Western part of the Guiana shield in Imataca (Venezuela) as well as the Western part of Para (Brazil). During the Eorhyacian oceanic stage, the North Amazonian Archean shield and the West African Archean shield separated from each other forming oceanic crust in the process (2.26-2.20 Ga) (Figure 2-3).

The two Archean shields together with oceanic crust form the setting for the Amazonian orogeny (Figure 2-3). The Amazonian orogeny can be subdivided into two sections being the main transamazonian orogeny which affected the entire Guiana shield and the late-transamazonian orogeny which only affected the central and Western part of the Guiana shield at a later stage. The main transamazonian orogeny can be further subdivided into a D1 and D2a phase on the basis of tectonics which together took place between 2.26 and 2.08 GA. The D1 phase 2.18-2.13 Ga, is characterized by the generation of tonalite-trondhjemite-granodiorite greenstone belts (TTG-greenstone) as a result of North-South convergence between the North Amazonian and West African cratons. The subduction of the oceanic-floor that had been produced from 2.26 to 2.20 Ga, and subsequent melting of it resulted in TTG melts. These have been dated at 2.18 to 2.16 GA (Figure 2-3). In Suriname the group of lithologies associated with the greenstone successions are identified as the “Marowijne” group. According to the lithological and isotopic data acquired in French Guiana greenstones consist essentially of submarine lavas. Turbidites belonging to the Armina formation were later deposited on top of the volcanics (Figure 2-2). These are part of a succession of siltstone/mudstone and greywacke that can be observed in the Koolhoven deposit.

Figure 2-2, Clear successions of siltstone and mudstone from the Armina formation were deposited in the form of turbidites.

The North-South convergence later changed into sinistral shearing strike slip movement along a NE-SW direction. This phase is recognized as the D2a phase (2.11-2.08 Ga) (Daoust, et al., 2011; Delor, et al., 2003). Deformation took place in compressional settings as well as extensional settings as a result of the strike slip movement. Pull-apart basins resulting from extensional deformation created space for sediment deposition (Daoust, et al., 2011; Kroonenberg & de Roever, 2010, Voicu, et al., 2001).

In Suriname the Rosebel formation consisting of sandstone and conglomerate was deposited in such pull-apart basins forming an unconformity with the underlying volcanic TTG-greenstone belt. Due to the presence of bedding and scour-and-fill structures the Rosebel formation has been interpreted to have been deposited in a high energy depositional setting such as a torrential fluvial environment. The Sediments of the Armina formation contain fragments of volcanic rock which is believed to be derived from the erosion of the associated previously formed volcanics. (Daoust, et al., 2011; Delor, et all., 2003). The conglomerates of the Rosebel formation contain clasts of mudstone, siltstone, and

volcanic rock hereby indicating that part of the conglomerate sediments finds their origin in the erosion of the previously deposited Armina formation (Daoust, et al., 2011; Delor, et al., 2003; Watson, 2008).

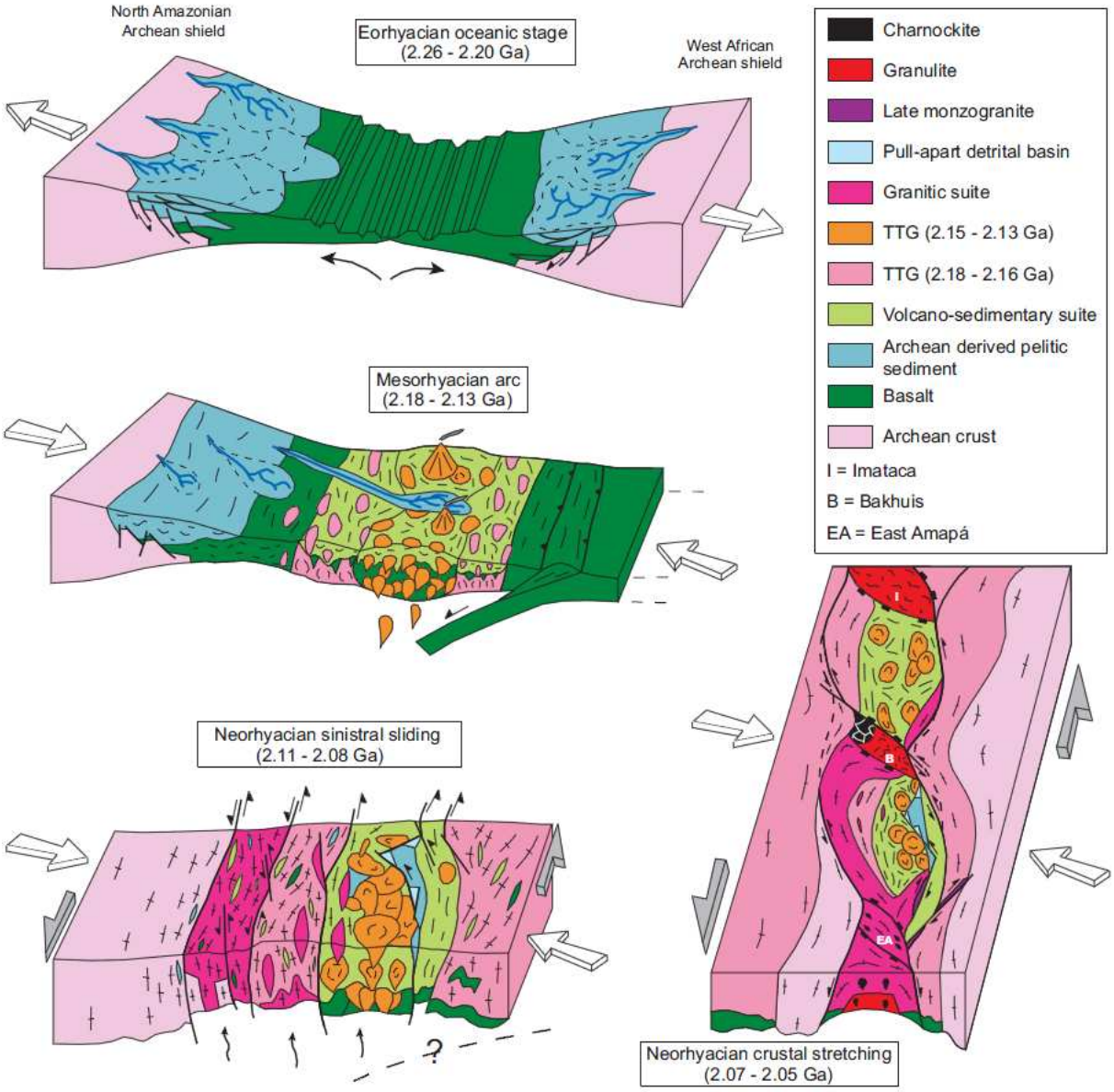

Figure 2-3, "Geodynamic evolution model for the Guiana shield Paleoproterozoic terrains" (Delor, et al., 2003).

2.2.2 Rosebel geology

Figure 2-4 represents the Rosebel concession. Except from the Rosebel pit all the pits are aligned along the two major shear zones that are present on the concession. The three different domains are referred to as:

- North trend: Koolhoven, Jzone, Pay Caro, East Pay Caro.
- Central domain with only the Rosebel pit.
- The South trend: Mayo, Roma and Royal Hill.

The pits along the Southern trend are aligned along an E-W trending major shear zone. The Northern trend is subdivided into a Northern and Southern mineralized trend (Appendix Figure 10-5). Pay Caro and East Pay Caro being situated on the Southern mineralized trend and Koolhoven together with Jzone on the Northern mineralized trend. Both mineralized trends are separated from each other by the volcanic rocks of the Armina formation. They are also both related to shear zones along the contact between the volcanic and sedimentary rock formations. Differences in strain capacity are assumed to be the cause for this.

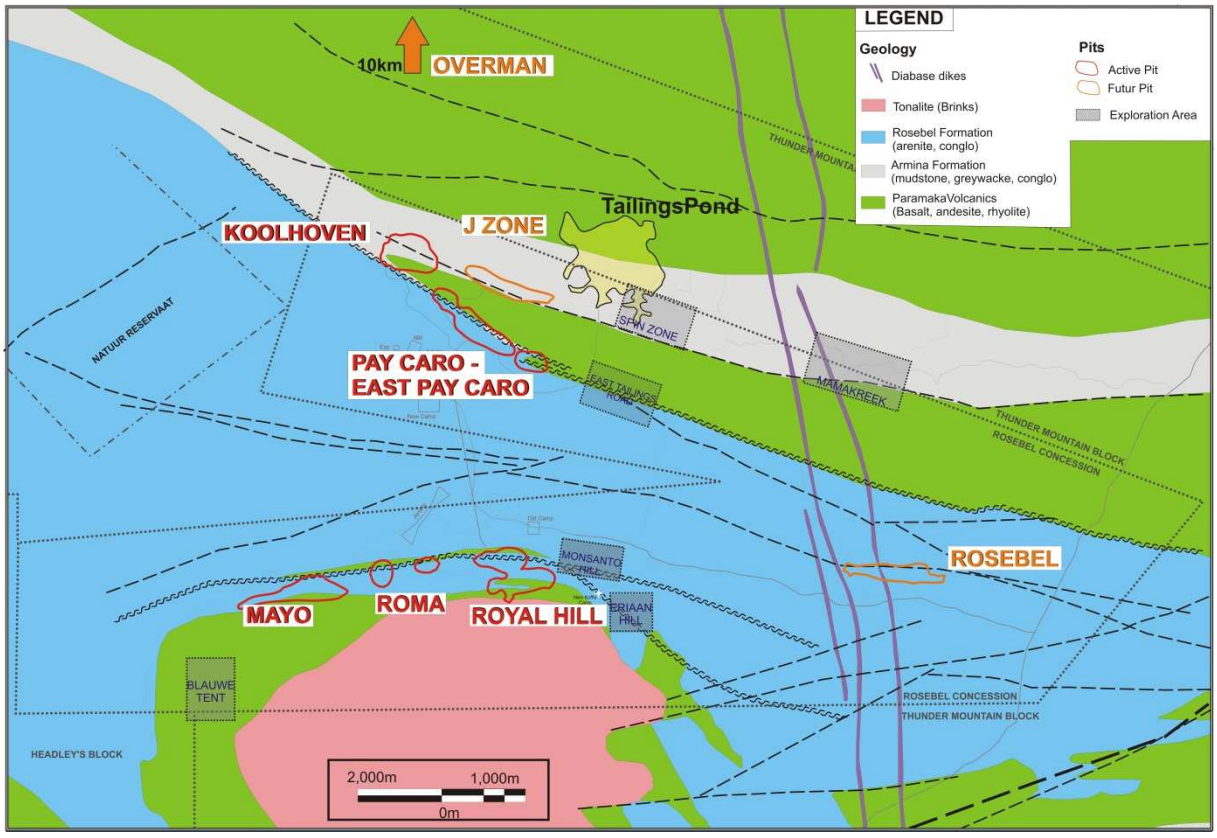

Figure 2-4, Geological map of the Rosebel concession (Daoust, et al., 2011).

The gold occurs in the form of coarse grains of free gold and is often attached to hematite, goethite and pyrite. Mineralization occurs both in shear and tension veins. Tension veins account for the greater portion of vein volume and total gold content.

In the North trend beside quartz and carbonate (ankerite & calcite) the veins also contain: plagioclase, hematite, chlorite, sericite, pyrite, and tourmaline. Zonations with plagioclase and hematite have been identified closer to the shear vein zone. Selvages have also been observed on the deposit scale. Pervasive alteration to chlorite, sericite, plagioclase, hematite, carbonate and

pyrite near the shear zone and alteration to chlorite, carbonate (calcite) and sericite away from the shear zone. Both mechanical traps such as anticline hinges and brittle conglomerate lenses and chemical traps along lithological contacts of different chemical composition are also considered to be present. Seven out of eight deposits are located along lithological contacts.

2.2.3 Koolhoven geology

The Northern mineralized trend in Koolhoven is characterized by three mineralized zones (Figure 2-6 & Appendix Figure 10-6) each parallel to each other along a WNW-ESE orientation. These mineralized zones are related to minor shear zones with a thickness of <1m. The shear zones with a strike of WNW-ESE are steeply south dipping. Gold is commonly found in the quartz-carbonate veins and is associated with pyrite alteration in the wall rock. The pyrite content ranges from 2 to 5 vol%. The Koolhoven should be regarded as a low grade ore deposit (Figure 2-5).

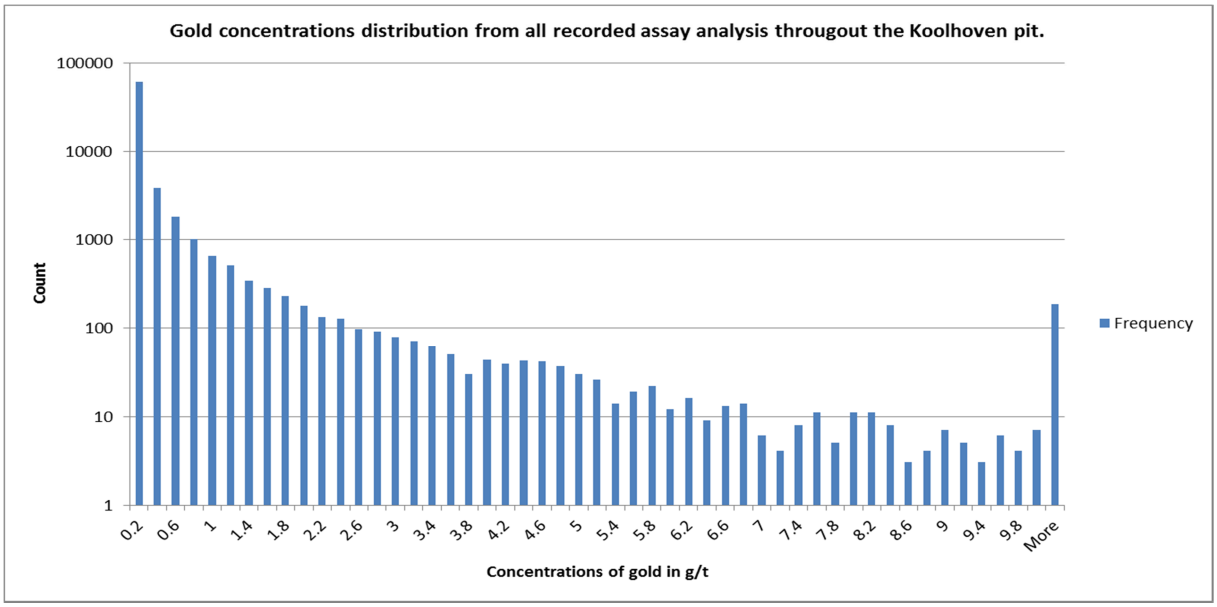

Figure 2-5, Gold concentration distribution from all available assay analysis of the Koolhoven deposit.

Lithologies found in the Koolhoven pit consist of andesite volcanic rock in the South. The turbiditic sequence overlaying the volcanics consists of mudstone, siltstone, and greywacke. In the North we find conglomeratic lenses. The complete sequence from turbiditic sediments to conglomeratic lenses lies conformably on the underlying volcanic. As explained before three mineralized trends are present in the Koolhoven pit. All three are associated with the presence of shear zones oriented WNW-ESE and are steeply dipping towards the South. Beside shear veins the deposit also hosts two sets of tension veins. The first set is WNW-ESE and has a dip of around 45 degrees towards the North. The second set is N-S and steeply dipping towards the West. Veins generally lack deformation.

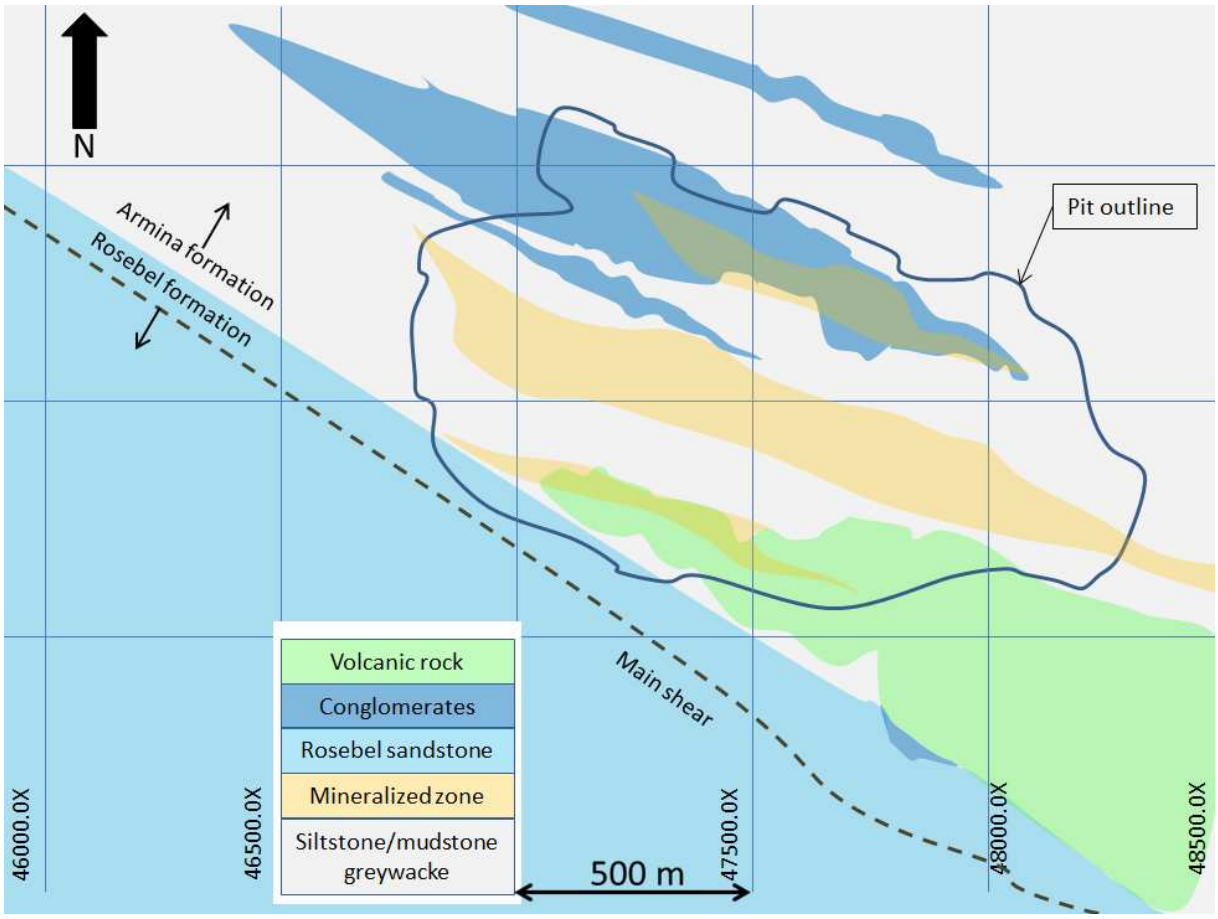

Figure 2-6, Simplified geological map of the Koolhoven pit.

2.3 Type of deposit

The Koolhoven deposit can be classified as a Greenstone hosted quartz-carbonate vein gold deposit (Appendix Figure 10-3 & Appendix Figure 10-4). These deposits are a subtype of the lode gold deposits and sometimes referred to as mesothermal, orogenic, shear-zone related quartz carbonate or gold only deposits (Dubé & Gosselin, 2007; Yeats & Vanderhor, 1998).

They form along major compressional to transtensional crustal-scale fault zones. Although they are present in deformed Greenstone terranes of all ages, Achaean terranes seem to host the most important deposits in terms of gold content. The gold tends to concentrate in settings affected by curvature, flexure and dilatational jogs, which have created space and pathways for the migration of hydrothermal fluid.

The deposits generally form at depths greater than five km and have vertical vein arrays that exceed one kilometre (Robert, et al., 1997; Robert, et al., 2007) (Appendix Figure 10-3).

As the name “greenstone hosted quartz-carbonate vein gold deposit” indicates, veins play a major role in relation to the deposit style. Different types of veins are present as a result of different stress & strain regimes. Furthermore they are important both as a conduit for hydrothermal fluids to flow and as open spaces where gold can precipitate.

Previous research (Eilu & groves, 2001; Dubé & Gosselin, 2007; Robert, et al., 1997; Robert, et al., 2007; Dubé & Gosselin, 2007, Daoust, et al., 2011) on the alteration and mineralogy of greenstone

hosted quartz-carbonate vein deposits reveal strong similarities. As the name of the deposit type suggests the bulk of the vein consists of quart and carbonate (ankerite, dolomite, calcite, siderite). Other minerals that may be present in the veins are: chlorite, white micas, tourmaline and scheelite.

On the regional scale the deposits are characterized by strong carbonate alteration. The alteration halos close to the deposit include carbonate alteration, sericitization and sulphidization of the vein selvage. The sulphide minerals present include: pyrite, chalcopyrite and pyrrhotite but only make up less than 10 vol% of the ore bodies. The alteration halos are also characterized by varying amounts of chlorite, calcite and magnetite. "In greenshist facies, the alteration zones are, from distal to proximal and according to the diagnostic minerals: calcite-chlorite, calcite-ankerite and sericite. In amphibolite facies, two zones are normally detected, a distal biotite and a proximal calc-silicate zone with no intermediate zone" (Table 2-1). More specifically research in French Guiana states: "Muscovite + chlorite + carbonates predominate in hydrothermally altered metavolcanic and metasedimentary rocks" (Milesi, et al., 2003, p.257).

	Greenschist	Amphibolite
Typical carbonate	Calcite (distal); ankerite (proximal)	Calcite
Dominant mica	Muscovite (sericite)	Biotite
K-feldspar	Unstable in the proximal alteration zone	Stable throughout the alteration sequence
Ca silicates	Not present	Diagnostic for the proximal zone
Ti minerals	Rutile only	Ilmenite and titanite more common
Dominant Fe sulphide	Pyrite	Pyrrhotite
Dominant As mineral	Arsenopyrite	Arsenopyrite or loellingite
Extent of CO_2 v. K alteration	Carbonation is more extensive	Potassic alteration is more extensive
Lateral extent of the alteration halo	20–200 m, in some cases >1–2 km	Less extensive; normally <20–50 m

Based on Mikucki & Ridley (1993), Cassidy *et al.* (1998), Eilu *et al.* (1998, 1999) and McCuaig & Kerrich (1998).

Table 2-1, Variation in alteration between greenshist and amphibolite facies (Eilu & Groves, 2001).

Ausspec International published a series of ten spectral analysis guides named the GMEX series. Volume 6 "Archean greenstone gold" reveals that several alteration zones around Archean greenstone gold deposits can be defined by spectral analysis. These zones show particular differences with the background signal in Table 2-2. The order of zones from distal to proximal location to the mineralized area is: Chlorite zone (Table 2-3), Carbonate zone (Table 2-4), muscovite & pyrite zone (Table 2-5). It is important to note that boundaries between the different zones are not sharp and that not all zones carry the same importance in relation to regional exploration campaigns and/or spectral analysis. This is especially true for the muscovite & pyrite zone which represents the location where the gold should be deposited. "Although this zone is of extreme importance in terms of Au mineralisation it could be considered as one of the least important in terms of the application of spectral geology to the exploration program. This is because even though this zone contains some characteristic spectral signatures it is more likely to be recognised by the geologist through logging and anomalous geochemical signature (e.g. Au)" (GMEX handbook 6, p.45).

Mineral	Occurrence
Actinolite or hornblende +/- chlorite	Typical of upper Greenshist and lower Amphibolite Facies.
White mica (paragonite)	Present in felsic rocks and some metasediments.
Talc, serpentine	Present in ultramafic rocks.
Notronite, saponite, montmorillonite, kaolinite	Common weathering products near surface and at greater depth on fractures.

Table 2-2, Background signal for Archean greenstone gold deposits (AusSpec international, 2008).

Mineral	Occurrence
Chlorite, carbonate (calcite +/- ankerite)	Typical of altered mafics and some metasediments.
White mica	Present in felsic and some metasediments.
Talc	Present in ultramafic rocks.

Table 2-3, Chlorite zone for Archean greenstone gold deposits (AusSpec international, 2008).

Mineral	Occurrence
Fe carbonate (siderite and ankerite)	It is rare to find carbonate alone in a spectrum. It would typically be observed with other minerals such as white mica and chlorite.
White mica	If present, may be termed the carbonate-muscovite zone.
Chlorite	If present, may be termed the carbonate-chlorite zone.

Table 2-4, Carbonate zone for Archean greenstone gold deposits (AusSpec international, 2008).

Mineral	Occurrence
White mica (phengitic)	Typically the dominant micaceous mineral.
+/- Biotite, phlogopite	May be the dominant mica in some cases.
Ankerite siderite	May also be present.
Pyrite	No discrete absorptions but have a quenching effect on the spectra if finely disseminated in a sample.

Table 2-5, Muscovite and pyrite zone for Archean greenstone gold deposits (AusSpec international, 2008).

Common metals associated with the deposit are: Ag, W, B, As, Mo, Sb, Te, Bi. Base metals such as: Cu, Pb and Zn only show slight enrichments. Au:Ag =5:1 (Robert, et al., 1997; Robert, et al., 2007) and up to 10:1 according to . (Eilu & Groves, 2001, p. 183) state: “the ores are enriched in Ag, As, Au, Ba, CO_2, K, Rb, S, Sb, Si, Te and W, and depleted in Na and Y relative to host-rocks. Base metals: Fe, Mg and Mn are rarely mobile in these settings”.

The halo dimensions vary in size depending on the host rocks. The halo may envelope an entire deposit (Robert, et al., 1997; Dubé & Gosselin, 2007). In General no distinct mineral zonation is observed (Robert, et al., 1997; Robert, et al., 2007; Dubé & Gosselin, 2007).

3 Data acquisition and methodology

3.1 Overview

The tree research questions will be dealt with in the same order as they have been listed in paragraph 1.2.

RQ1) To differentiate the different lithologies from each other major element contents will be measured using lithium borate fusion XRF. The lithology characteristics form the starting point of the gold deposit. Furthermore results from the lithology differentiation will allow to relate the other acquired results to specific lithologies on the basis of measured values instead of visual interpretations.

RQ2) To test if specific elements are related to the occurrence of gold a large dataset has been gathered using a X-50 Mobile XRF unit (portable XRF). The elements contents will be compared to the gold content derived from a pre-existing data base as will be explained below. Because the quality of the data acquired with the relatively cheap portable XRF procedure is uncertain the results will be compared to a selection of samples that have been tested in parallel using ICP-MS and ICP-AES in a laboratory.

RQ3) The presence of alteration halos will be investigated using an analytical spectral device measuring spectra in the VNIR range. Importance of studying alteration halos is clearly explained in (Thompson, et al., 1996, p.1) “In particular, alteration is ubiquitous in an around hydrothermal mineral deposits. The distribution and mineralogy of this alteration relates to the hydrothermal environment, and hence, the type of mineral deposit. More importantly for mineral exploration, hydrothermal alteration around mineral deposits commonly form halos that provide a target which is much larger than the deposit itself”.

Thin sections will be used to control the results of the lithology differentiation and the alteration mineralogy. Furthermore the thin section are used describe rock textures.

The Koolhoven deposit has been chosen for this research project because it has the best coverage of boreholes outside the pit. This characteristic is crucial to test the presence of alteration halos

The data used for this research project originates from a pre-existing database and newly acquired data. Rock samples taken from the boreholes were used for several analyses to be able to cross validate results. The sampling process for new data is summarized in Figure 3-1.

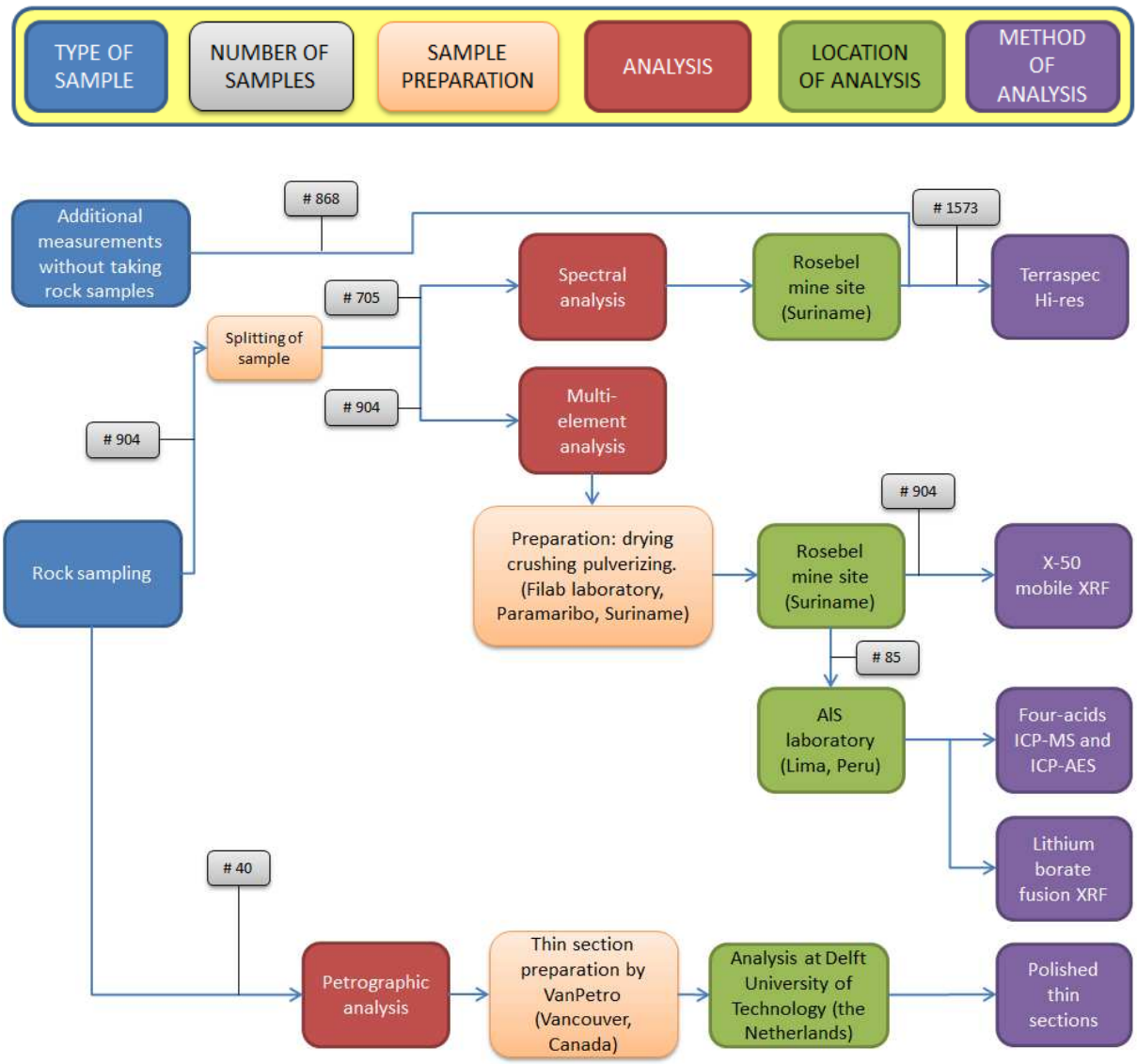

Figure 3-1, Flowchart displaying the systematic of sampling.

The samples were selected from 28 different boreholes throughout and around the pit (Figure 3-4). All the different lithologies have been sampled. Figure 3-4 shows only a small part of the boreholes drilled in the Koolhoven pit. Not all drilled boreholes were available for the research project because condemnation boreholes outside the pit are generally not stored and because the tropical weather had deteriorated the quality of the boxes such that they could not be handled without falling apart. Out of the 28 selected boreholes three have been selected because they contain intervals with higher gold content (Figure 3-2 and Figure 3-3). These are boreholes KHD-508, KHD-566 and KHD-583. Table 3-1 summarizes the number of samples selected from each borehole.

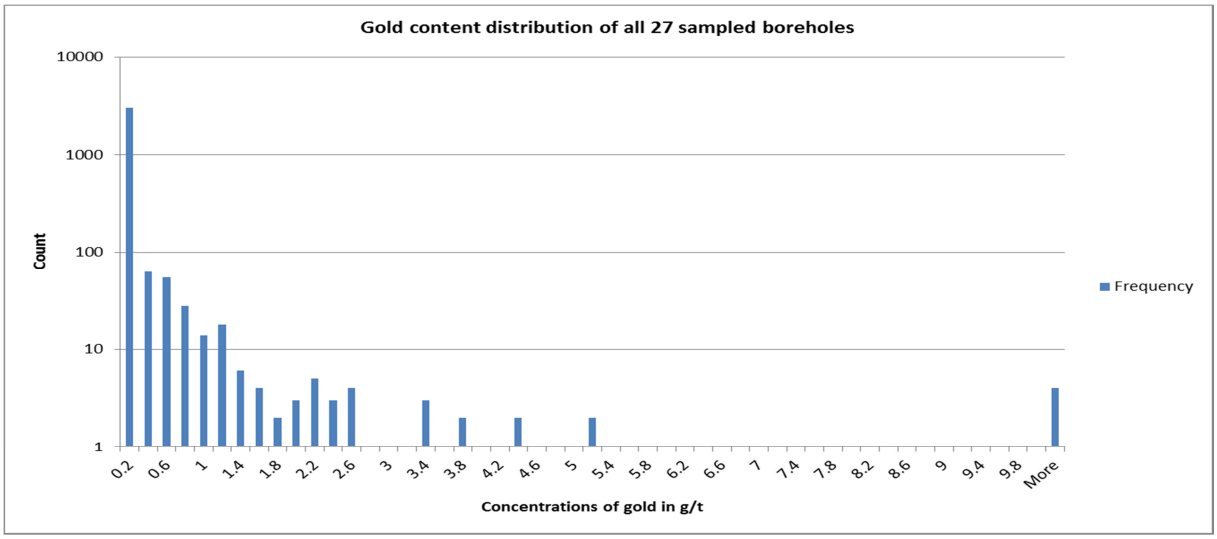

Figure 3-2, Gold concentration distribution of the 27 boreholes used for multi-element and VNIR sampling.

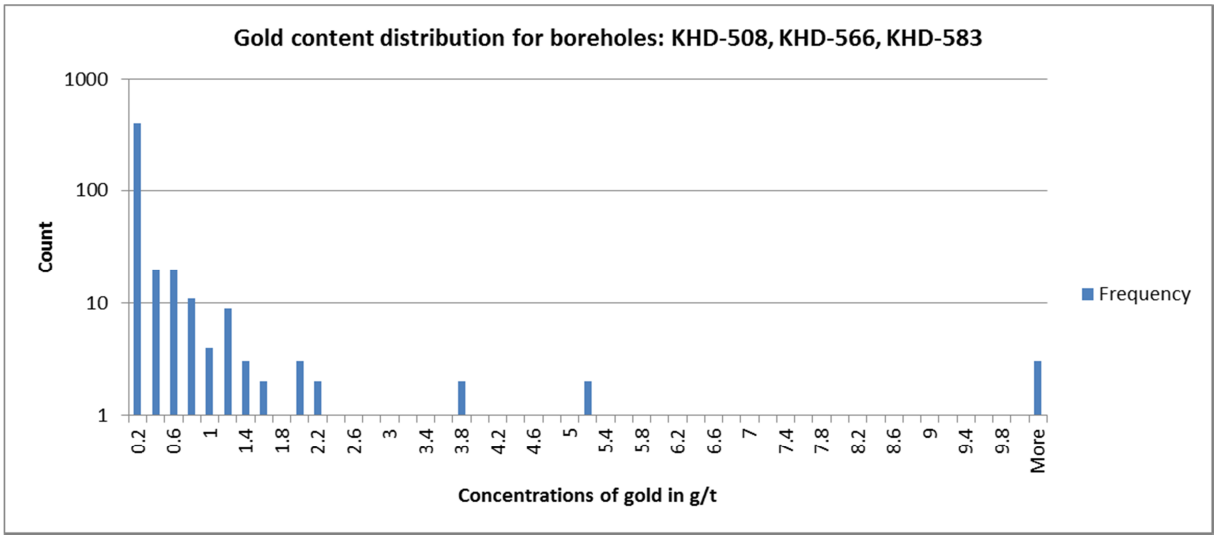

Figure 3-3, Gold concentration distribution of boreholes KHd-508, KHD-566 and KHD-583.

Because some samples used for the multi-element could not be splitted these were not measured using the VNIR spectrometer. Therefore boreholes contain more portable XRF data points then spectral measurements. The samples that could not effectively be splitted were shallow located unconsolidated saprolite samples. Once dry these samples would fall apart during handling.

In the case that the number of spectral measurements exceed the number of portable XRF data points additional spectral measurements were taken directly on the core without taking a sample for multi-element analysis.

The number of portable XRF measurements includes the samples that have also been analysed by the laboratory.

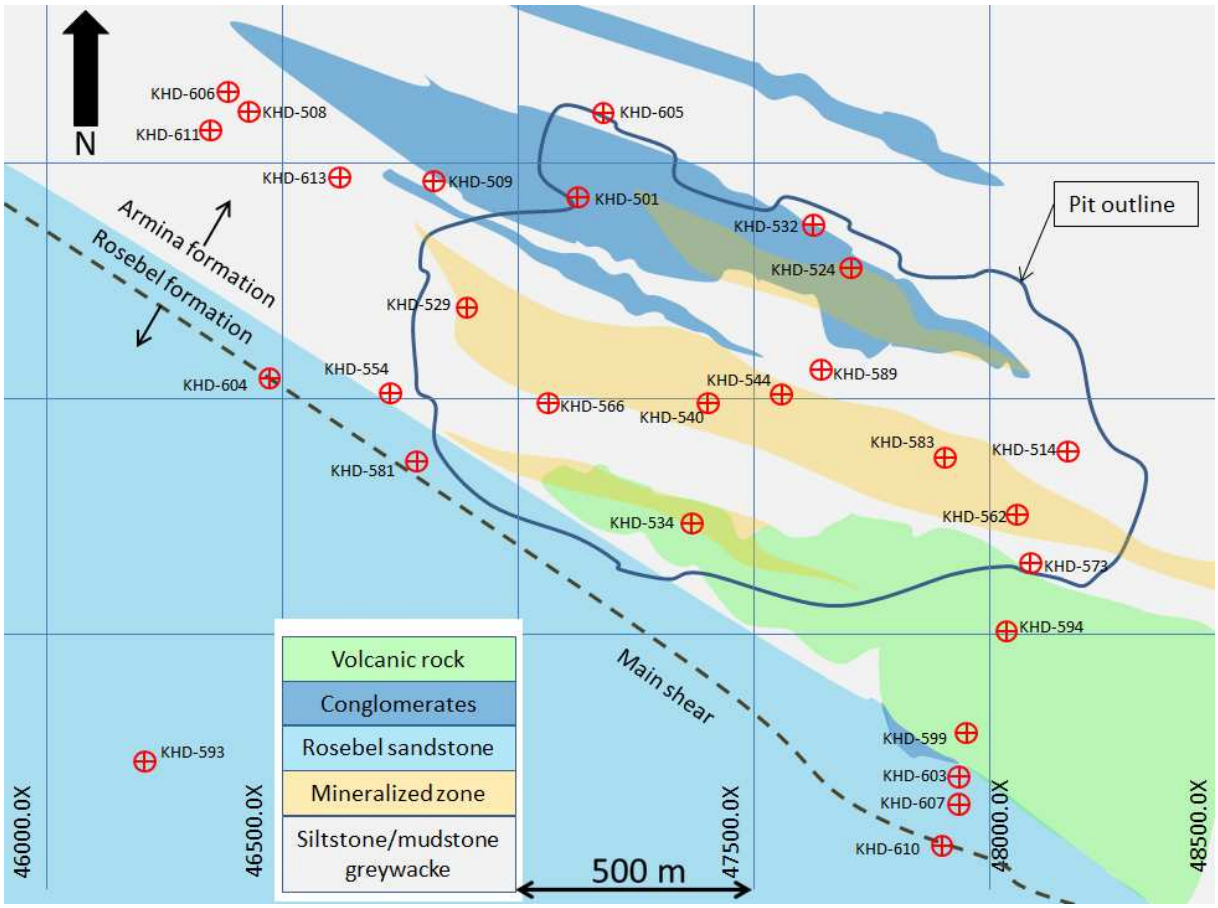

Figure 3-4, The Koolhoven with the sampled boreholes in red.

Borehole ID	Number of portable XRF measurements	Number of laboratory analysis (fusion XRF and four acids ICP-MS & ICP-AES	Number of spectral measurements	Number of thin-sections
KHD-501	20	-	16	1
KHD-508	55	-	222	-
KHD-509	24	-	21	-
KHD-514	46	3	54	1
KHD-524	27	3	22	3
KHD-529	28	2	22	-
KHD-532	34	7	27	4
KHD-534	30	5	27	4
KHD-540	28	1	25	-
KHD-544	32	4	28	2
KHD-554	28	3	19	3
KHD-562	18	3	16	2
KHD-566	55	-	192	-
KHD-573	44	6	37	2
KHD-581	36	6	29	-
KHD-583	52	-	222	-
KHD-589	35	-	202	-
KHD-593	27	4	19	-
KHD-594	32	7	161	5
KHD-599	38	5	35	3
KHD-603	-	-	-	2
KHD-604	25	3	18	-
KHD-605	36	4	29	7
KHD-606	11	1	10	-
KHD-607	36	5	34	-
KHD-610	35	8	28	-
KHD-611	23	3	20	1
KHD-613	49	2	38	-
Total	**904**	**85**	**1573**	**40**

Table 3-1, Overview of the samples and analysis performed.

3.2 Existing database

All boreholes drilled are systematically logged and analysed for gold content. The gold content is analysed on 1.5 meter intervals using fire assay. Exceptions for the length of the interval are made depending on vein concentrations and if visible gold is found or not while logging. The logging continuously performed by the Mine Exploration department. The database includes information on lithology, mineralogy, alteration, deformation, and veining. This information was available together with pictures of all the drill cores.

3.3 Petrography

3.3.1 Introduction

The petrographic part consists of several datasets. First the pre-existing drill logs which are made for every drill hole are used to identify the large scale trends such as lithology. Field notes and descriptions made during the course of this research project are also used as support. Furthermore 40 polished thin sections have been made for petrographic studies to characterize both the lithology and special features which are only detectable on the micro scale. Analysis of the polished thin section together with the gold content may reveal the timing of gold mineralization and or links to other minerals. Besides characterizing the lithologies the focus will be on the study of veins because these are believed to contain the gold. Both the veins as the surrounding host rock will be analysed.

3.3.2 Procedure

Selection of samples is based on visual interpretation. The samples were dispatched to Vancouver Petrographics (VanPetro). VanPetro prepared a total of 39 polished thin sections of 26*46 mm and one polished thin section of 50*50 mm. Analysis of the thin sections was performed at Delft University of Technology. The emphasis of the analysis is characterization of the different lithologies and features based on mineralogy and textures. Minerals were determined optically by microscopy analysis. Where doubts remained an electron microprobe was used to define the chemical composition of the mineral. For detailed description of electron microprobe technology the reader is referred to (Gill, 1997). Although optical analysis of textures is prone to be subjective depending on the geologist performing the analysis. For interpretation of textures the work of Spry (1969) was used.

3.3.3 Sampling

The thin sections have been selected as to capture the features characterizing the overall different geologies as well as special features with emphasis on the veins. The spread of thin section over the entire mine is therefore not even. The locations of the samples may be separated by 20 meters in a single borehole while in other cases such as polished thin sections LC426 to LC429 four polished thin sections have been selected on an interval of 40 cm to capture the characteristics of a single shear vein. Care was taken to sample in fresh rock to ensure good quality polished thin sections.

3.4 Multi element geochemistry

3.4.1 Introduction

Four different methods of data acquisition have been used to obtain the multi-element data. A Mobile X-50 XRF unit was used on mine-site to obtain a large dataset of 904 samples. Of these 904 samples 85 were sent to ALS laboratory in Lima (Peru) for quantitative analysis (Figure 3-1 & Appendix Figure 10-7). Here four-acid ICP-MS & ICP-AES was used to report the widest possible

concentration range (Table 3-3). Lithium borate fusion XRF was used to measure the content of major elements (Table 3-4). The quantitative data from the laboratory analysis serves as reference for the data obtained with the portable XRF unit.

3.4.2 Procedure

Sampling of the boreholes was followed by cleaning the samples. The first preparation stage was performed by Filab Suriname and included: drying, crushing and pulverizing of all samples. The 904 samples were packed in plastic bags to be ready to be analysed with the field portable XRF unit. 85 pulverized samples derived from fresh rock only intervals were selected to be analysed by ALS laboratory in Lima (Peru) using quantitative methods as stated above.

3.4.3 Sampling

A total of 904 samples of a length varying between 20 cm and 50 cm were obtained throughout 27 boreholes (Table 3-1). Care was taken to avoid veins and other non-representative features such as intervals containing large gains of sulfides. The samples were split with one part used for the multi-element analysis and the second part for spectral measurements.

3.4.4 Desktop XRF

The portable XRF unit used for the experiments is an X-50 Mobile XRF System manufactured by InnovXsystem. The device has three different setups. All three are optimized for a different range of elements. At the stage of this research project only the 3-beam setup had been calibrated and therefore was used. Within this setup not all elements are measured with the same accuracy (Table 3-2& Appendix Figure 10-9). Although the results from the desktop XRF unit are not as accurate as the results obtained under laboratory conditions the results should mainly be regarded as qualitative instead of quantitative. The benefit of using the portable XRF unit is that once the device has been bought the operating costs are minimal: pulverization, plastic bags, and man hours. Pulverization of the samples may already have been done for other analysis such as gold assay and there for may not need to be done.

Using the desktop XRF therefore allows us to perform many more measurement than we would by sending samples to be analysed by a private laboratory. Although care has been taken to take representative samples, outliers may have been selected and be present in our data set. Not only will it be easier to detect an outlier when the number of samples is greater but if it would not be detected the effect of the outlier will be lower as well.

Soil 3-Beam	Primary	Secondary
Beam 1 – 50 KV	As, Sr, Zr, Mo, Ag, Cd, Sn, Sb, Ba	Ti, V, Cr, Mn, Fe, Co, Ni, Cu, Zn, W, Hg, Se, Pb, Bi, Rb, U, Nb, LE, La, Ce
Beam 2 – 35 KV	Fe, Co, Ni, Cu, Zn, Se, Pb, Bi, Rb	Ti, V, Cr, Mn, W, Hg, As, U, Sr, Zr, Nb, Mo, LE
Beam 3 – 10 KV	P, S, Cl, Ca, Ti, Cr, Mn	Sc, V, Fe, LE

Table 3-2, Characteristics of the 3-Beam setup for the portable XRF unit. Primary elements are elements for which the beam is optimized and should therefore yield correct values. The elements listed under secondary are also measured but with less accuracy.

3.4.5 Four acids, ICP-MS & ICP-AES

Four acids refer to the four acids being used to dissolve the samples prior to the actual analysis. The acids include: hydrochloric, nitric, per-chloric and hydrofluoric acids. Both ICP-MS as ICP-AES have been used to report the widest possible concentration range. For detailed description of both

analysis methods the reader is referred to (Gill, 1997; Balaram, 1996; Jenner, et al., 1990). Four-acids solution was used because hydrofluoric acid attacks the silica matrix of the rock samples. In the process silica will also exit the solution due to evaporation. The loss of Si is normally an advantage because it reduces the amount throughout which the trace elements are dispersed. This result in higher concentrations of trace elements in the solution and therefore better detectability. The analysed elements and ranges of values are represented Table 32. The results from the four-acid ICP-MS and ICP-AES analysis will be used as reference for the data gathered with the portable XRF unit.

48 elements by four-acid, ICP-MS and ICP-AES

ANALYTES & RANGES (ppm)								CODE
Ag	0.01-100	Cs	0.05-500	Na	0.01%-10%	Sr	0.2-10,000	ME-MS61
Al	0.01%-50%	Fe	0.01%-50%	Nb	0.1-500	Ta	0.05-100	
As	0.2-10,000	Ga	0.05-10,000	Ni	0.2-10,000	Te	0.05-500	
Ba	10-10,000	Ge	0.05-500	P	10-10,000	Th	0.2-10,000	
Be	0.05-1,000	Hf	0.1-500	Pb	0.5-10,000	Ti	0.005%-10%	
Bi	0.01-10,000	In	0.005-500	Rb	0.1-10,000	Tl	0.02-10,000	
Ca	0.01%-50%	K	0.01%-10%	Re	0.002-50	U	0.1-10,000	
Cd	0.02-1,000	La	0.5-10,000	S	0.01%-10%	V	1-10,000	ME-MS61m
Ce	0.01-500	Li	0.2-10,000	Sb	0.05-10,000	W	0.1-10,000	
Co	0.1-10,000	Mg	0.01%-50%	Sc	0.1-10,000	Y	0.1-500	
Cr	1-10,000	Mn	5-100,000	Se	1-1,000	Zn	2-10,000	
Cu	0.2-10,000	Mo	0.05-10,000	Sn	0.2-500	Zr	0.5-500	

Table 3-3, The elements and their ranges measured by using four-acids ICP-MS and ICP-AES by ALS laboratory in Lima, Peru.

3.4.6 Fusion, XRF

Fusion refers to the lithium borate fusion method used to prepare the sample prior to the actual XRF analysis. No silicates are known to resist to fusion digestion (Gill, 1997). It is therefore the preferred method to quantitatively analyse the silicate content of rock samples. The fusion preparation also eliminates particle size effects which are for example encountered in pressed powders or direct measurements on the core sample (Hutton & Elliott, 1980). This method is used to analyse the samples for major elements (Potts & Webb, 1992). The major elements together with their respective ranges of detections are listed in Table 3-4. For detailed descriptions of the analysis method the reader is referred to (Gill, 1997; Thomas & Haukka, 1976; Ramsey, et al., 1995;

ANALYTES (%)								CODE
SiO_2	0.01-100	MgO	0.01-100	TiO_2	0.01-100	BaO	0.01-100	ME-XRF06
Al_2O_3	0.01-100	Na_2O	0.01-100	MnO	0.01-100	LOI	0.01-100	
Fe_2O_3	0.01-100	K_2O	0.01-100	P_2O_5	0.01-100			ME-ICP06
CaO	0.01-100	Cr_2O_3	0.01-100	SrO	0.01-100			

Table 3-4, The elements and their ranges measured by using lithium borate fusion XRF by ALS laboratory in Lima, Peru.

3.4.7 Tests

Several tests were performed to analyse the quality of the data and consistency of the measurements. Tests performed include:

Desktop XRF:

- 10 repeated measurements on calibration disc without changing the location

- 10 repeated measurements on the calibration disc while changing the location of the measurement
- 10 repeated measurements on two pulp samples LC1143 and LC1153.
- 20 measurements of empty plastic bags.
- Cross validation of samples analysed with the X-50 Mobile XRF and analysed by ALS laboratory using four acids ICP-MS and ICP-AES.

ALS laboratory

- Repeated the four acids ICP-MS and ICP-AES analysis for samples: LC010, LC048, LC058, LC069 and LC087.
- Repeated the lithium borate fusion XRF analysis for the samples: LC012, LC017, LC034, LC036, LC059, LC083 and LC093.
- Included standards and blanks throughout the analysis.

3.5 Visible and near infrared spectral analysis

3.5.1 Introduction

The spectral analysis is used to recognize fine grained minerals, compositional variations and define the type of alteration. It is very useful and fast because minimal sample preparation is required. Reflectance spectroscopy has been around since the first half of the 20th century , however it is only 15 years ago that the use of portable short wave infrared (SWIR) spectroscopy truly started to increase.

Various subdivisions of the wavelength ranges are commonly used. In this research project the term “visible and near infrared (VNIR)” will refer to the total range from 400 nm to 3000 nm. The range from 1000 to 2500 nm will be referred to as the “short wavelength infrared (SWIR)” range. The current spectrometers generally detect the visible near infrared (VNIR) and therefore include the short wavelength infrared (SWIR) (Appendix Figure 10-10). The SWIR range however does relate to the chemical composition while the rest of the VNIR does not. Minerals such as: clays, carbonates, phyllosilicates, chlorites and some sulphates may successfully be identified using SWIR spectroscopy.

Besides recognizing mineral groups SWIR spectroscopy can be used to define the mineral composition, crystallinity and relative proportion of minerals within a rock sample.

The fact that the devices can be carried into the field, that the samples required minimal preparation except from being dry, make mineral spectrometry a valuable tool in exploration. All these factors can be used to define a temperature and chemical zoning in an alteration system.

3.5.2 Procedure

For the spectral analysis of the boreholes a Terraspec Hi-Res spectrometer was used. This device measures wavelengths from 350nm to 2500nm. The samples selected for the spectral analysis using the Terraspec Hi-Res are first left to dry for two days. The rock samples are then thoroughly

scratched to remove any oxidation on the surface and dirt. Although the risk of having drilling mud is minimal because the measurements are taken on the split surface, any residue will be removed during the scratching process. The split surface was chosen because it ensures no outside light source can enter the probe. The curvature of the outside surface of the borehole is not suitable because gaps remain between the rock surface and the probe. Drilling mud residues are also more likely to be present on the round surface.

To avoid side effects caused by moisture in the air the measurements are taken in the afternoon. At this time of the day the risk of morning dew, which is an important factor in tropical environment, is minimized. The water absorption feature not related to the rock characteristics is therefore also minimized.

The spectral device is switched on an hour in advance to heat up before taking the first white balance reference. Because the device continues to heat up after one hour it is recalibrated on regular intervals of 15 minutes during the first two hours. After two hours the calibration was performed every half hour. The integration time for each measurement has been fixed at ten seconds to optimize the spectra quality.

3.5.3 Sampling

For the majority of the boreholes the spectral measurements are taken on the same samples that are analysed using the desktop XRF device. These consist of twenty centimetre long half core samples taken on an average interval of five meters. To capture changes on the scale of one borehole at a time five boreholes: KHD-508, KHD-566, KHD-583, KHD-589 and KHD-594 were selected. For these five boreholes the measurement spacing was lowered to one meter interval. Boreholes: KHD-508, KHD-566, KHD-583 contain higher gold concentrations.

3.5.4 Extra information

To relate the spectral data to the geological setting several more parameters are imported for each measurement from the pre-existing database into the “The spectral geologist 7” software (TSG7). Rock description, rock type, alteration and gold content are all extracted from the pre-existing database. The gold content is based on 1.5 meter of half core in which the spectral measurement is taken and therefore the gold content is not specific for an exact measured spot. For the rock type two different groups are recognized, namely: sedimentary rock and volcanic rock. The rock description characterizes the sample in more detail differentiating between for example, conglomerate, sandstone, greywacke, siltstone/mudstone and volcanics.

3.5.5 Tests

During the data acquisition care has been taken to avoid measuring veins and large sulphide mineral grains. This precaution is however limited by the ability to see the veins and sulphide grains. Small veinlets and finely dispersed sulphides may go unnoticed. Two sets of measurements have therefore been taken to test the influence of measurement location on a sample and the effect of scratching. The goal is to discover if rock which looks homogeneous will yield the same results if measured on different locations and if removing the surface oxidation by scratching changes the results. For this, ten measurements are taken on different locations on the same sample before scratching the sample (Figure 3-5). After scratching the sample 10 measurements are taken on the same location. By

separating the measurements before and after scratching the effect of location on the sample can be analysed. By combining both sets of data before and after scratching the effect of removing the surface layer of the sample will be quantified (Figure 3-6). The red interval in Figure 3-5 has not been measured because it contains a large pyrite which was large enough to be detected with the naked eye.

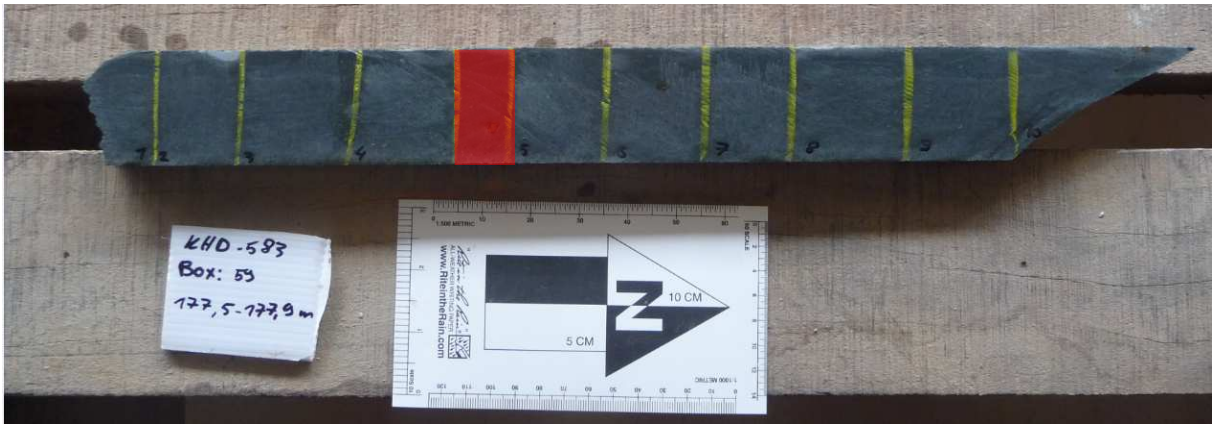

Figure 3-5, one sample divided into 10 intervals to test the spectral measurements. Note that the interval between four and five (marked in red) is not included due to the presence of a pyrite grain.

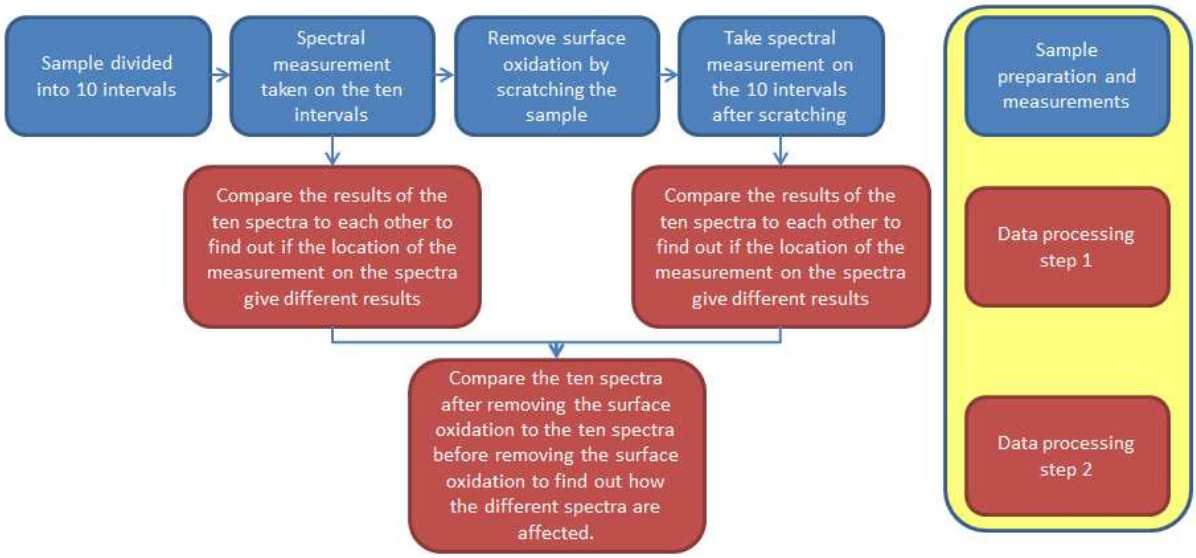

Figure 3-6, Systematic of testing the effect of varying spectral measurement location on a rock sample.

3.6 Partial least squares regression

3.6.1 Introduction

Partial least squares regression (PLSR) will be used to analyse both the spectral data as the multi-element data. "Partial least squares regression (PLSR) is a technique that can be used to predict or analyse a set of dependent variables from a set of independent variables or predictors" (Abdi, 2007).

The principles of this technique will shortly be discussed below with the use of Figure 3-7. For more information the reader is referred to (Abdi, 2007). The simulations were produced using the SIMPLS script in Matlab software.

3.6.2 Procedure

The general equation describing PLSR is shown here under (Equation 1).

$$\hat{y} = \beta_0 + \beta_p x_p$$

Equation 1, General equation for PLSR simulation.

$\hat{y}$= the prediction of variable y.

$x_p = (x_1, x_2, x_3, ..., x_p)$ is a row vector with p measured variables.

β_0 and β_p are the calibration coefficients.

The entire procedure can be subdivided into four general steps:

Step 1, consists of dividing the dataset in two parts. One part is used to determine β_0 and β_p while the second part will be used to cross validate β_0 and β_p. The subdivision is random for every simulation however the size of each subset is fixed to 2/3 of the data points to be used to determine β_0 and β_p and 1/3 for the cross validation step.

Step 2, involves the determination of calibration factors β_0 and β_p.

Step 3, tests the consistency of β_0 and β_p. β_0 and β_p are applied on the same dataset x1 and y1 with which they have been determined. This is performed by plotting the R^2 values of y and $\hat{y}$ against the number of components used to calculate $\hat{y}$. A high correlation factor R^2 between $\hat{y}1$ and y1 means that β_0 and β_p are indeed accurate and consistent for the data set from which they have been determined.

Step 4, is aimed at testing β_0 and β_p against new data. The cross validation step involves subset 2 consisting of y2 and x2. A high R^2 means that β_0 and β_p are valid for other data points as well and therefore the calibration factors can be applied to new data.

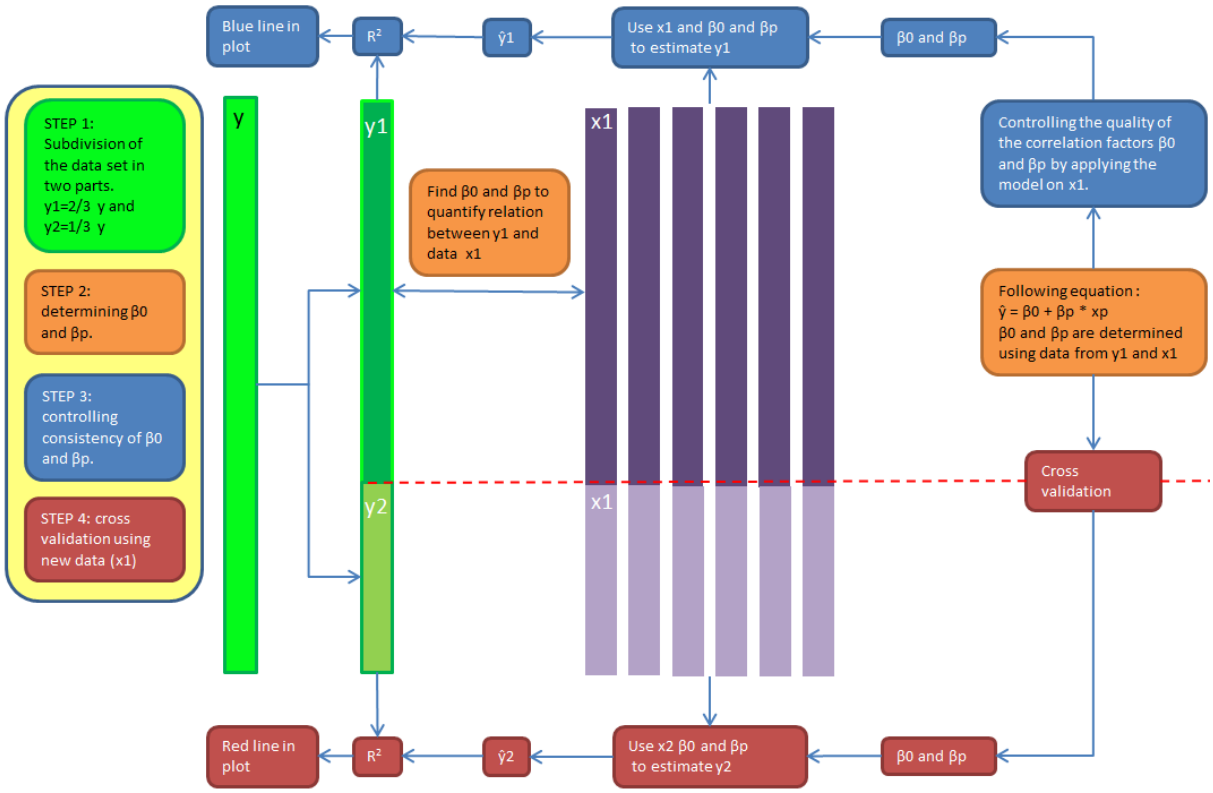

Figure 3-7, Schematic representation of the PLSR procedure.

The quality of the PLSR procedure will depend on the range of the data as well as the size of the data set. Because the technique is based on variation, enough variation in dataset y and x must be present. Furthermore although R^2 is used to quantify correlation the trends of both the consistency test as the cross validation test must be examined. In an ideal case both lines representing the R^2 as function of the number of elements follow the same trend indicating that β_0 and β_p behave the same for y1 & x1 as for y2 & x2.

PLSR will be performed on the spectral data and multi-element dataset.

3.6.3 Spectral data

In the case of spectral data noise will play an important role in the PLSR simulation. Spectra with a high noise to signal ratio may negatively influence the results. The derivative is determined over a span of four nm. Although the derivative will not represent the same as the reflectance it can still be used because changes in reflectance will be represented as a specific derivative value. Only samples derived from fresh rock are used.

As shown in Figure 3-8 the PLSR simulations are performed on three data sets. All the fresh rock samples, sedimentary samples only and at last volcanic samples only.

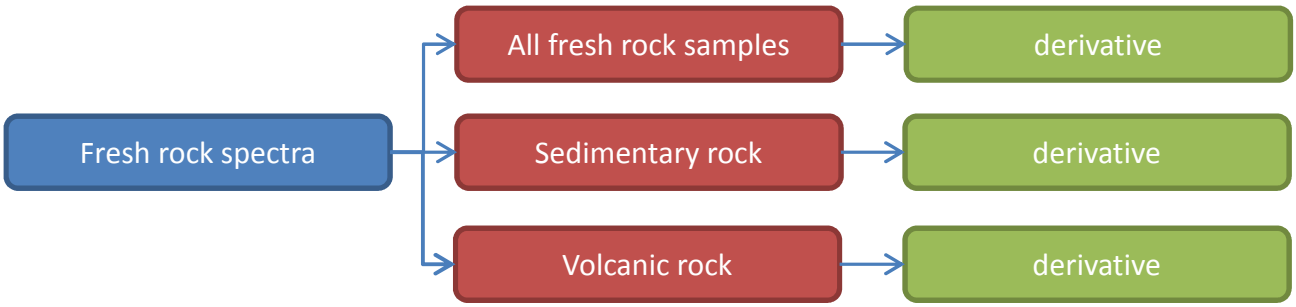

Figure 3-8, Subdivision of the data sets used for the PLSR simulation with spectral data.

3.6.4 Multi-element data

For the multi-element analysis the best data set in the sense of size will be the dataset acquired with the portable XRF unit. Figure 34 shows the subdivision of data sets used for the PLSR simulations.

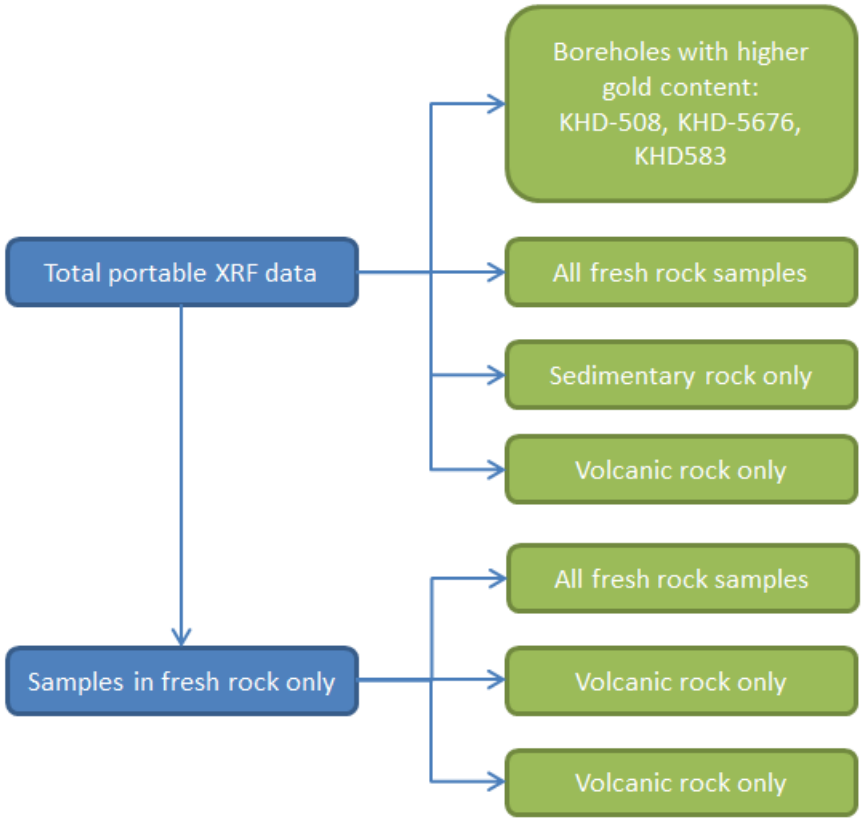

Figure 3-9, subdivision of data sets used for the PLSR simulation with multi-element data.

4 Data processing

4.1 Spectral data

The spectra are imported in The Spectral Geologist 7 (TSG7) software for interpretation and further processing.

A total of 1573 spectra have been gathered and imported into TSG7 software to be analysed. The Spectral Assistant (TSA) is used to interpret the spectra. To ensure that the interpretation of the spectra is reliable, spectra at regular intervals were controlled by interpreting these separately. For this the hull quotient corrections is applied prior to interpretation. Furthermore automatic feature extraction was applied to all spectra. All the features were extracted after the hull quotient correction was applied except for the mean values at 1350 nm and 1650 nm (Table 4-1, Table 4-2 and Table 4-3). For further reading on feature extraction the reader is referred to.

Wavelength of deepest absorption for features:	Range (nm)	Indicative for
AlOH	2180-2228	White mica composition
FeOH	2240-2270	Chlorite composition
MgOH-CO_3	2300-2370	Carbonate composition
Non specific	2180-2370	Dominant mineral group

Table 4-1, subdivision of data sets used for the PLSR simulation with multi-element data.

Relative absorption depth for features:	range
AlOH	2180-2228
H2O	1880-1940
MG-OH Ca	2300-2370
Deepest feature between 1180-2370nm	2180-2370

Table 4-2, Elements for which the relative depth of absorption is measured. These values are important to determine relative proportions of minerals.

Mean value at	Used for
2164 nm	Kaolinite crystallinity
2180 nm	Kaolinite crystallinity
1350 nm reflectance	Fe^{2+} slope
1650 nm reflectance	Fe^{2+} slope

Table 4-3, Mean values measured at several specific wavelengths. These are used to calculate the kaolinite crystallinity and the Fe^{2+} slope.

Some of these values directly indicate mineral characteristics. For example the wavelength position of the AlOH absorption differentiates between the different types of white mica's (Table 4-1). Other parameters can be calculated by combining the above values. The following procedure was used.

- Dominant mineral group is defined by determining the wavelength position of the deepest absorption feature between 1180 and 2370 nm.
- White mica composition directly depends on the wavelength position of the AlOH absorption.
- White mica crystallinity: Depth ALOH absorption / depth of water absorption. Values < 1 mean that het white mica is of low crystallinity. Values > 1 mean that the white mica is of moderate to high crystallinity.
- White mica: chlorite and/or carbonate relative proportion: Depth ALOH/ depth MgOH-Ca absorption.
- Relative proportion of smectite: Depth water/depth of deepest absorption feature between 2150 and 2370. Values < 1 imply that smectite is subordinate. Values > 1 imply that smectite is more dominant
- Kaolinite crystallinity: Mean value at 2180nm / mean value at 2164 nm.
- Chlorite composition: depends on wavelength of absorption of the FeOH feature.
- Carbonate composition: depends on the wavelength of absorption of the MgOH-CO_3 feature.
- Fe2+ slope: Mean value at 1650/ mean value at 1350. Both measured in reflectance spectrum.

Whenever the term relative is used in the results of spectral data a parameter of a rock sample is compared to the same parameter of another rock sample(s) in the same data set. Values obtained from the spectral analysis do not always fit pre-determined ranges and are therefore only useful when compared to other values in the same dataset.

The data is displayed in TSG7 in the form of scatterplots and histograms. Using this method up to 3 parameters can be plotted to try and find trends irrespective of the position of the measurement.

If the result indicates that halo's may be present in and/or around the gold deposit the data will also be displayed in three dimensions using Surpac 6.1 software. This will relate the data spatially compared to the local geology.

In the case of the partial least squares regression all spectra were first imported into ViewSpecPro 6.0 software to obtain the first derivative. The first derivative values were then imported into Matlab software to perform the actual regression.

4.2 Multi-element data

4.2.1 Laboratory data

ioGAS software was used to treat the multi-element data. Harker plots were made to display and interpret the data acquired with the fusion XRF method.

4.2.2 Portable XRF data

The first step of the processing stage is the validation of the acquired data. The next three steps have been performed using Microsoft Excel software.

- For the data acquired with the portable XRF unit the standard deviation calculated for the tests mentioned in paragraph 3.4.4. Elements with a standard deviation smaller than 5% of the average measured element content will be accepted.
- Whenever the average concentration of a specific element in the plastic bags exceeds the average concentration of the same element over the entire data set of samples the element will be discarded.
- The dataset from the portable XRF data is plotted versus the data acquired by the ALS laboratory in Peru to cross validate the results. Values resulting in a correlation factor R^2 below 0.9 will not be used.

According to these tests the elements will be evaluated and used in partial least squares regression in Matlab and plotted downhole using ioGas software.

5 Results

5.1 Petrographic analysis

5.1.1 Overview

The first part of the petrographic analysis is based on field observations made during the sampling process. Secondly the thin sections are partially used to as a reference for the results obtained with the multi-element analysis and the VNIR spectral analysis. The element content of the different lithologies may directly be related to the presence of specific minerals recognised in the thin sections. Secondly, the VNIR spectral analysis detects minerals with Al-OH, Mg-OH and Fe-OH bonds that are active in the SWIR range while more minerals are likely to be present. Using the results from the petrographic study will also enable to define to define if specific mineral responses in the VNIR analysis are being overshadowed by other minerals. Besides characterizing the lithologies the focus of the petrographic analysis was the study of veins. The characterization of veins deserves attention because this is where the gold is concentrated. Textures from both the host rock and the veins may give clues concerning the timing of veining, gold deposition and or pressure regime. Pictures of the rock samples used for thin section analysis together with their location can be found in Appendix B. Although all thin sections have been analysed and described the results presented in this chapter consist of a concise summary of the most striking features only.

5.1.2 Field observations

The field observations made during the sampling process are simple yet valuable to understand the geological evolution of the Koolhoven pit and put the thin sections in a geological context. The volcanics in the South are overlain by an interval of siltstone/mudstone which shows clear turbidite textures (Figure 5-1). In the North conglomerate is found (Figure 5-4) which suggests a shallowing of the depositional environment. A gradual change from siltstone/mudstone to conglomerates in the North can be evaluated as well. From South to North the lithologies evolve from siltstone/mudstone (Figure 5-1) to fine grained greywacke with a high content of matrix material (Figure 5-2). More towards the north the greywacke contain coarser clasts (Figure 5-3). The transition from this greywacke to conglomerate is also gradual. The clast size increases up to the size of pebbles and the greywacke is interbedded by conglomeratic lenses. This gradual transition leads to the massive conglomerate layers that are found in the North (Figure 5-4).

The quartz and carbonate can be recognized in the veins. The vein selvages show bleaching on occasions and sulfide prophyrblasts.

Figure 5-1, Siltstone/mudstone interval. Sample LC063, KHD-611, 138 m.

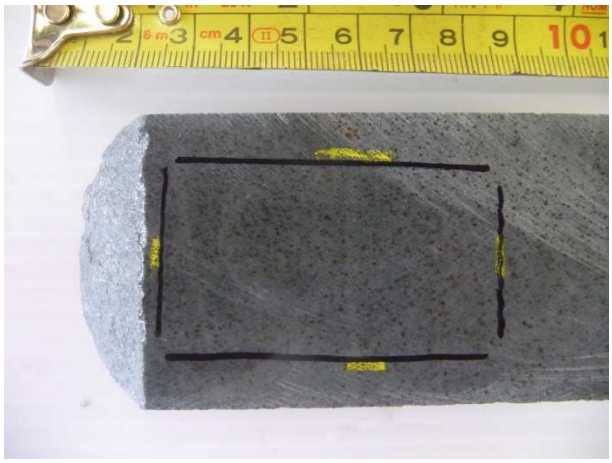

Figure 5-2, Fine greywacke close to the siltstone/mudstone interval. Sample LC066, KHD-573, 138m.

Figure 5-3, Coarse greywacke close to the conglomerate interval. Sample LC035, KHD-524, 128 m.

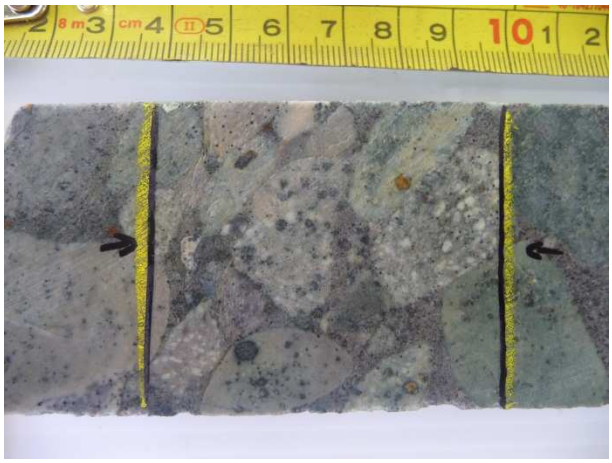

Figure 5-4, Conglomerate rock in the North of the Koolhoven pit. Sample LC281, KHD-501, 125 m.

Besides recognising different lithologies and gradual changes several alteration characteristics were observed. Bleached zones around veins were found together with high concentrations and larger grains of pyrite and chalcopyrite close to the veins. Carbonate spots (Figure 5-5) were also observed. Sericitization close to veins occurred, often related to shear zones.

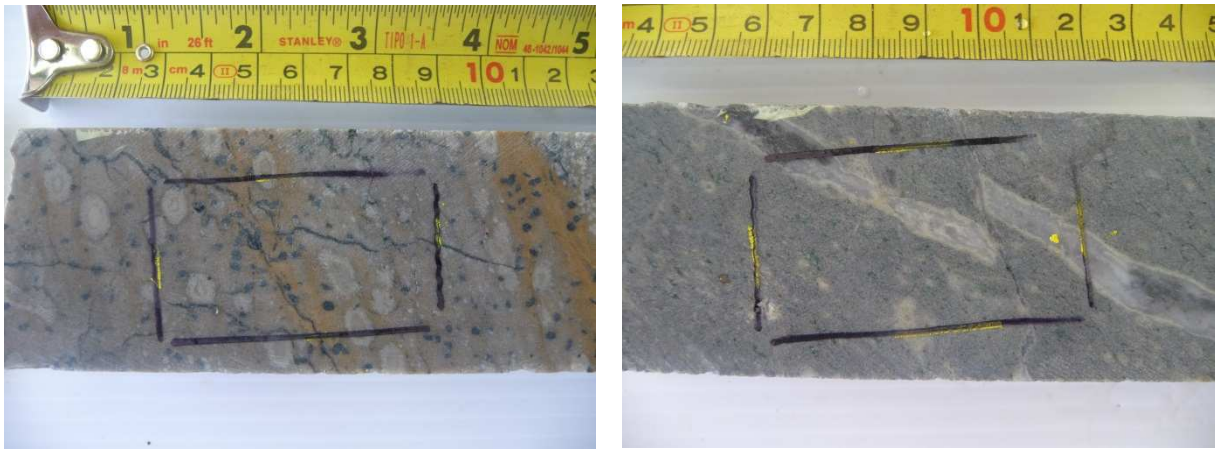

Figure 5-5, Carbonate spots. On the left sample LC133, KHD-534, 128 m. On the right sample LC131, KHD-534, 155 m.

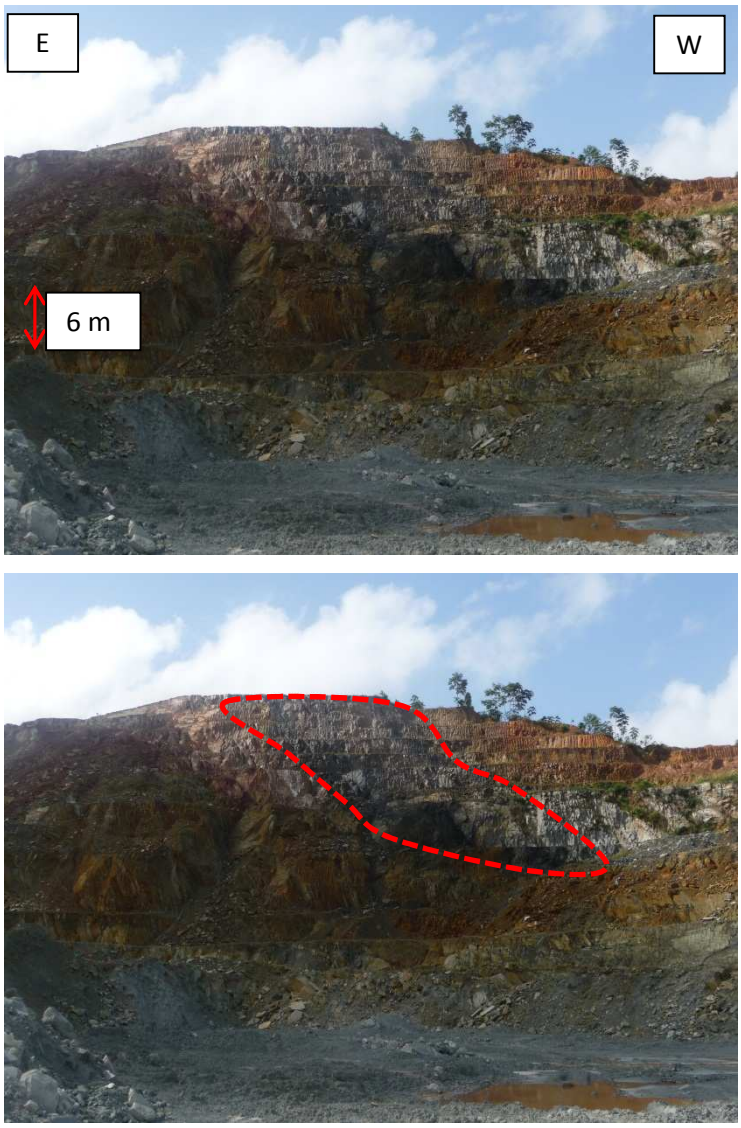

Figure 5-6, Exposure of a graphite layer on the South wall in the East of the pit.

At last an important observation made in the pit is the presence of a graphite layer parallel to the shear zones. The graphite layer is exposed in on the South side of the pit in the East (Figure 5-6). Graphite is known as a reducing agent that leads to the precipitation of gold from solution by altering the aqueous complex carrying gold.

5.1.3 Thin sections

5.1.3.1 Host rock

5.1.3.1.1 Host rock mineralogy

The minerals observed in the thin sections include: quartz, carbonate (calcite, dolomite), white mica, chlorite, pyrite, chalcopyrite, magnetite, hematite, rutile, clay minerals and feldspar including plagioclase.

The feldspars are restricted to thin sections LC002 and LC089 of the volcanic rocks, and are present in the form of phenocrysts evenly distributed throughout the matrix.

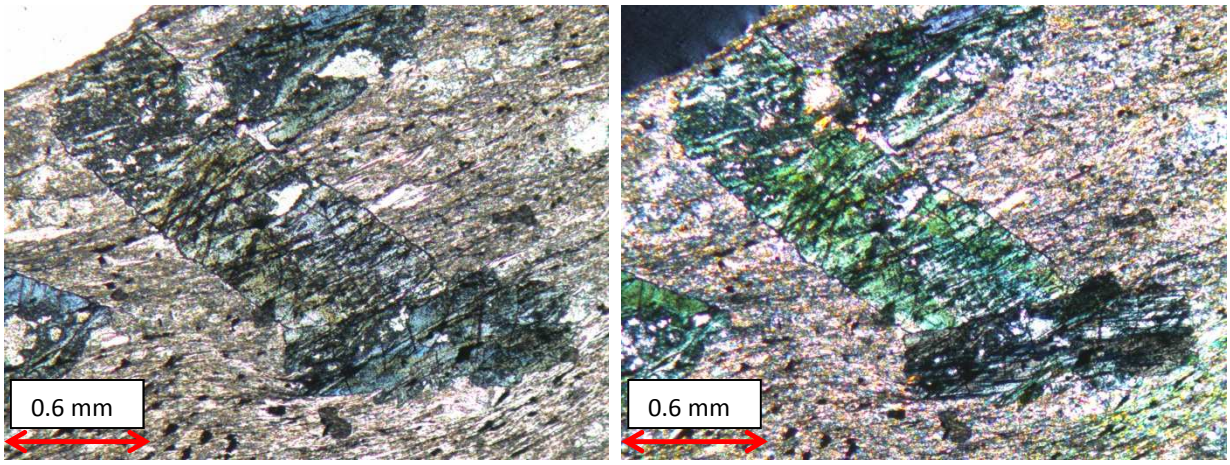

Figure 5-7, LC002 (KHD-599, 79 m). Transmitted light with parallel polars (left) and crossed polars (right).

Plagioclase is found in conglomerate in boreholes KHD-532 and KHD-501.

In the thin sections White mica is present in the form of sericite. The sericite either forms thin bands as part of the foliation (Figure 5-13) or represents the bulk of the rock sample. An increase in sericite content near shear veins has been observed in the cores.

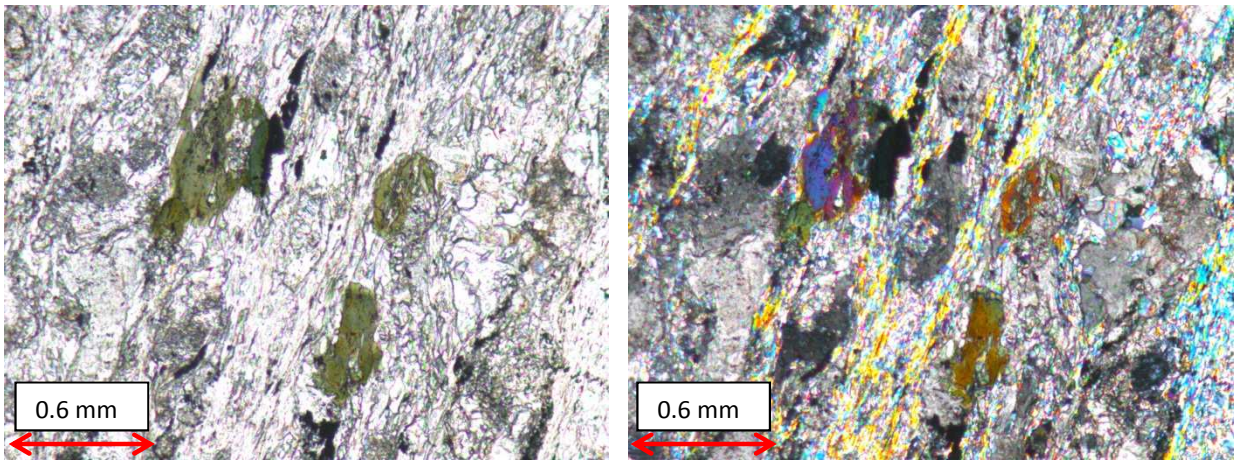

Figure 5-8, LC094 (KHD-594, 98 m). Transmitted light with parallel polars (left) and crossed polars (right).

No exact carbonate can be named, yet different types of carbonate have been identified. Diamond shaped carbonate grains suggest the presence of dolomite.

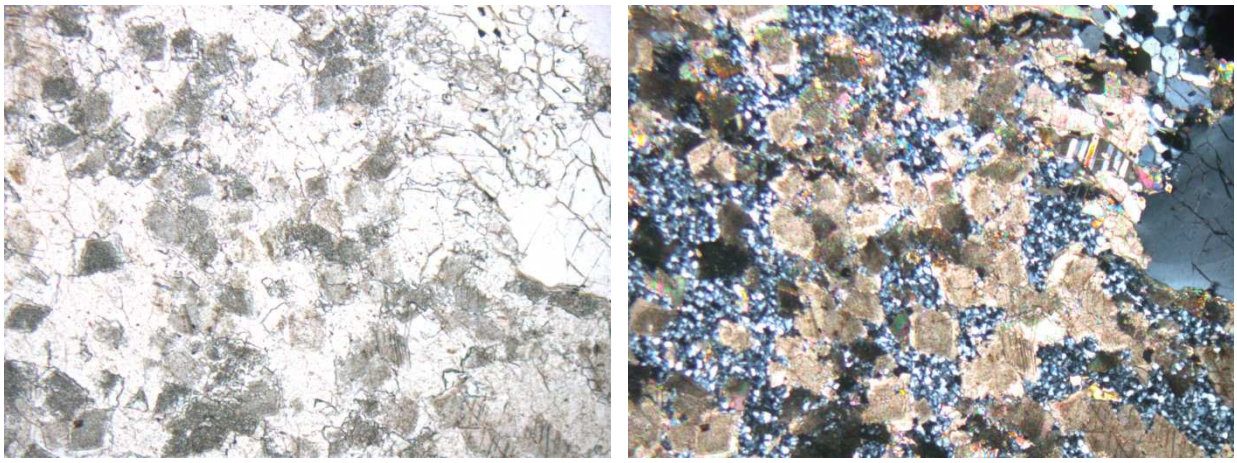

Figure 5-9, Diamond shaped carbonate grains. Transmitted light with parallel polars (left) and crossed polars (right).

Hematite is only present in the form of inclusion within magnetite. Chalcopyrite and pyrite occur both separated from each other or combined. Pyrite is the dominant mineral of the both. Chlorite is present in the form finely dispersed crystals parallel to the foliation. Rutile has been found finely distributed in very small quantities.

5.1.3.1.2 Host rock textures

A variety of textures can be observed throughout the different lithologies. From core samples several indicators of directional forces are found throughout the thin sections. Schistosity is recognized by crystal orientation.

Pressure shadows around more rigid minerals (pyrite and quartz) have been identified. Multiple recrystallization stages including different minerals are recognized in the case of thin section LC705 #1 (Figure 5-10 & Figure 5-11). Two stages of carbonate recrystallization (indicated in yellow and blue) and two stages of quartz recrystallization (indicated in red and green) around a pyrite grain are shown in (Figure 5-11).

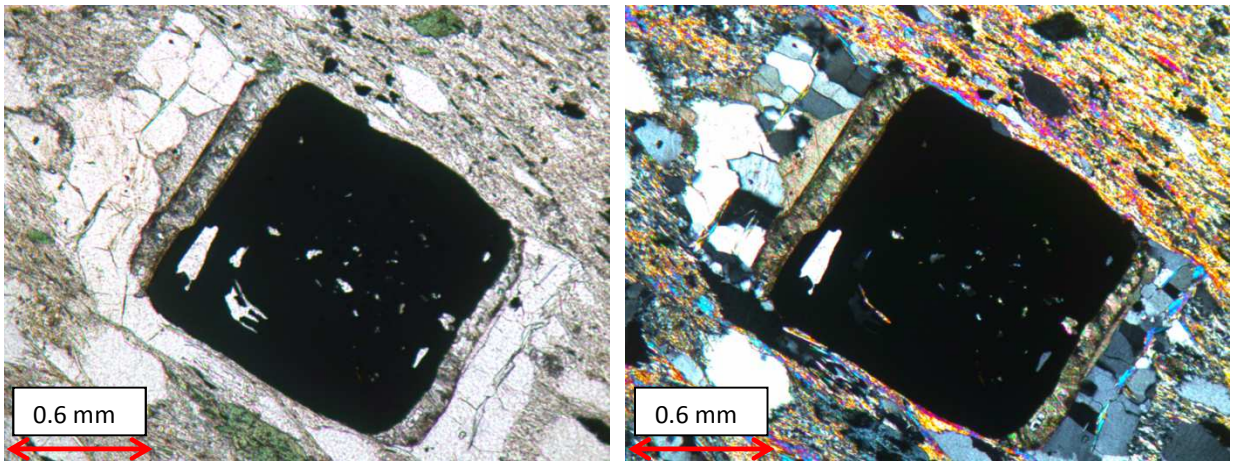

Figure 5-10, Sample LC705 # 1 (KHD-603, 128 m). Transmitted light with parallel polars (left) and crossed polars (right).

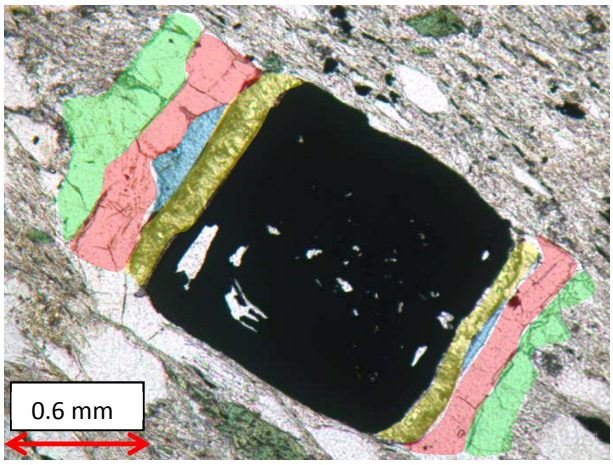

Figure 5-11, Four symmetric recrystallization stages around a pyrite grain, Sample LC705 # 1 (KHD-603, 128 m). Transmitted light with parallel polars.

Figure 5-12 shows pressure shadows around quartz grains. The quartz grain also displays different extinctions which also suggest that it has been subjected to pressure and mechanically deformed.

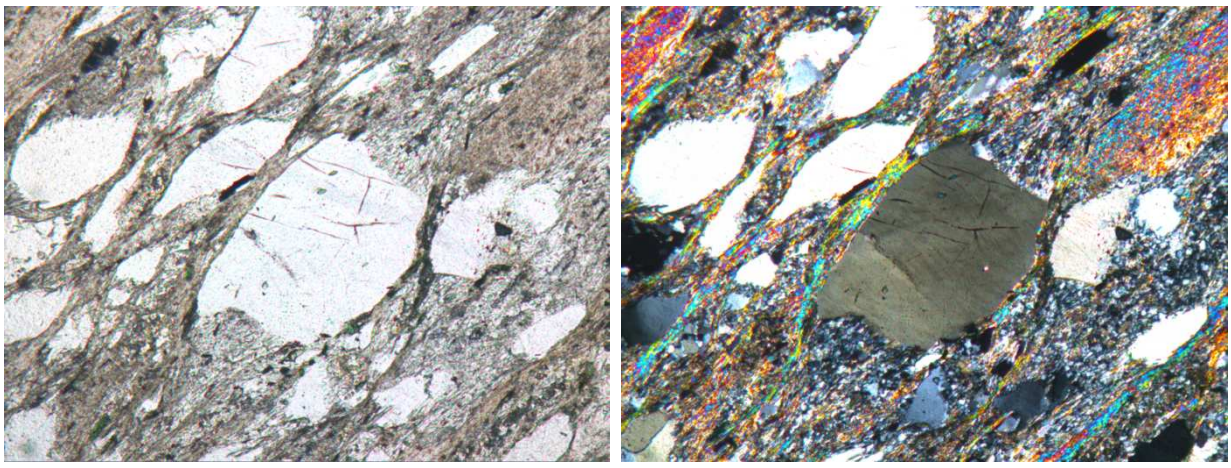

Figure 5-12, Pressure shadow on both sides of a quartz grain, sample LC705 #1 (KHD-603,128). Transmitted light with parallel polars (left) and crossed polars (right).

5.1.3.2 Veins

5.1.3.2.1 Mineralogy

Mineralogy in the veins is dominated by quartz and carbonate and to a lesser extent by chlorite. Accessory minerals that have been identified in the veins are tourmaline and white mica. This is in accordance with Dubé & Gosselin (2007). See chapter 2. Mixing of these minerals through the vein occurs with quartz always as the major mineral followed by carbonate and chlorite.

5.1.3.2.2 Vein types

Tension veins, shear veins and veinlets/fissures occur throughout the deposit. Tension veins have been recognized by their lack of deformation and displacement, sharp boundaries between vein and host rock and internal "comb" texture when present. Tension veins often display a repeating suite of minerals. In the presence of unmixed[1] quartz and carbonate the carbonate concentrates on the sides

[1] "unmixed" in relation to mineralogy in veins refers to to a systematic succession of bands of specific minenrals parallel to the vein sides.

of the vein while the quartz occupies the centre of the vein (Figure 5-13). When chlorite is present in the vein together with carbonate and quartz the succession from the sides of the vein to the centre is: chlorite, carbonate, quartz (Figure 5-18). This is only valid if the minerals are present in layers (Figure 5-18).

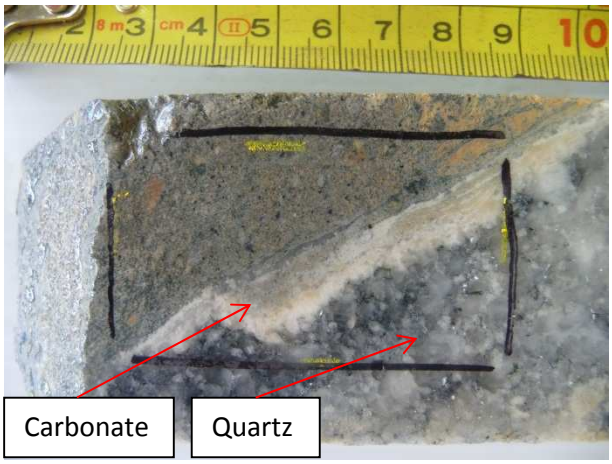

Figure 5-13, Separation of quartz and carbonate in a vein. Sample LC427 (KHD-605, 171.3 m).

Shear veins display major deformation and no clear boundary between vein and host rock. They may occur in the form of shear zones in which the host rock has been entirely deformed. The larger shear veins are generally associated with sericite (Figure 5-14).

Figure 5-14, Shear vein interval, sample LC701 (KHD-544, 160m).

5.1.3.2.3 Timing of veins

Timing is not the same for all veins. Several indicators for timing differences have been recognised throughout the thin sections. Timing is relative to: other veins, deformation, and mineral crystallization.

Intersections of veins: this is the easiest indicator of timing and gives a relative timing between two different veins. Figure 5-15 shows several intersections. The intersections between veins are sharp. Displacement may also occur (sample LC131 Figure 5-15).

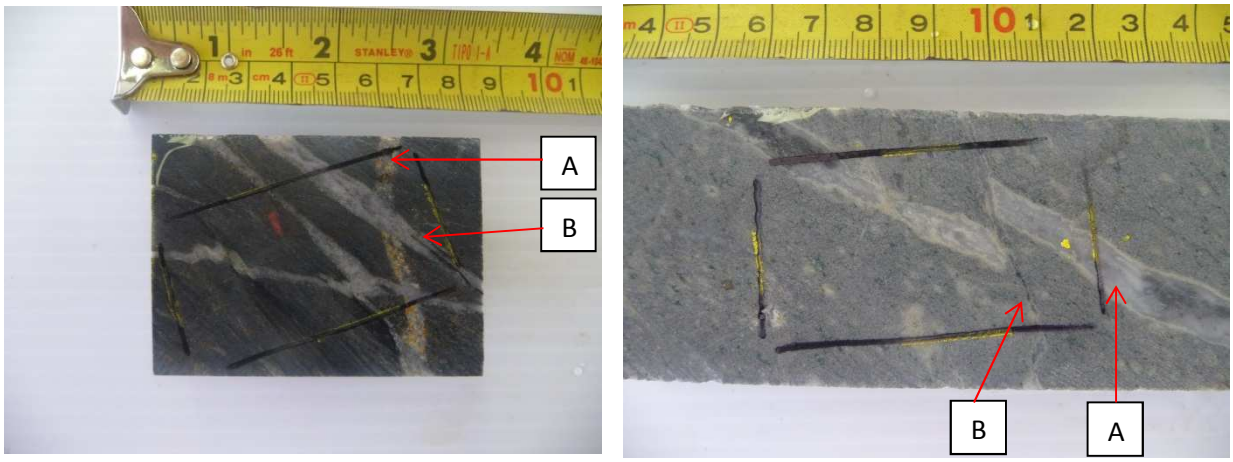

Figure 5-15, left: LC299 intersection of several veins (KHD-544, 112.4 m). Right: LC131 vein intersection with displacement (intermediate volcanic, KHD-534, 155 m).

Vein deformation indicates that the vein has been subjected to directional forces. If we assume that these forces were applied to the entire deposit the deformed veins must have been created before the non-deformed veins. This is valid under the assumption that the host rock behaves the same. In the Koolhoven different grades of deformation are found. While Figure 5-16 shows clear deformation of a vein. Thin sections LC705 #1 and #2 both show no apparent deformation however the internal orientation of the quartz grain is parallel to the foliation indicating it has been affected by directional pressure as well. The overall deformation of veins throughout the Koolhoven pit is minor. Also on pit scale the tension veins show minor deformation indicating that the veining happened after the major deformation phase.

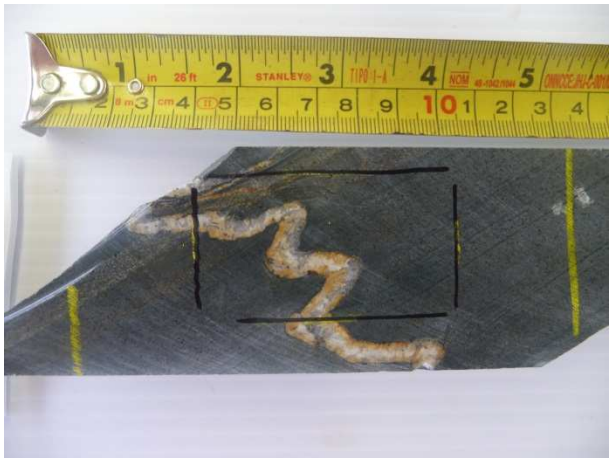

Figure 5-16, LC084 (KHD-562, 74.5 m).

The bleached area in thin sections LC705 #1 and #2 (Figure 5-17) also gives an indication of the relative timing of both veins. Two veins parallel to each other and with the same textures are present in the sample. In thin section LC705 #2 however the host rock on both sides shows differences in colour. The description suggests that the vein in thin section #2 was created and mainly crystalized before the bleaching around the vein in thin section #1 took place. The vein in thin section #2 would hereby have worked as a barrier for bleaching.

Figure 5-17, left: LC705 #1 & #2 displaying two parallel tension veins and a clear bleaching zone (KHD-603, 128.5m). Right: LC096 display of a light colour bleached zone (KHD-594, 120.8m).

Textures: the internal crystal texture of veins also give an indication of directional pressure regimes. Crystal orientation parallel to the foliation grain boundary recrystallization and cracking of large crystals all three indicate that the sample has been subjected to directional pressure.

5.1.3.2.4 Bleached zone

The bleached zone in the case of thin section LC096 (Figure 5-17) is characterized by a decrease in chlorite compared to the non-bleached zone. Furthermore pyrite is present in the bleached zone and not outside. The bleaching process would hereby have removed the chlorite and brought sulfides together with carbonates. The presence of sulfides in combination of specific minerals only has also been recognised in other thin sections such as in thin section LC084 (Figure 5-18). In thin section LC084 both pyrite and chalcopyrite are present in the carbonate but outside. In the non-bleached zone magnetite is present.

In the case of thin sections LC705 #1 & #2 (Figure 5-17) the difference in coloration is the same as in thin section LC096. A decrease in chlorite in the bleached zone gives it a lighter colour. Again the pyrite is also concentrated in the bleached zone. The vein separating both zones is suggested to have been formed before the bleaching took place and hence functioned as a barrier (paragraph 5.1.3.2.3).

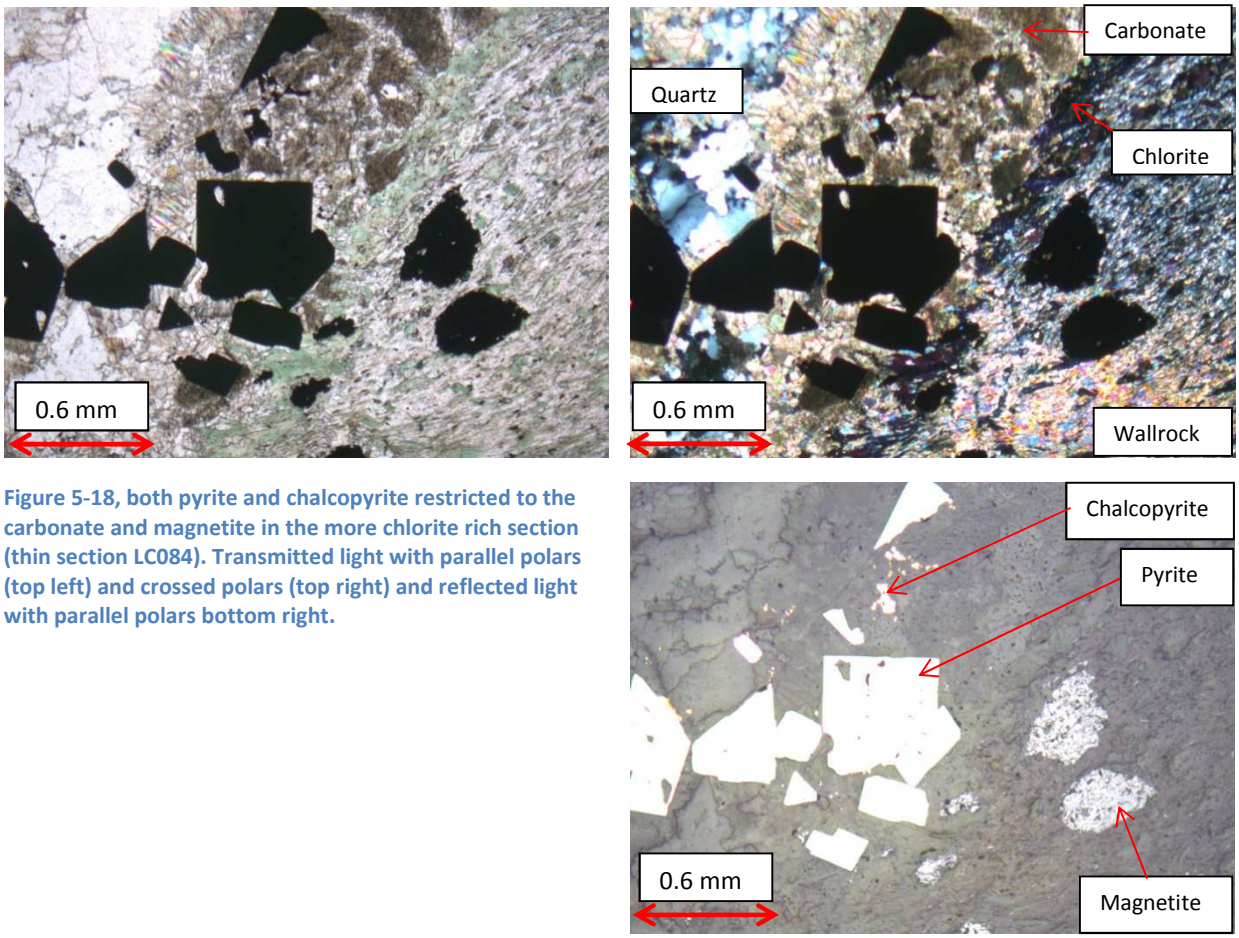

Figure 5-18, both pyrite and chalcopyrite restricted to the carbonate and magnetite in the more chlorite rich section (thin section LC084). Transmitted light with parallel polars (top left) and crossed polars (top right) and reflected light with parallel polars bottom right.

5.1.3.2.5 Relative vein orientation

From the thin sections the vein orientation can only be defined relative to each other. The first indication of varying orientation is the fact that veins form intersections. Intersections occur between both types of vein (shear and tension) and also within the same type of veins. Both shear veins and tension veins group to form sets yet in different ways. On the mine scale three different shear zones were observed parallel to each other (Figure 5-19). These are in reality numerous shear veins with the same orientation in the Koolhoven deposit. They concentrate in three locations, thereby forming sets. In between these shear zones, shear veins are not as frequent. These three minor shear zones are parallel to each other and to the major shear zone to the South. The same spread of shear vein is also visible on the microscopic scale. Thin sections being small they generally only include one part of a larger shear vein (Figure 5-14) or only one single shear veinlet.

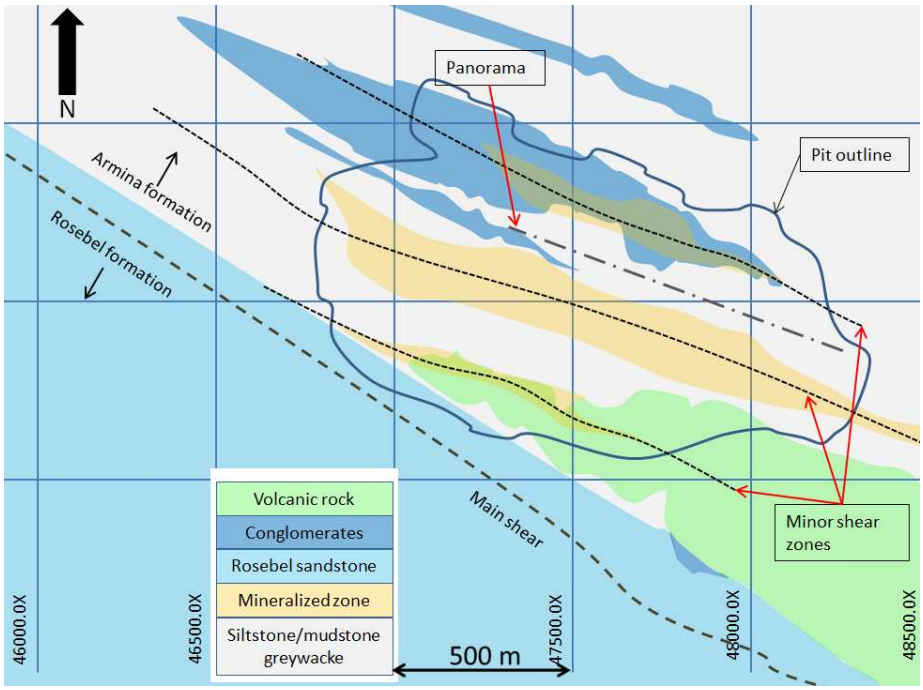

Figure 5-19, Systematic map of the Koolhoven deposit displaying the minor shear zones parallel to the main shear. The panorama location of Figure 5-21.

In contrast to shear veins, tension veins display evenly distributed sets. This is recognizable on the mine scale (Figure 5-21) as well as on the borehole and microscopic scale (Figure 5-20). Although tension veins are not as thick as shear veins the higher frequency with which they occur means they are important in volume. No distinction could be made between the two sets of tension veins mentioned in chapter 2.

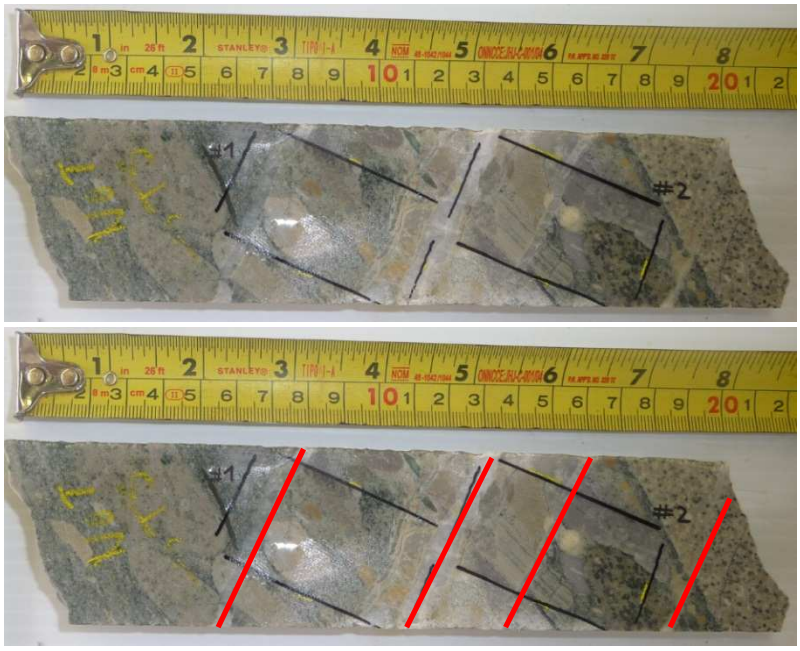

Figure 5-20, Parallel tension vein in sample LC040, (KHD-532, 150 m).

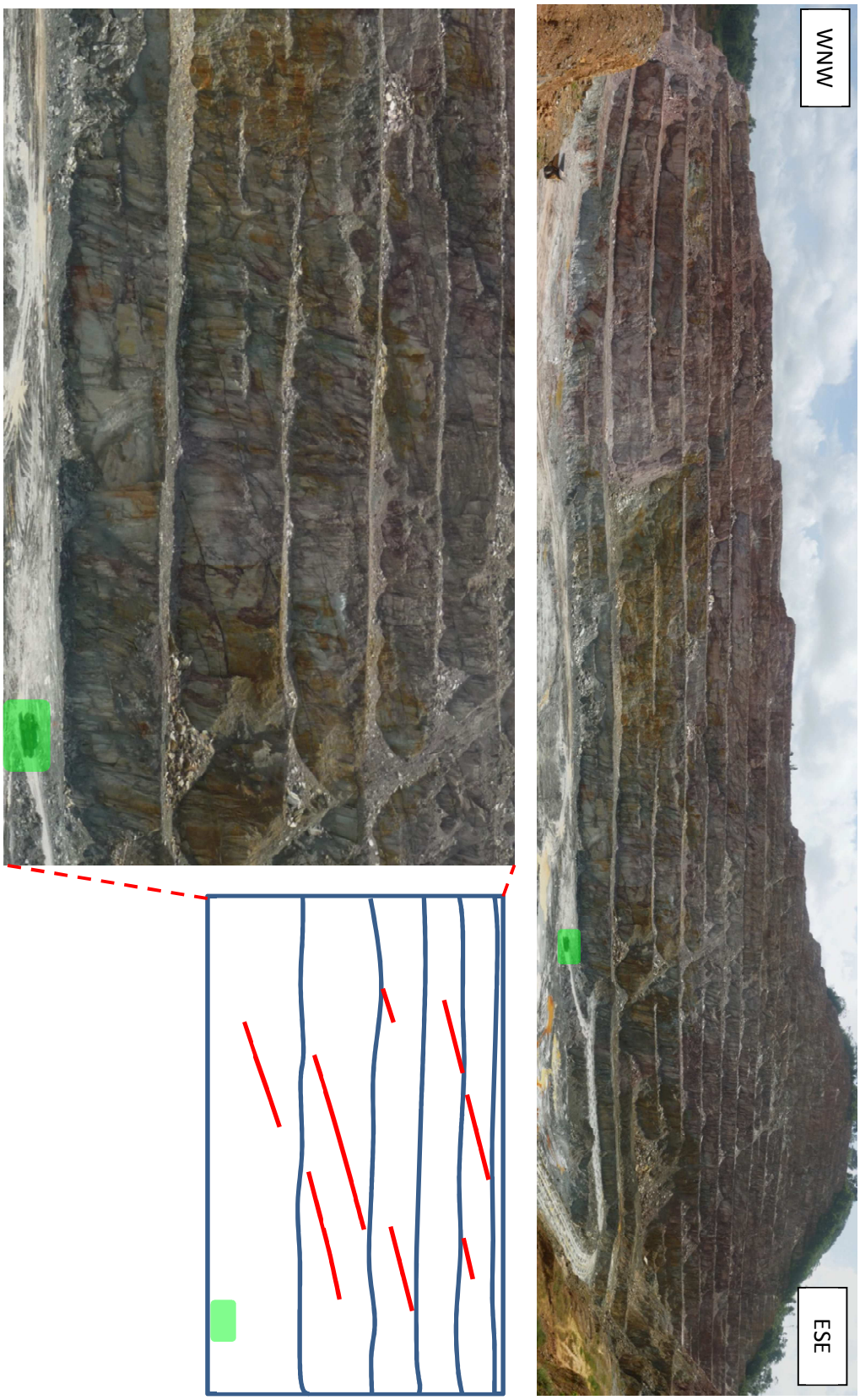

Figure 5-21, Panorama view of the Koolhoven pit showing the parallel tension veins. A car is highligted in green as scale the location of the panorama is found in Figure 5-19.

5.1.4 Summary

Although the polished thin section have been analysed visually and analysis may therefore vary per person, the thin sections represent a valuable data set.

Similarities between the vein textures on mine scale and microscopic scale are found. Several generations of veins have been recognized in the thin sections. Although deformation has affected some veins and recrystallization of the minerals has taken place the majority of the veins show only small indications of deformation hereby suggesting the veining is late compared to the major deformation fase.

On average throughout the thin sections carbonate is present in higher concentrations than chlorite. This characteristic will be important to take into account when analysing the VNIR results.

It is known that thin section LC705 #1 partially includes a vein with a high content of gold (visible gold was present but not intersected by the thin section). The bleached zone around this vein may be the most proximal alteration characteristic linked to the deposition of gold. The bleached zones are characterized by the presence of sulfidic minerals such as pyrite and chalcopyrite, higher content of carbonate (compared to the non-bleached rock) and absence of chlorite.

In accordance with the background presented in chapter 2, the minerals found suggest a proximal location to the gold mineralization.

5.2 Multi-element analysis

5.2.1 Overview

As can be seen in Figure 5-22 the multi-element data was obtained by using several different preparation and methods of analysis. As a first step the validation of the different data sets will be discussed. Data validation will start with the data obtained by the laboratory since this is assumed to be of quantitative quality and planned to be used as a reference for the cross validation of the portable XRF data. Next, the different processing steps originally planned to be applied to the various datasets are discussed with the aim to clarify the obtained results.

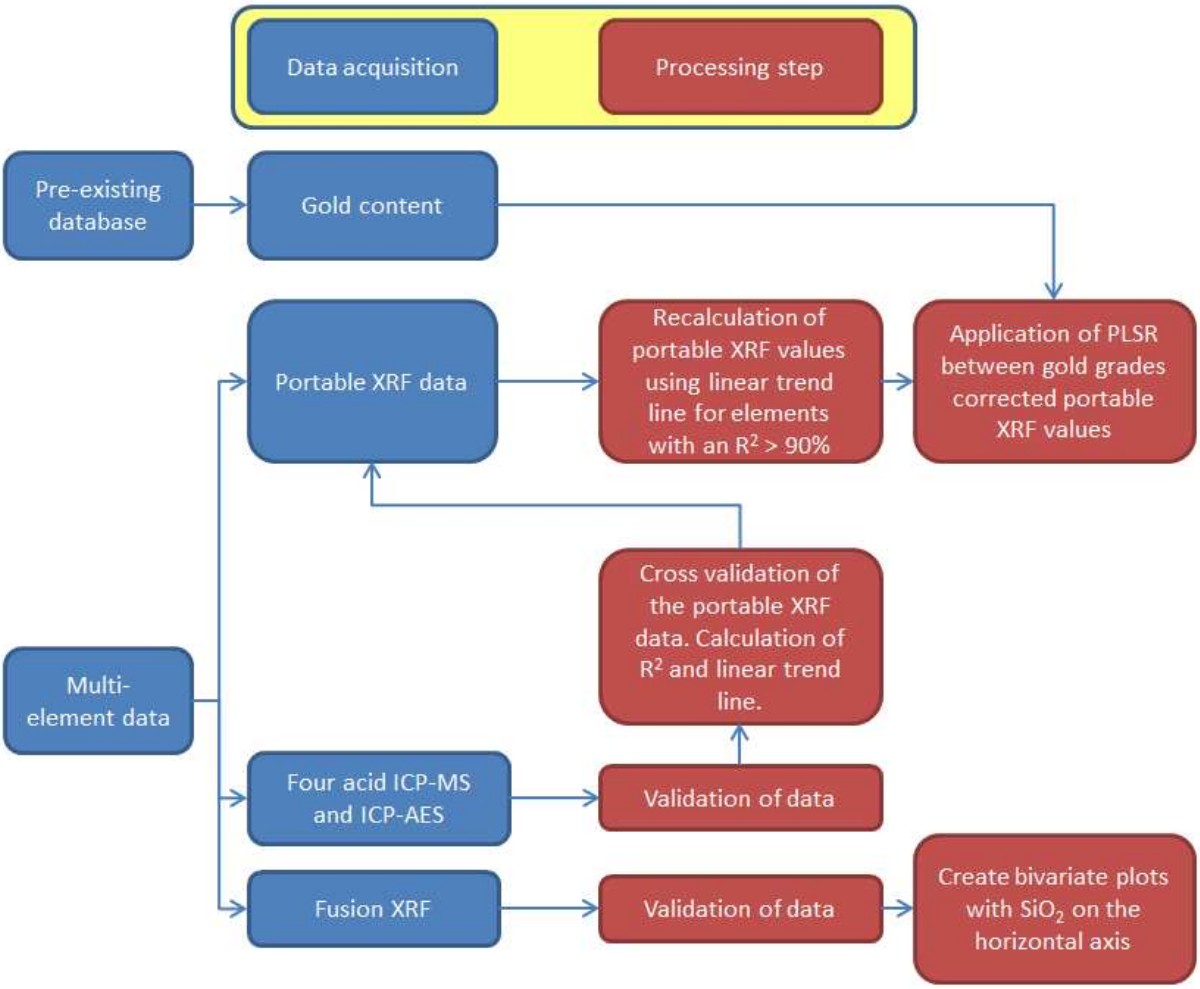

Figure 5-22, Proposed processing workflow for multi-element data.

The results for the fusion XRF and four-acids ICP-MS and OCP-AES are displayed in Appendix B. The results obtained from the X-50 Mobile XRF are displayed in Appendix C.

5.2.2 Validation of laboratory data

Validation of the laboratory data is crucial since this will be our reference for the validation of the portable XRF data. Two sets of analysis were performed by the ALS laboratory: four acids ICP-MS & ICP-AES and fusion XRF. For both these data sets the results are displayed in Appendix C together with duplicate analysis of several submitted samples, standards and blanks.

5.2.3 Lithology differentiation using major elements

5.2.3.1 Overview

In this part the major elements will be used to define compositional differences by which the different lithologies can be separated from each other. The possibility of separating lithologies on the basis of element content will:

- Give important information to understand the forming of the deposit and the geological evolution.
- Enable to control the lithological interpretation in the pre-existing database that is used in this project.
- Enable us to link the results found in the other analysis to specific lithologies based on analytically measured values instead of visual interpretation.

The element contents measured by the fusion XRF analysis where plotted against the SiO_2 values in the form of scatter plots. The specific use of SiO_2 values on the horizontal axis for scatter plots is also known as Harker plots. All data points where first separated on the basis of their interpreted lithology: volcanic, siltstone/mudstone, greywacke, sandstone and conglomerate according to the available drill logs from the pre-existing database. It is important to note that while the sedimentary rocks are separated into different groups the volcanics are grouped into one single group, namely volcanic rock, and no differentiation is made in the beginning. This has been done because of the restricted amount of data points available for volcanic rock and because according to Figure 3-4 all samples were selected from the same volcanic rock formation. Conglomerates which are only represented by three data points from borehole KHD-532 should also be treated with care since they may be subject to local anomalies and may not be representative for all conglomerates encountered in the Koolhoven pit.

First a selection of bivariate plots is made. Then the plots including both volcanic and sedimentary rocks are described. Element contents will be used to separate the lithologies from each other and also to differentiate between the different types of volcanic rock. In a second stage only the sedimentary rocks will be described. The goal is to be able to separate the lithologies on the basis of geochemistry. Except from separating the lithologies from each other the result may give information on the relationship between the different lithologies. The analysis will be based on relative differences. Whenever the terms highest or lowest are used, these relate values specific to one lithology to the values belonging to the other lithologies.

5.2.3.2 Choosing the bivariate plots to be used

Before the characterization of the different lithologies is described, the bivariate plots should be evaluated. The evaluation of the different plots will be based on:

- Absolute concentrations of the different elements. Whenever the total range of values from one specific element is small it must be questioned whether the difference is representative for the lithology.
- Expected behaviour of the different lithologies. Several characteristics are to be expected per lithology. Sandstone is expected to contain the highest SiO_2 values and yield low values for the other elements. This is assumed because particles containing other elements than SiO_2 will have been degraded during transportation because they are not as resistant to erosion and weathering as quartz grains (SiO_2).
- Mobility of the elements. Paragraph 2.3 stated that iron, magnesium and manganese are rarely mobile in quartz carbonate vein gold deposits. This will greatly depend on the local geology and conditions. It is not mentioned if this holds in tropical environment where the rainfall may be much higher.

On the basis of absolute concentrations not all elements can be classified as major elements. BaO, Cr_2O_3, MnO, P_2O_5 and SrO do not yield values above 1 w%. TiO_2 only yields three values above 1 w%. It was decided to use major-elements for the differentiation of lithologies. Depending on the other evaluations the elements who do not qualify as major elements will be used to support other findings or dismissed.

Following the assumptions listed above the behaviour of sandstone is first evaluated to control the obtained results. Sandstone indeed yields the highest values of SiO_2 which partially confirms that the interpretation from the pre-existing database is indeed correct. Sandstone also shows the minimal values for the rest of the 12 other elements. This is the case for Al_2O_3, Fe_2O_3, MgO, P_2O_5, TiO_2. The elements CaO and MnO do not strictly follow the assumptions but compared to the other lithologies sandstone still displays relatively low values. Several elements do however not follow the assumptions at all. This is the case for BaO, Cr_2O_3, K_2O, Na_2O and SrO. It is decided not to use BaO, Cr_2O_3, and SrO for the differentiation of lithologies because all three do not qualify as major-elements and do not follow the expected trend for sandstone.

The siltstone/mudstone lithology should contain less silica than the sandstone and more Al_2O_3 which is representative for clay minerals. This is clearly displayed in the Al_2O_3 vs SiO_2 plot hereby indicating that the interpretation form the pre-existing database also holds for siltstone and mudstone.

No assumption can be made on the composition of greywacke and conglomerates because these may greatly vary in composition depending on the matrix and clasts composition. It is also not possible to make assumptions on the basis of volcanic rocks because all samples were grouped together while they may be of different composition.

The Mobility of elements should be taken into account. It is however not an absolute measure since mobility of elements greatly depends on the local conditions. Considering that the Koolhoven deposit is located in rainforest environment and therefore high amounts of rain have precipitated throughout the years. This will have depleted the deposit of mobile elements.

On the basis of this primary evaluation of the results it is decided to only discard the elements BaO, Cr_2O_3, and SrO.

Figure 5-23 displays the colours used to separate the data points of different lithologies and the colours used to group them. The lithology name is in the colour of the data points. The box colours represent the colour which has been used to group the data points. Greywacke A together with siltstone/mudstone are grouped together for reasons explained below. All the Harker plots are displayed together in the Appendix: Figure 10-11 to Figure 10-23.

Figure 5-23, Legenda for the Harker plots.

5.2.3.3 Volcanic & sedimentary rock

On the basis of SiO_2 content three different ranges can be recognized each containing specific lithologies (Figure 5-24).

The volcanic rocks display the largest range of SiO_2 values from LC074 43.8% to LC099 74.6%. Out of the 16 data points for volcanics 10 however represent the lowest SiO_2 values. Although this does not show a clear distinction from the rest of the lithologies it must be reminded that the volcanics have not been separated into subgroups yet. The sandstones represent the higher SiO_2 values LC017: 66.5% SiO_2 to LC059: 79.2 % SiO_2. The range from LC042 53% to LC034 67.1% SiO_2 contains data points of all lithologies yet the bulk consists of siltstone/mudstone, greywacke and conglomerate (Figure 5-24).

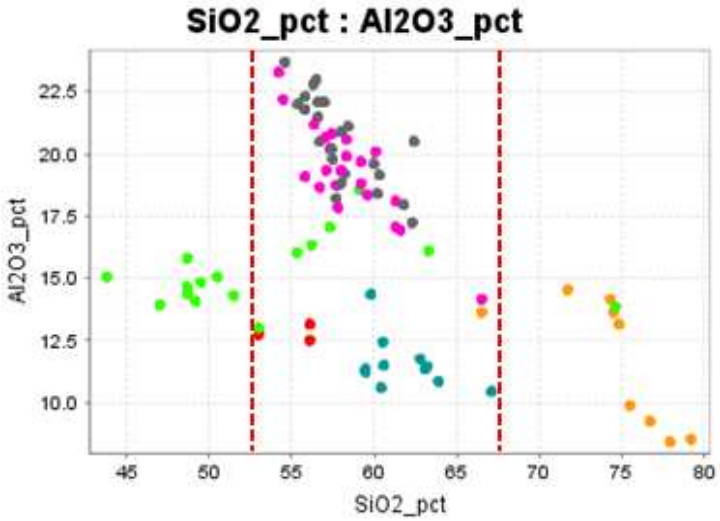

Figure 5-24, Subdivision of The SiO_2 range.

Lithology	Lower boundary % SiO_2	Upper boundary % SiO_2
Volcanic	43.8	74.6
Siltstone/mudstone	54.6	62.4
Greywacke	54.2	67.1
Sandstone	66.5	79.2
conglomerate	53.0	56.1

Table 5-1, SiO_2 ranges for the different lithologies.

The bulk of the volcanic rocks tend to have a low content of SiO_2 yet this is not a conclusive distinction from the rest of the lithologies. Three other major elements can be used to separate the volcanic rocks from the sedimentary rocks. CaO and MgO are to be considered as most appropriate (Figure 5-25). In both cases the volcanic rock show higher values compared to the sedimentary rock with the exception of conglomerates.

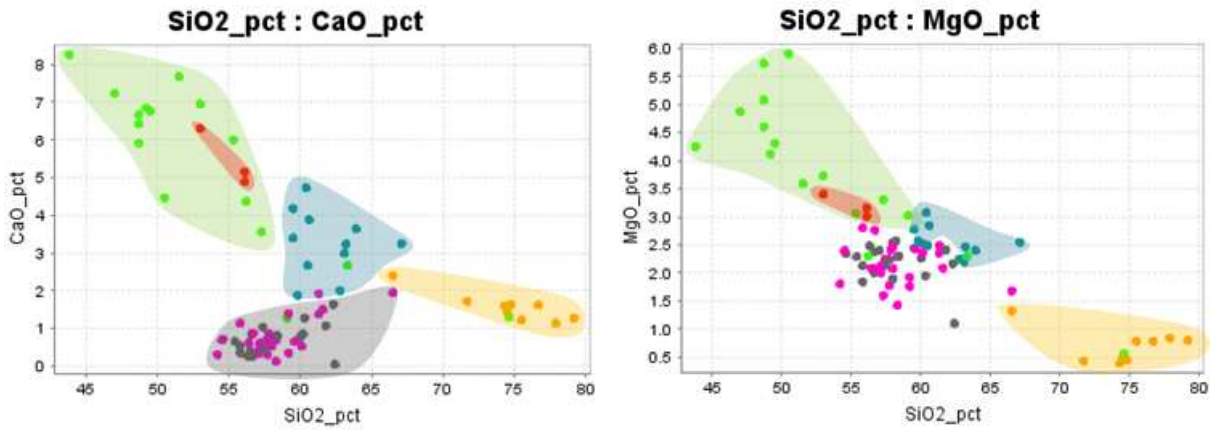

Figure 5-25,The two clusters for volcanic rock in teh CaO and MgO plots also include the conglomerate rock.

Although CaO and MgO were seen as the best diagnostic elements for volcanic rocks both areas shown in Figure 5-25 show that the three conglomerate points are included. In both cases the conglomerates show the highest values of Cao and MgO for the sedimentary rocks.

It is observed that for volcanic rock in the plots showing Al2O3, CaO and MgO the outliers (outside the green surface) remain the same. This suggests systematically different chemical compositions of the volcanic rock. On the basis of SiO2 content the volcanic rock can already be further subdivided into mafic intermediate and felsic rock (Table 5-2). The SiO_2 values for the volcanic rock indicate that the bulk of sampled rock is of mafic composition. Based on this result several assumptions can be made. Mafic rock is assumed to be rich in iron and magnesium according to (Skinner, et al., 2004). CaO may also be enriched compared to felsic rock (Skinner, et al., 2004). Subsequently the felsic rock should have lower values of Fe2O3, MgO, CaO. Looking at the different plots all these assumptions are confirmed.

Figure 5-26, Figure 5-27 and Figure 5-28 clearly supports the mafic intermediate and felsic subdivision. In all three elements: MgO, Fe_2O_3 and CaO a decrease is visible from high MgO, Fe_2O_3 and CaO for mafic rock to low concentrations of CaO and MgO for felsic rock. These consistent results further support the quality of the choice of element to use for the analysis.

Classification	SiO2 range
Mafic	mafic <55 w%
Intermediate	55 w% < intermediate < 65w%
Felsic	65 w% < felsic

Table 5-2, SiO_2 ranges for mafic, intermediate and felsic rock classification ((Rafferty, 2012)).

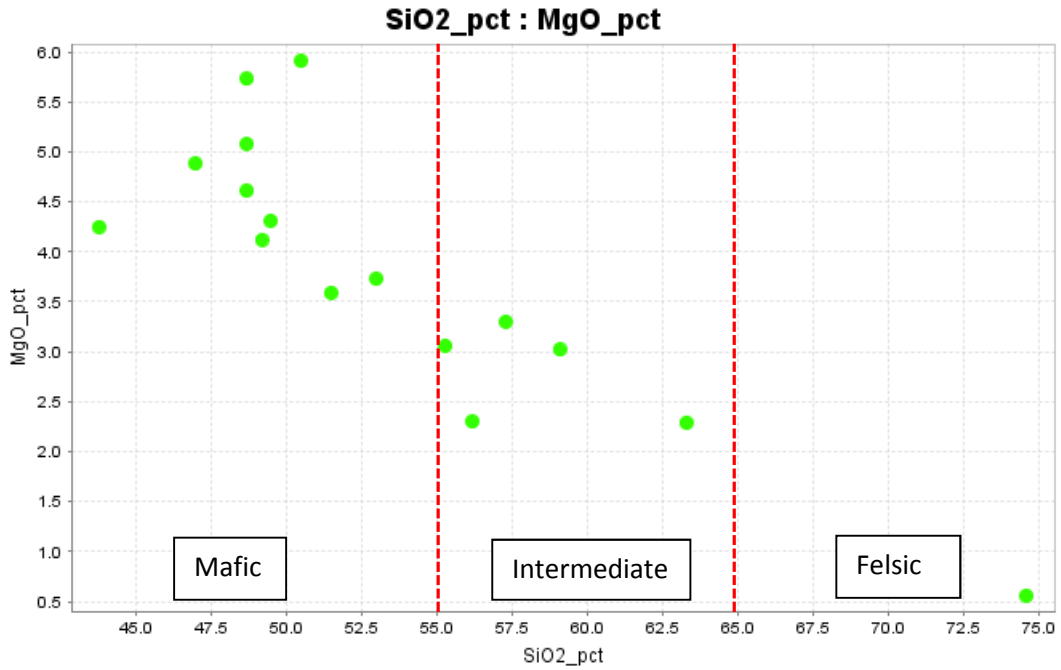

Figure 5-26, MgO vs SiO_2 bivariate plot for volcanic rock samples only.

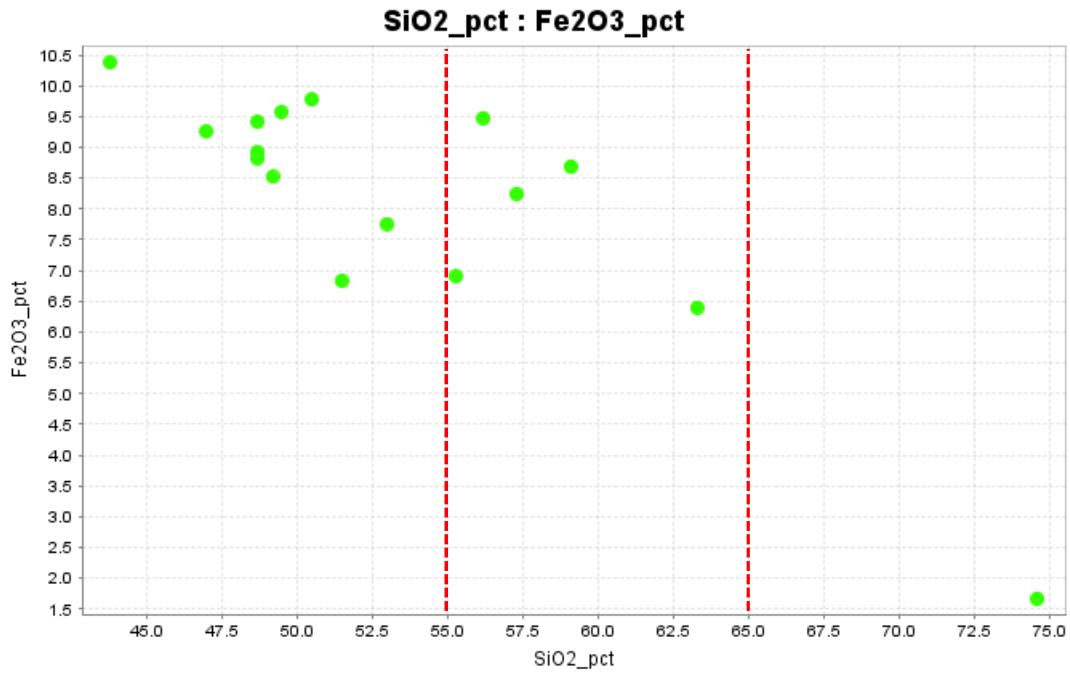

Figure 5-27, Fe_2O_3 vs SiO_2 bivariate plot for volcanic rock samples only.

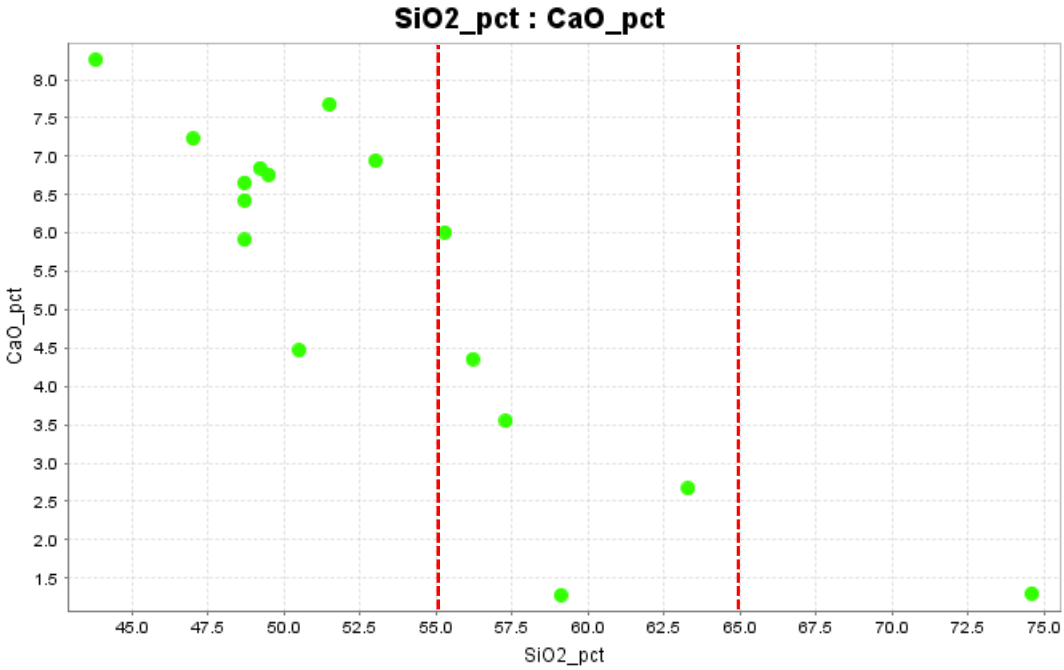

Figure 5-28, CaO vs SiO_2 bivariate plot for volcanic rock samples only.

As discussed in paragraph 5.2.3.2 the elements SiO_2, Fe_2O_3, MgO, P_2O_5 and TiO_2 show clear differences between sandstone and the remaining lithologies. (Figure 5-29). In all four scatter plots the sandstone display the lowest values except for SiO_2 for which sandstone represents the highest values. These factors suggest a high sediment maturity. According to paragraph 5.2.3.2 both Fe2O3 and P2O5 should only be used to support the other results but no regarded as conclusive.

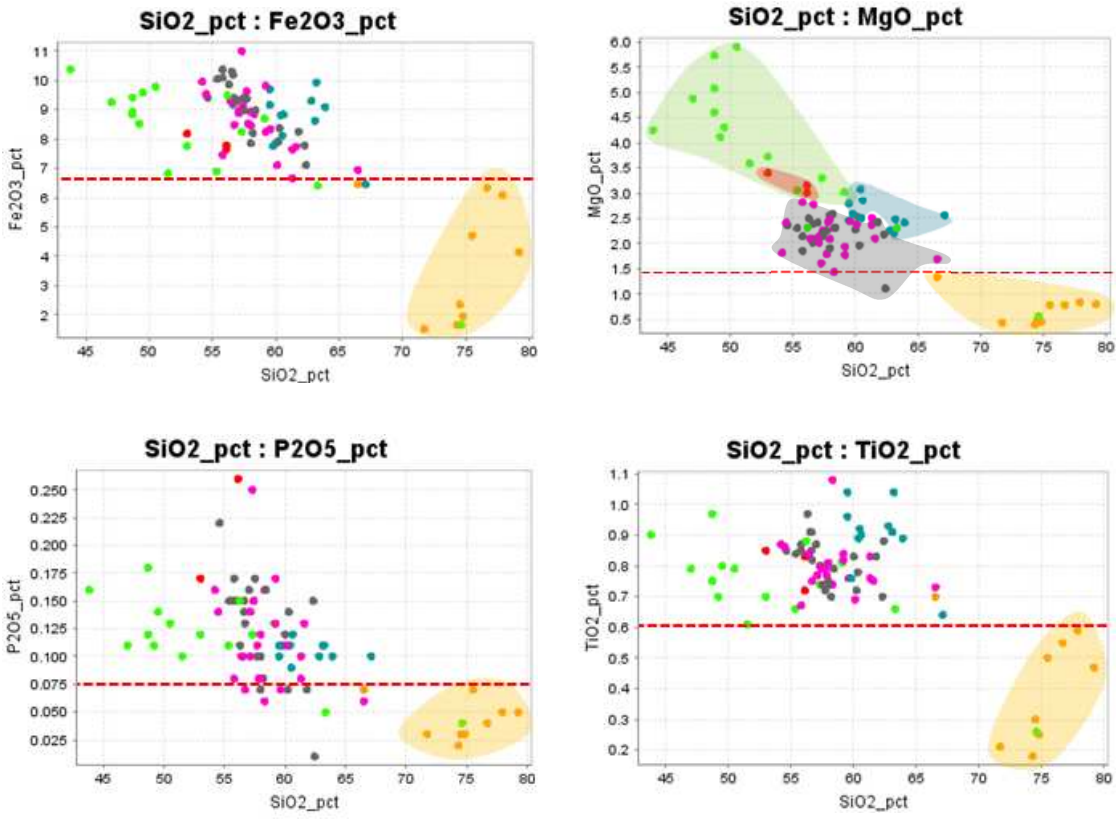

Figure 5-29, Differentiation of the sandstone on the basis of low: Fe_2O_3, MgO, P_2O_5 and TiO_2.

In addition, as was mentioned in paragraph 5.2.3.2 the combination of high SiO_2 content and low Al_2O_3 concentrations support the assumption that the sandstone contains few clays and is a mature sediment (Figure 5-30).

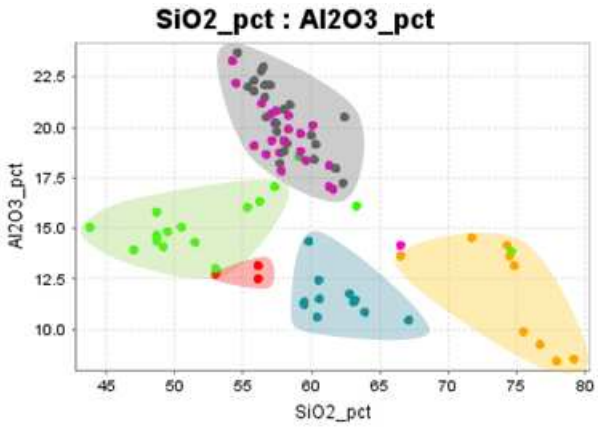

Figure 5-30, Sandstone displays the highest SiO_2 values and relatively low Al_2O_3 herby indicating that the rock has a low clay mineral content.

Conglomerates are only represented by three data points and are mixed with the other lithologies in all scatterplots except for MnO vs SiO_2 (Figure 5-31). Here the three data points for conglomerate clearly display higher MnO values. The lowest being sample LC040 0.31w%. The MnO range is from 0 to 0.45 w% and should therefore not be regarded as a major element. It is difficult to judge if these results are representative when including the volcanic data points however it cannot be dismissed that the three data points representing conglomerate show a clear difference from the other sediments.

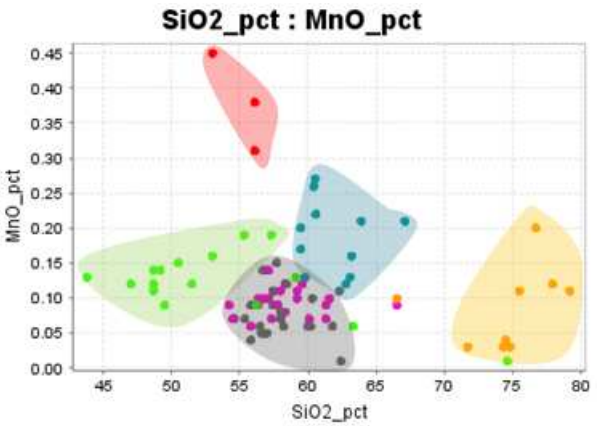

Figure 5-31, MnO is the only element by which conglomeratic rock can be differentiated from the other lithologies in the presence of volcanic rock.

The samples derived from greywacke rock show varying groupings and have therefore been subdivided into two groups: greywacke A and greywacke B. The choice to separate both these groups is based on the large number of greywacke samples and relative tight grouping of the data points. The subdivision was primarily conducted to see if the same samples repeatedly displayed a different trend. The subdivision is clearly visible in the Al_2O_3 vs SiO_2 plot (Figure 5-32). First Greywacke B shows slightly higher SiO_2 values. The difference between the two groups is however more apparent when

looking at the Al_2O_3 values. Greywacke A follows the trend of siltstone/mudstone within a range of 14.15% Al_2O_3 (LC016) to 23.3% Al_2O_3 (LC053) while greywacke B shows lower values 10.45% Al_2O_3 (LC034) to 14.35% Al_2O_3 (LC039). More variations between the two groups are visible in: CaO (Figure 5-25), K_2O (Appendix Figure 10-17) and MnO (Figure 5-31).

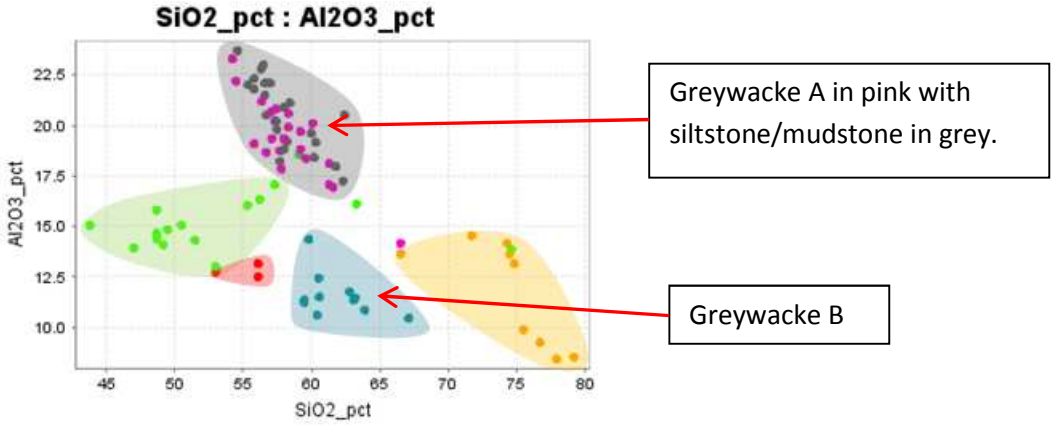

Figure 5-32, A difference between greywacke A and B is visible in the Al_2O_3 plot.

The data points representing siltstone/mudstone are closely linked to the ones of greywacke A. Both are separated from the other lithologies including greywacke B by their high Al_2O_3 values mainly (Figure 5-33). Al_2O_3 is an indicator for clay minerals and therefore suggests that both siltstone/mudstone and greywacke A are less mature sediments. They also display the lowest CaO values (Figure 5-25) although this is not such a clear difference compared to Al_2O_3.

5.2.3.4 Sedimentary rock only

The second stage includes only sedimentary rocks and reveals even more characteristics that can be used to separate lithlogies, especially for conglomerate.

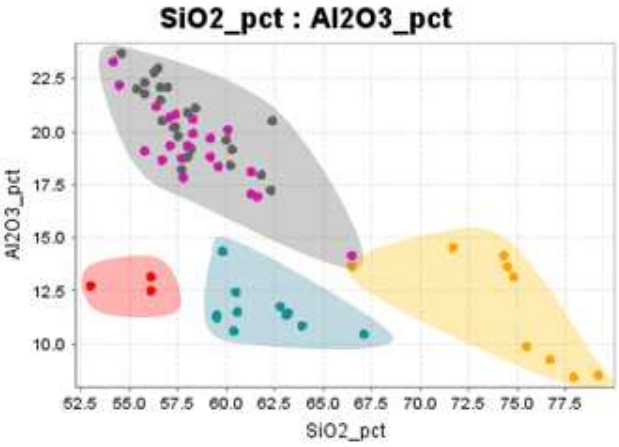

Figure 5-33, Bivariate plot for Al_2O_3 and SiO_2. Clear distinctions between the different lithologies can be made. Siltstone/mudstone and greywacke A however remain grouped.

The distinction between the different sediments is best displayed in the Al_2O_3 plot (Figure 5-33).

Conglomerates now have more elements by which they can effectively be recognized. Due to the exclusion of volcanic rock, conglomerates represent the highest three values for CaO and three out of the four highest values for MgO (Figure 5-34). Within the sedimentary lithologies the conglomerates

can also be separated by combining both their low SiO_2 content and relatively low Al_2O_3 (Figure 5-33). In this graph the conglomerate data points display a clear cluster separated from the rest of the sediments. The fact that volcanic rocks and conglomerates are distinguished from the other by the same elements indicates that they may be related in composition.

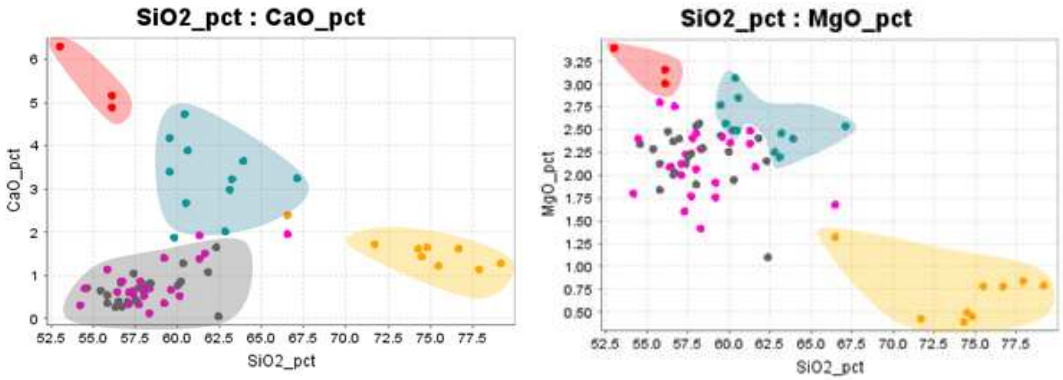

Figure 5-34, With the exclusion of volcanic rock, conglomerate can also be differentiated on the basis of the CaO and MgO content.

The subdivision of greywacke into greywacke A and B has remained due to the following reason. Greywacke A systematically follows the trend of siltstone/mudstone. Greywacke B does not always differ from greywacke A. However in each plot in which differences between the two greywacke can be observed it are the same data points that differ.

An important point to note is the relation between greywacke B and the conglomerates. Whenever the greywacke B group does not follow the same trend as greywacke A it seems to follow the trends from the conglomerates. The values of conglomerate may either fall within the range of values for the same element for greywacke B or a gradual change of concentration of a specific element is observed from conglomerate to greywacke B to greywacke A. The first is the case for Al_2O_3 and K_2O (Figure 5-35) while the latter is true for CaO and MnO (Figure 5-36).

The two groups greywacke A and B have been separated from each other on the basis of chemistry. Greywacke B data points are all derived from three boreholes in the North of the mine namely: KHD-605, KHD-532 and KHD-524 (Figure 5-37). The fact that the conglomerate data points are derived from borehole KHD-532 suggest that beside a differentiation on the basis of lithology location also plays an important role.

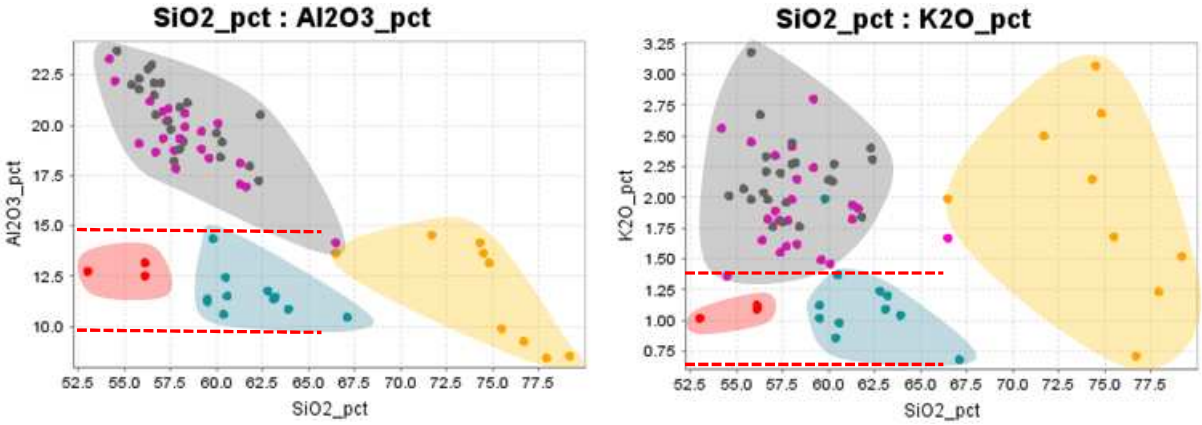

Figure 5-35, Elements for which conglomerate and greywacke B share the same values.

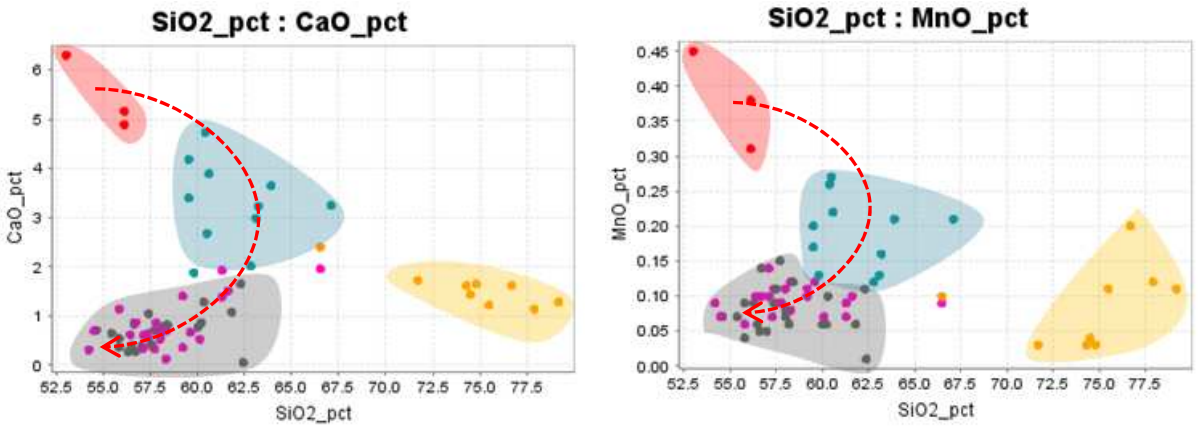

Figure 5-36, Gradual change in CaO and MnO content from conglomerate through greywacke B to siltstone/mudstone and greywacke A.

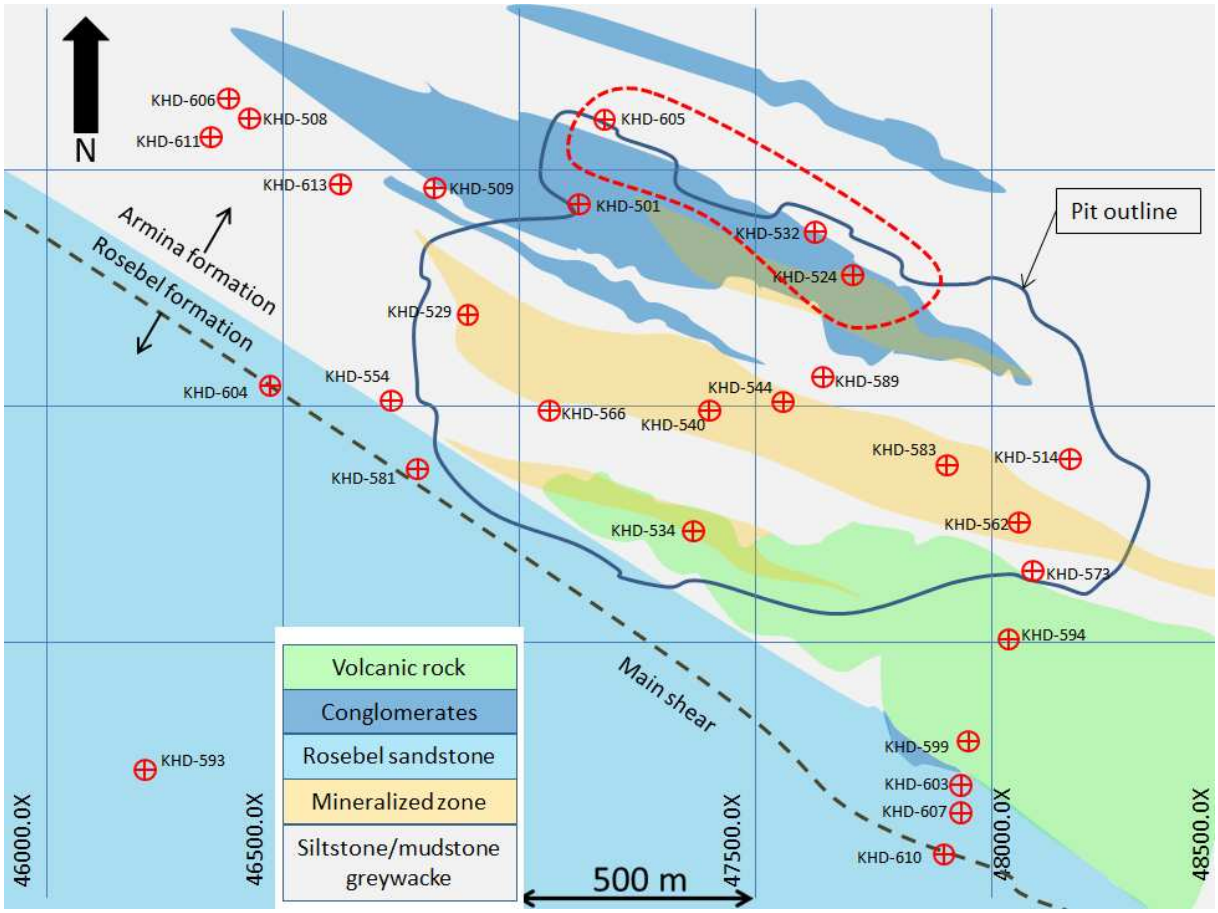

Figure 5-37, The Koolhoven pit with the three boreholes containing greywacke B and the conglomerates encircled.

5.2.4 Path-finder elements

Using the criteria stated in chapter 4.2.2 that elements with a standard deviation greater than 5 % of the average measured value and the results displayed in Appendix Table 10-1 to Appendix Table 10-5, elements will either be used or discarded from further analysis.

From the 10 measurements on the same spot of the calibration disc it is concluded that the elements: Ag, Ba, Bi, Cd, Ce, Hg, La, P, Pb, Rb, S, Sb, Sc, Se, Sn, V and W should not be used because their standard deviation exceeds 5% of the average element content Appendix Table 10-1.

The 10 measurements on different spots of the calibration disc (Appendix Table 10-2) show that he elements: Ag, Ba, Bi, Cd, Ce, Cl, Hg, La, P, Rb, S, Sb, Sc, Se, Sn, U, V and W have a standard deviation above 5% of the average measured value.

The reproducibility of the measurements was also tested using the pulps of samples LC 1153 and LC 1143. The results are displayed in Appendix Table 10-3 and Appendix Table 10-4. According to Appendix Table 10-3 the elements As, Ba, Cd, Ce, Cl, Cr, Hg, La, Mo, Nb, S, Sb, Sc, Sn and V are not accurate. Appendix Table 10-4 shows that the elements: As, Cd, Ce, Cl, Hg, Ca, Mo, Nb, P, S, Sb, Sc, Sn and V have a standard deviation above 5% of the average measured value.

The elements: Ca, Co, Cu, Fe, K, Mn, Ni, Sr, Ti, Zn and Zr are the only elements that have passed all four tests (Table 5-4).

Plastic bags have been tested using the portable XRF unit and the values have been compared to the overall dataset of the rock samples. Not all plastic bags were detected. As a measure, the average values for the plastic bags were subtracted from the average values of the rock samples for the same elements. Values for the rock samples are a composite value of the plastic bags and the rock pulps. Negative values therefore imply that the response from the plastic bag overshadows the response from the pulp. This is valid for the elements: As, Cd, Ce, La, Nb, P, Sn, U and W (Appendix Table 10-5). It must be reminded that the 20 plastic bags have been tested but only 5 were detected. This also evokes doubts upon the consistency of the element content in the different plastic bags. Although the plastic bags show great variability in concentrations it is important to note that these are the elements that have failed the previous four tests.

In chapter 3.4 the statement was made that the data acquired with the field portable XRF unit would not be as accurate as the data acquired under laboratory conditions with the various methods listed in chapter 3.4 (four-acid ICP-MS and ICP-AES) The assumption was made that data acquired by ALS laboratory using the four-acid ICP-MS and ICP-AES method is quantitative and should therefore be used as a reference for all elements.

By plotting the results obtained from the portable XRF unit versus the data obtained using four-acid ICP-MS and ICP-AES it becomes clear that not all elements are measured accurately. Even elements for which the 3-beam setup is optimized do not all correlate with the reference data. Several elements including Rb and Zn (Figure 5-38 & Figure 5-39) show a correlation between the two datasets but with a systematic error. Although the data points are aligned along a diagonal line the ranges are different. Since the pulps for the portable XRF unit are the same as for the four-acid ICP-MS and ICP-AES analysis the error must be a calibration error. The R^2 value being higher than 90% we assume that the values are correlated to each other but not calibrated. The formula for the trend

lines together with the R^2 are displayed in the top right corner of the graph, y representing the values from the portable XRF unit and x the values obtained by the laboratory.

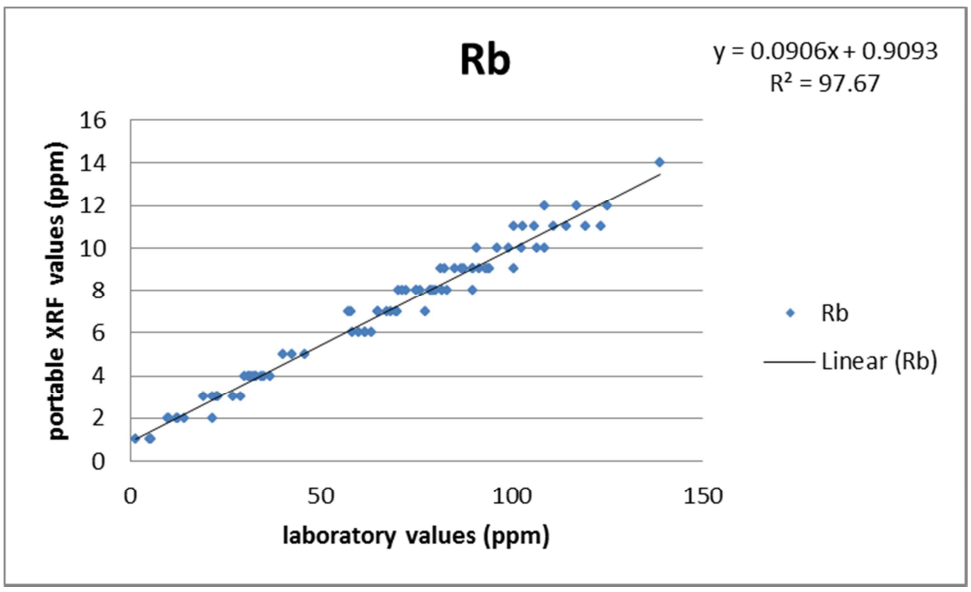

Figure 5-38, Plot of the data acquired by the portable XRF unit versus data acquired in the laboratory for Rb.

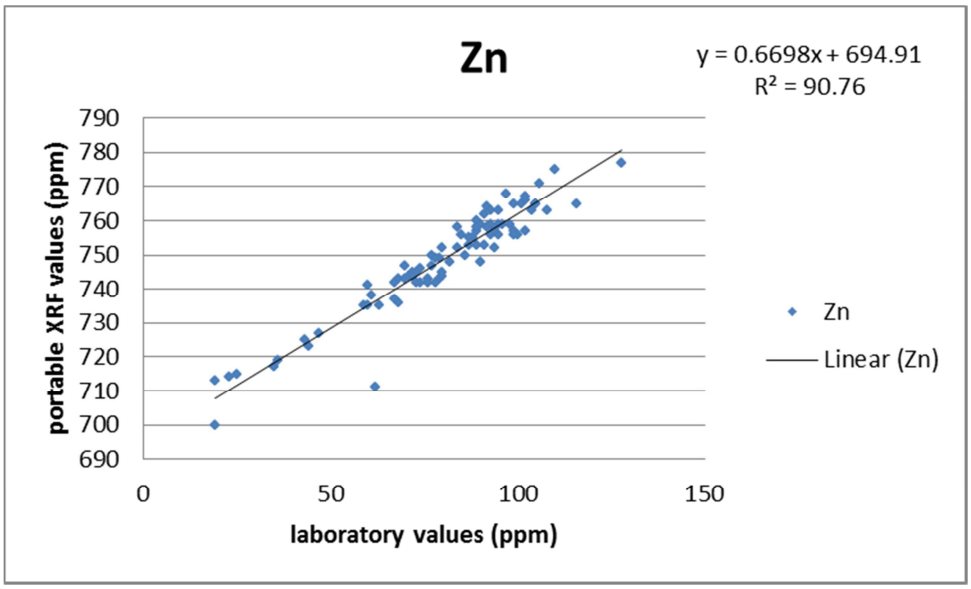

Figure 5-39, Plot of the data acquired by the portable XRF unit versus data acquired in the laboratory for Zn.

Other elements for which the portable XRF unit is optimized according to in the 3-beam setup (Table 5-3) yield poor correlation with the reference data. For example Ni (Figure 5-40) for which the portable XRF unit has a LOD of 5-8 ppm is not recorded for several concentrations of more than 40 ppm. The measurements are also not consistent since the portable XRF unit does detect several concentrations below 10 ppm but fails to record several concentrations above 40 ppm (Appendix Table 10-6). For the element Ni trying to calibrate does not make sense since the R^2 is to low and would not be improved by using the trend line to convert the portable XRF values. It must be concluded that both the quantitative and qualitative characteristics of the portable XRF unit are to be doubted.

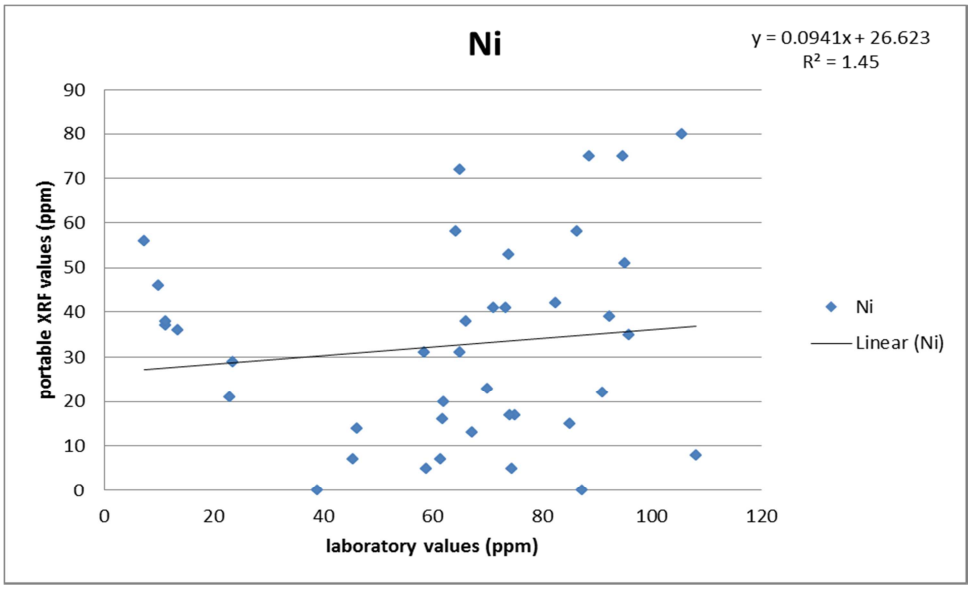

Figure 5-40, Plot of the data acquired by the portable XRF unit versus data acquired in the laboratory for Ni.

The trend line formula's for the elements with R^2 > 90% data indicate that two errors are present. In the case of Rb and Zn which are both measured by the second beam of 35 KV, both errors are present but are not systematic. From the formula for the trend line for Rb a scaling error of 0.01 is present with an offset of less than one ppm. The offset being minimal the trend line for Rb could be roughly reduced to a scaling error namely a factor 10. In the case of Zn first a scaling error of 0.67 between the two data sets is present followed by an offset of 695 ppm. Since both Rb and Zn are being measured by the second beam in the 3-beam setup and display varying errors no overall correction can be applied over the total dataset

By using a linear trend line to recalibrate the data, the R^2 is not affected however the ranges of value are conform to each other. This method of calibration should be used with great care since we have a limited range of values. Values outside the measured range may behave differently therefore extrapolation should be avoided.

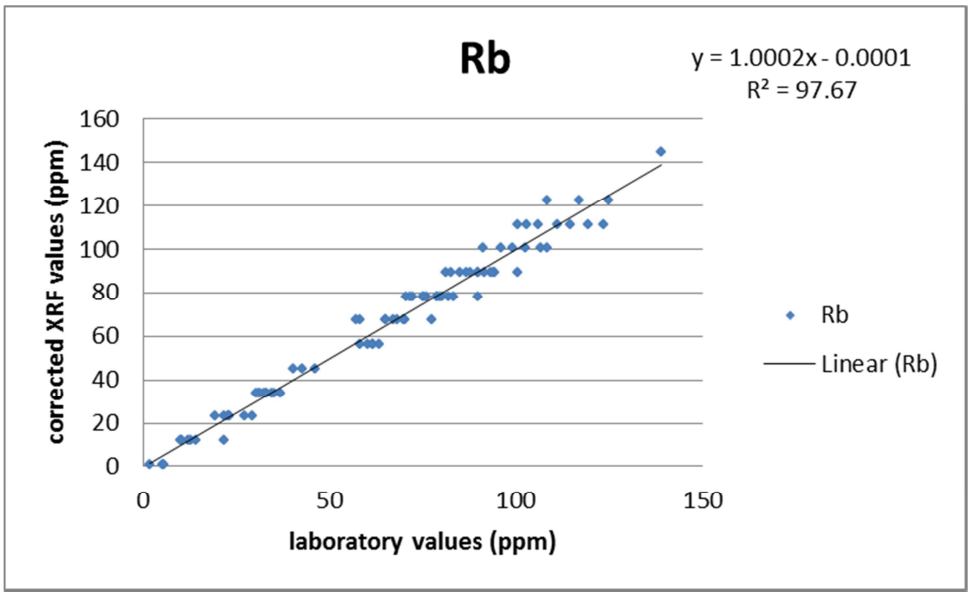

Figure 5-41, Plot of the corrected data acquired by the portable XRF unit versus data acquired in the laboratory for Rb.

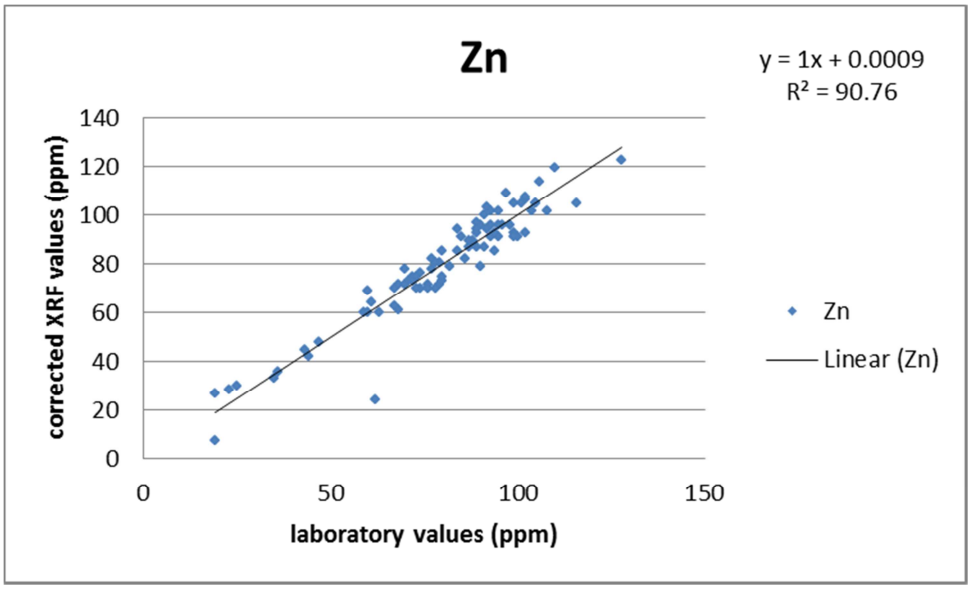

Figure 5-42, Plot of the corrected data acquired by the portable XRF unit versus data acquired in the laboratory for Zn.

Table 5-3 summarizes the data validation between the data acquired with the portable XRF unit and the data acquired by the laboratory. The R^2 value could not be obtained for all elements due to the following reasons:

- Some elements were recorded by the laboratory to have concentrations below the LOD of the portable XRF unit (Ag, Bi, Cd).
- The element is not being recorded by ICP-MS and/or ICP-AES as is the case for Cl and Hg.
- Not enough values were recorded to create a solid trend line. This is the case for example for Se, Sn, U and W
- In the case of Nb all the data points are clustered in a small range. Although 82 portable XRF data points and 84 laboratory data points have been measured the limited range makes fitting a trend line impossible.

As can be seen in Table 5-3 the R^2 are either above 90% or far below with the highest being 47% for Co and the next highest 24% for Ti. A total of twelve elements produce an R^2 value above 90%. Only the data of these elements should be considered further.

The only elements which have shown reproducible results, a standard deviation lower than 5 % of the average measured value and a correlation factor R^2 higher than 90% are: Ca, Cr, Cu, Fe, K, Mn, Sr, Zn and Zr (Table 5-4).

Element	Beam	R^2 in %	Number of measured values from XRF	Number of measured values from ICP-MS and ICP-AES	Laboratory max ppm	Laboratory minimum ppm	Laboratory average ppm
Ag	1	None	0.00	81.00	0.41	0.01	0.07
As	1	92	84.00	84.00	192.50	0.30	17.56
Ba	1	98	84.00	84.00	1120.00	120.00	467.86
Bi	2	None	2.00	79.00	0.34	0.01	0.08
Ca	3	99	81.00	84.00	56300.00	300.00	15427.38
Cd	1	2	57.00	77.00	0.32	0.02	0.08
Ce	1s	6	83.00	84.00	94.90	17.20	42.84
Cl	3	None	79.00	NR			
Co	2	47	84.00	84.00	53.10	1.20	28.74
Cr	3	93	84.00	84.00	501.00	75.00	171.94
Cu	2	93	84.00	84.00	254.00	0.60	45.60
Fe	2	95	84.00	84.00	74500.00	10100.00	54144.05
Hg	1s 2s	None	82.00	NR			
K	2	96	83.00	84.00	25400.00	1000.00	13054.76
La	1s	1	78.00	84.00	46.20	7.60	20.83
Mn	3	99	84.00	84.00	3220.00	90.00	865.33
Mo	1	2	84.00	82.00	6.07	0.05	0.46
Nb	1s 2s	18	82.00	84.00	17.20	1.00	3.67
Ni	2	1	39.00	84.00	108.00	7.30	68.15
P	3	None	4.00	84.00	1120.00	50.00	477.14
Pb	2	None	27.00	84.00	18.50	1.80	8.00
Rb	2	98	84.00	84.00	139.00	1.60	66.03
S	3	1	45.00	60.00	20500.00	100.00	1786.67
Sb	1	0	47.00	84.00	9.08	0.11	2.69
Sc	3s	0	83.00	84.00	37.60	3.20	22.99
Se	2	None	84.00	6.00	1.00	1.00	1.00
Sn	1	None	20.00	84.00	5.30	0.40	1.23
Sr	1	99	84.00	84.00	526.00	80.30	161.54
Ti	3	24	84.00	83.00	5740.00	680.00	2449.76
U	1s 2s	None	1	84	4	0.3	1.53
V	1s 2s 3s	15	84	84	189	9	130.57
W	1s 2s	None	2	84	26.7	0.2	3.17
Zn	2	91	84	84	128	19	80.35
Zr	1	91	84	84	390	49.9	132.97

Table 5-3, Summary of the data validation between the values acquired with the portable XRF unit and the laboratory. The letter "s" in the "beam" column refers to "secondary" meaning that he beam detects this element as secondary element, see paragraph 3.4.4.

Element	Plastic bag test	Calibration disc same spot	Calibration disc different spots	Sample LC1143	Sample LC1153	Cross correlation with laboratory	Element passes all tests
Ag	-	FAIL	FAIL	-	-	-	FAIL
As	-	-	-	FAIL	FAIL	PASS	FAIL
Ba	-	FAIL	FAIL	PASS	FAIL	PASS	FAIL
Bi	-	FAIL	FAIL	-	-	-	FAIL
Ca	-	-	-	PASS	PASS	PASS	PASS
Cd	FAIL	FAIL	FAIL	FAIL	FAIL	FAIL	FAIL
Ce	FAIL	FAIL	FAIL	FAIL	FAIL	FAIL	FAIL
Cl	-	PASS	FAIL	FAIL	FAIL	-	FAIL
Co	-	PASS	PASS	PASS	PASS	FAIL	FAIL
Cr	-	PASS	PASS	PASS	PASS	PASS	PASS
Cu	-	PASS	PASS	PASS	PASS	PASS	PASS
Fe	-	PASS	PASS	PASS	PASS	PASS	PASS
Hg	-	FAIL	FAIL	FAIL	FAIL	-	FAIL
K	-	PASS	PASS	PASS	PASS	PASS	PASS
La	FAIL	FAIL	FAIL	FAIL	FAIL	FAIL	FAIL
Mn	-	PASS	PASS	PASS	PASS	PASS	PASS
Mo	-	PASS	PASS	FAIL	FAIL	FAIL	FAIL
Nb	FAIL	-	-	FAIL	FAIL	FAIL	FAIL
Ni	-	PASS	PASS	-	-	FAIL	FAIL
P	FAIL	FAIL	FAIL	FAIL	-	-	FAIL
Pb	-	FAIL	PASS	-	-	-	FAIL
Rb	-	FAIL	FAIL	PASS	PASS	PASS	FAIL
S	-	FAIL	FAIL	FAIL	FAIL	FAIL	FAIL
Sb	FAIL	FAIL	FAIL	FAIL	FAIL	FAIL	FAIL
Sc	-	FAIL	FAIL	FAIL	FAIL	FAIL	FAIL
Se	-	FAIL	FAIL	PASS	PASS	-	FAIL
Sn	FAIL	FAIL	FAIL	FAIL	FAIL	-	FAIL
Sr	-	-	-	PASS	PASS	PASS	PASS
Ti	-	PASS	PASS	PASS	PASS	FAIL	FAIL
U	FAIL	PASS	FAIL	-	-	-	FAIL
V	-	FAIL	FAIL	FAIL	FAIL	FAIL	FAIL
W	FAIL	FAIL	FAIL	-	-	-	FAIL
Zn	-	PASS	PASS	PASS	PASS	PASS	PASS
Zr	-	-	-	PASS	PASS	PASS	PASS

Table 5-4, Summary of all passed and failed tests per element.

Due to the varying inconsistencies in the desktop XRF database questions regarding the validity of the dataset arise. The choice has been made to use the 12 elements which yield a correlation factor above 90% for further analysis. This choice is based on the fact that two in-dependable analysis methods have yielded results correlated to each other but not calibrated. Although the elements As, Ba and Rb did not pass all tests they are still included because the correlation factor both data sets exceeds 90%. The data is deemed useful to create new hypothesis which will have to be tested with more valid data. It must clearly be noted that the results presented below are not conclusive. The fact that the trend lines obtained from the cross validation plots for the 12 elements using 85 samples will be used on the remaining 819 desktop XRF data points implies that extrapolation will be performed. The following analysis (PLSR & evaluation of downhole plots) will not be based on

absolute concentration but on changes in concentrations. These changes will remain after the calibration of the values. Since the results will only be used to potentially create new hypothesis which should be tested with more valid data extrapolation is acceptable.

5.2.4.1 Partial least squares regression

Chapter 3 stated that the portable XRF data would be the most suitable because of its large size compared to the data set acquired by the laboratory. Paragraph 5.1.3 however, proved that only 12 elements could successfully be cross validated with the laboratory data. The input values for the PLSR simulations will therefore be restricted to the corrected values of the 12 elements with an R^2>90% together with their respective gold contents.

The resulting R^2 values belonging to the different simulations using PLSR are displayed in Table 5-5 and Table 5-6. It is directly recognized that the R^2 values obtained from the various simulations do not indicate any useable correlation. This is valid for all the samples and the samples derived from fresh rock only.

The best results are the ones from the volcanics which yield an average R^2 of 29% for the consistency test and 18% for the cross validation test. Although these results are better a look at the size of the data set reveals that the PLSR simulation for volcanic rocks uses 91 samples. The overall R^2 values for all four simulation sets seem to improve as the size of the data set decreases. This suggests that using more data enhances the chance of including random variations which would decrease the quality of the determination of β_0 and β_p resulting in poor predictions.

All rock	Simulation	Number of samples	R^2 in % for consistency test	R^2 in % for cross validation test
ALL samples	1	904	0.46	0.23
	2	904	3.6	-0.3
	3	904	2.9	-0.25
	4	904	0.45	0.28
	5	904	0.47	0.13
Sediments	1	813	0.52	0.32
	2	813	0.6	0.09
	3	813	3.2	-0.4
	4	813	0.6	0.28
	5	813	15.5	0
	6	813	1.2	0.3
Volcanics	1	91	34.5	27
	2	91	24.5	12
	3	91	32	23
	4	91	27	15
	5	91	32	10
	6	91	25	20
Three boreholes	1	162	53	3
	2	162	70	2
	3	162	40	5
	4	162	12.5	10
	5	162	45	2
	6	162	73	1

Table 5-5, Results of the PLSR simulations on the corrected portable XRF data for all rock samples.

Fresh rock only	Simulation	Number of samples	R^2 % for consistency test	R^2 % for cross validation test
All samples	1	644	2.4	1.3
	2	644	2.3	1.4
	3	644	2	1.6
Sediments	1	565	2.3	1.3
	2	565	8.2	0
	3	565	2.5	1.7
Volcancis	1	79	14	3.8
	2	79	10.5	7
	3	79	13	5

Table 5-6, Results of the PLSR simulations on the corrected portable XRF data for fresh rock samples only.

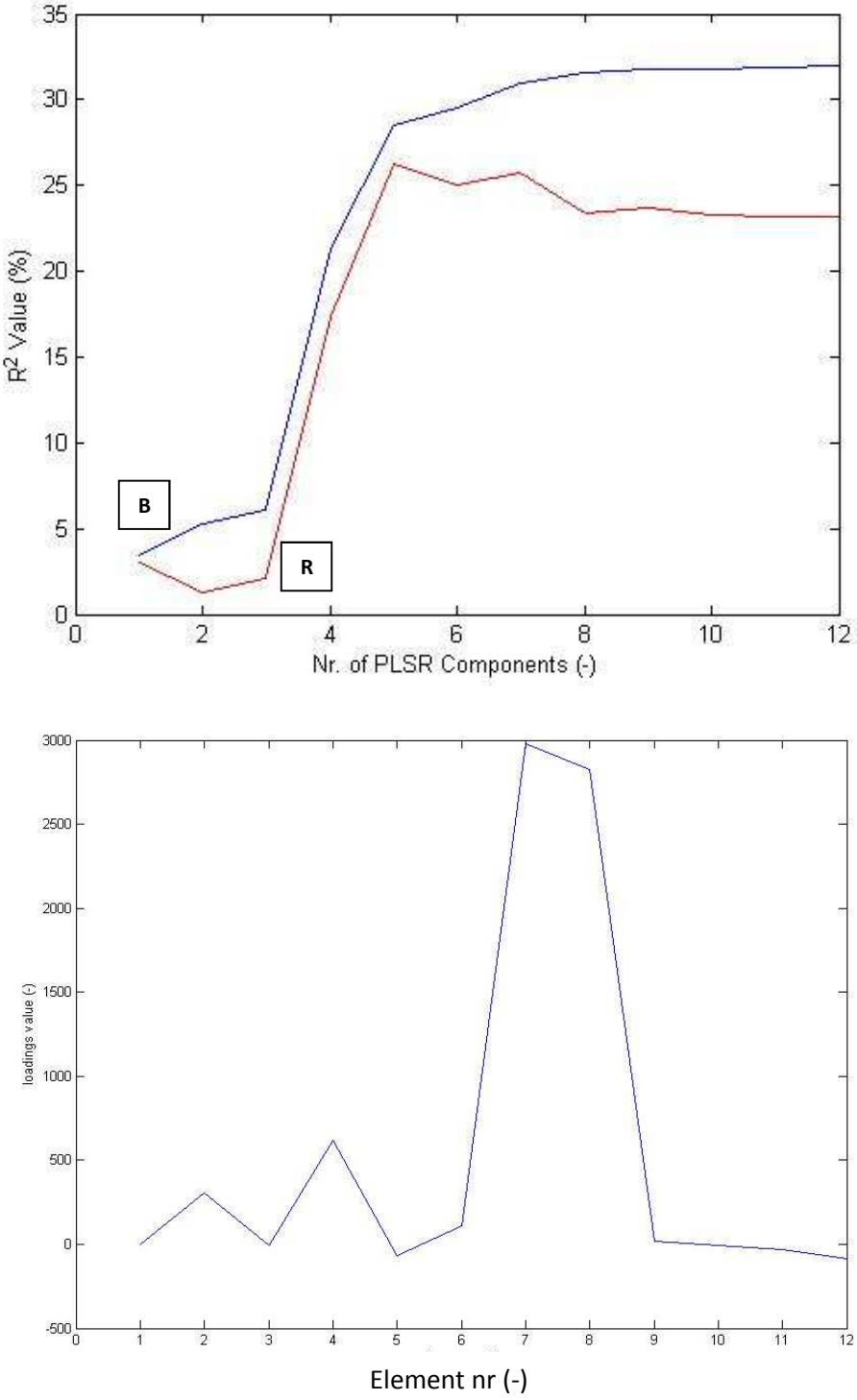

Figure 5-43, R^2 values for the PLSR simulation 3 of all volcanic rock samples (top). Elements belonging to component 4 (bottom).

Because of their higher R^2 values the results from the volcanic rocks are further investigated. The aim is to define which element or elements most influence the R^2 value. The graphs for the six PLSR simulations for volcanic rock show a dramatic increase in R^2 from 3 to 4 components (Figure 5-43).

The increase in R^2 value from 3 to 4 components is therefore mainly caused by element 4, 7 and 8 of the X matrix which represent: Cr, K and Mn. None of these three elements had been identified as being the result of the plastic bag in paragraph 5.1.3. The result therefore relate to the rock sample.

Beside absolute values for R^2 the trends of the plots were also analysed. Two types of trends have been observed. These are depicted in Figure 5-44 and Figure 5-45. As was shown in Figure 5-43 the blue line represents the R^2 % value obtained by comparing the true gold content to the predicted gold content using y1 and x1 (two thirds of the dataset used to obtain β_0 and β_p). The red line represents the R^2% value obtained by cross validating the β_0 and β_p using new data y2 and x2 (one third of the dataset). The blue line will be referred to as "line B" and the red line will be referred to as "line R).

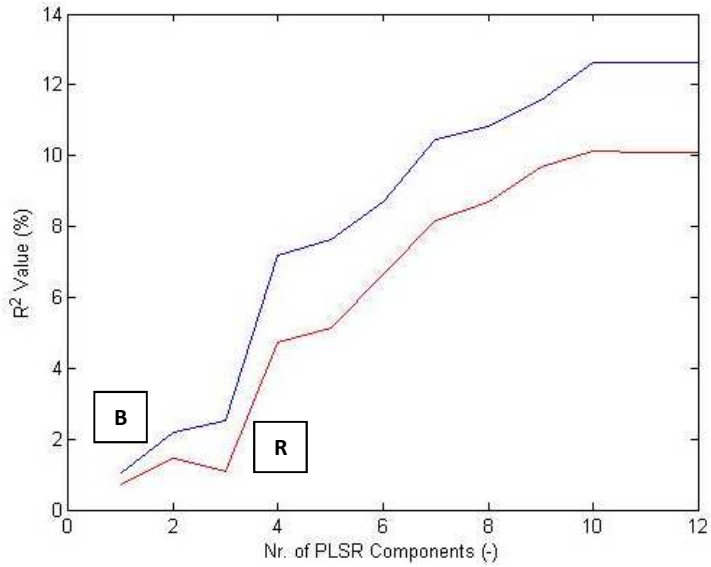

Figure 5-44, Plot displaying line B and line R for three boreholes in simulation 4.

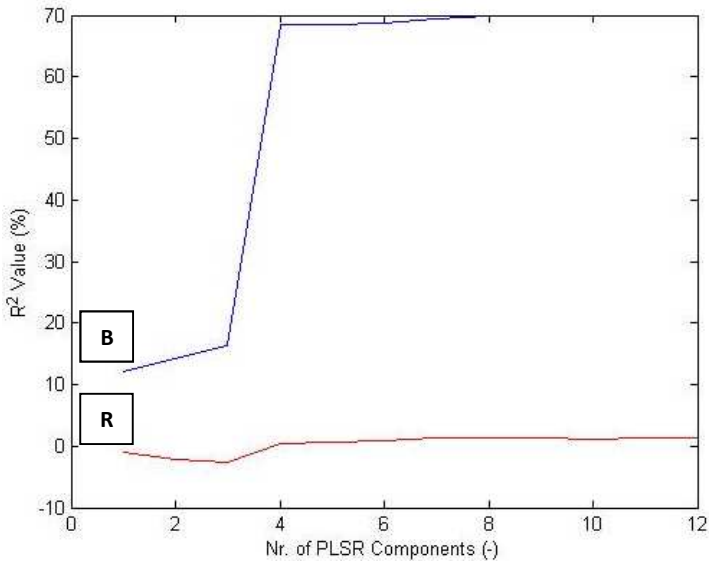

Figure 5-45, Plot displaying line B and line R for three boreholes in simulation 2.

In an ideal situation line B would reach an R^2 value of 100 % and line R would follow the exact same path.

In Figure 5-44 line R does follow line B closely. With more than four components used line B and line R start to divert from each other slightly.

Figure 5-45 displays a different trend from Figure 5-44 while the same data was used.

The differences observed are:

- Line B achieves a far higher R^2 of 70% compared to maximum of 12.5% for simulation 4.
- No significant increase in R^2 is obtained by using more than four components.
- Instead of a gradual increase of R^2 by using more components line B in simulation 2 increases dramatically from R^2 15% to 69% from 2 to 3 components.

Because the total dataset and PLSR analysis remain the same the differences should be caused by the subdivision of the total dataset into two parts. At each simulation a new random subdivision of data points is produced. The sizes of both these sub-datasets do not vary however their content does. As stated chapter 3 best results are to be expected when a large range of gold concentrations are used to determine β_0 and β_p. This also implies that β_0 and β_p will be optimized for a larger range of gold concentrations and may not be optimal when working with small variations.

These characteristics could be the cause of the difference between Figure 5-44 and Figure 5-45.

This effect can best be described using Figure 5-46 and Figure 5-47. Figure 5-46 should be linked to Figure 5-44 and Figure 5-47 to Figure 5-45.

The red boxes represent five rock samples with gold concentrations of 1, 5, 10, 20 and 40 g/t. The other samples (the bulk of the dataset) has gold concentrations bellow 0.5 g/t. In Figure 5-46 the five red boxes are evenly distributed over both y1 and y2. To determine β_0 and β_p we therefore have three samples with Au>= 1g/t and plenty of low gold concentrations leading to a poor coverage. In Figure 5-47 all five samples with Au>= 1g/t are present in y1. The coverage of gold concentrations is therefore better and β_0 and β_p are determined more accurately which results in a higher R^2 in the consistency test (Figure 5-46).

Cross validation

In Figure 5-46 two samples with Au>= 1g/t are available for the cross validation step. The β_0 and β_p that have been determined can now be cross validated using a dataset of the same range.

In Figure 5-47 all the high gold concentrations were concentrated in y1. Therefore for the cross validation part only samples with Au<= 0.5 g/t are available. β_0 and β_p which were determined on a range of 0 to 50g/t are now being cross validated against a dataset with a range of 0 to 0.5g/t resulting in poor predictions and therefore a low R^2.

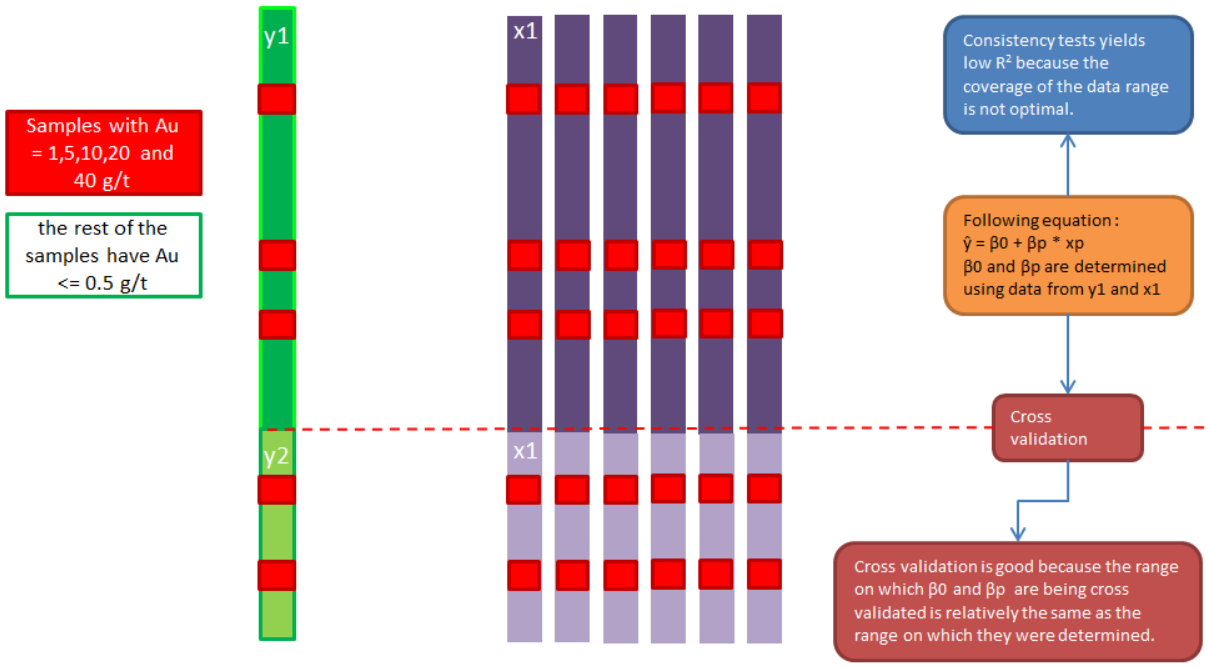

Figure 5-46, Systematic representation of data distribution in the two subsets. In this case an even distribution of samples with high Au concentrations over both subsets.

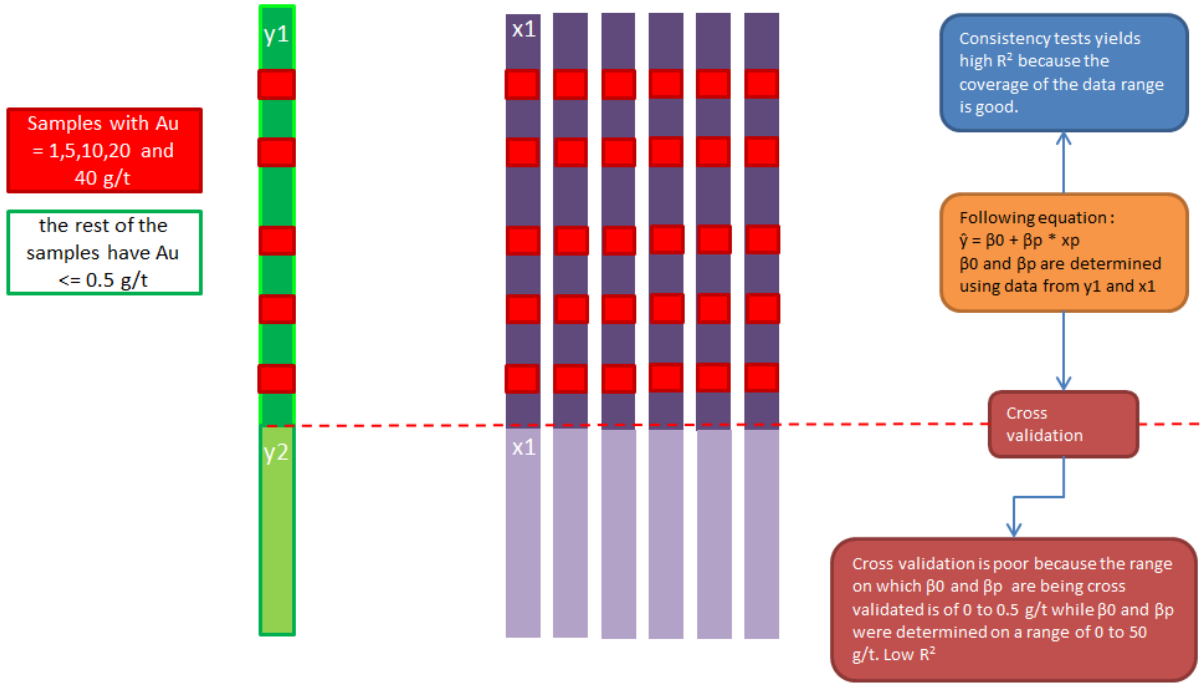

Figure 5-47, Systematic representation of data distribution in the two subsets. In this case an uneven distribution of samples with high Au concentrations over both subsets.

5.2.5 Re-evaluation of data processing method.

5.2.5.1 Issues concerning the calibration of the portable XRF data

The use of ordinary least squares regression (OLS) has long been accepted as the conventional method to calibrate data. The calibration performed previously between the portable XRF data and data from the laboratory uses this method of regression.

Several inconsistencies in the application of ordinary least squares regression mentioned in Rollinson (1993) and Weltje & Tjallingii (2008) are directly observed in the data used in this research project hereby implicating that the previously performed calibration and hence the following analysis is not correct.

As could be observed in paragraph 5.2.4 trend lines did not pass through the origins. This may result in negative predictions of values close to zero. As a result and as mentioned paragraph 5.2.4 using the results of ordinary least squares regression outside the range on which it has been determined is likely to result in erroneous predictions. Both on the lower boundary as on the higher boundary of the range.

Another issue is the total sum constraint. Concentrations are by definition expressed as a proportion of unity. This implies that by definition element concentrations are related to each other since if one element concentration increases one or more other element concentrations must decrease in order to obtain a total sum of proportions equal to unity. To calibrate the data adequately the total sum constraint must be respected. This however may not be the case when the element concentrations are calibrated one by one using OLS as has been done paragraph 5.2.4. This means that a bivariate approach was used to solve a multivariate problem. Instead calibration should be performed including all elements.

The fact that the measured concentrations of elements in the portable XRF dataset do not sum up to unity proves that part of the rock chemistry is not being measured and represented in the data. Comparing the samples to each other would implicate that different total amounts of detected elements are compared to each other. It is then no longer possible to define if changes in chemical compositions are a quality of the rock sample or of the measurement.

5.2.5.2 Proposed solution

To solve these issues the use of log-ratios is suggested (Rollinson, 1993). The theory behind this technique will be illustrated in several severely simplified steps. For more extensive background on the use of log-ratios the reader is referred to (Rollinson, 1993) and for the specific applications of these principles for the calibration of the portable XRF data the reader is referred to (Weltje & Tjallingii, 2008). In the analysis of geochemical data the interest is often to define relative changes and not necessarily changes in absolute values. Ratios, which capture the difference in concentrations but not the absolute concentration between two elements, are therefore a suitable tool to use. The use of ratios also enables the treatment of element concentrations when not all elements have been measured since only relative changes are analysed and not absolute values.

Ratios however have the undesirable characteristics of being asymmetric. A/B will behave differently than B/A. This problem was solved by taking the log of both ratios. This yields the same number but of opposite sign. The difference in sign will yield the same correlation coefficient but positive or negative. The application of log-ratios for calibration of the portable XRF data is illustrated in (Weltje

& Tjallingii, 2008). The idea is to rewrite the general calibration equation (Equation 2) using log-ratios.

$$W_{ij} = K_j I_{ij} M_{ij} S_i$$

Equation 2, General equation for the conversion of net intensities into element concentrations in a controlled environment (Weltje & Tjallingii, 2008).

W_{ij} is the concentrations of element j in sample i

K_j is the calibration constant for element j specific to the device. This represents the sensitivity of the device

I_{ij} represents the net intensity of element j in sample i.

M_{ij} is the matrix effect which corrects for scattering, absorption and enhancement effects in I_{ij}.

S_i represents the homogeneity and variations in measurement geometry compared to the standard measurement configuration

Rewriting the general equation using log-ratios yields the "log-ratio calibration equation" (LRCE) as proposed by (Weltje & Tjallingii, 2008) (Equation 3).

$$\ln\left(\frac{W_{ij}}{W_{iD}}\right) = \alpha_{jD} \ln\left(\frac{I_{ij}}{I_{iD}}\right) + \beta_{jD}$$

Equation 3, Log-ratio calibration equation (LRCE) (Weltje & Tjallingii, 2008).

α and β represent the matrix effect and detection efficiency (transformed to log-ratios).

An important change in the equation is the elimination of S_i which represented the measurement geometry which are difficult and maybe impossible to define in a poorly controlled measurement environment. Solving this equation is done using partial least squares (PLS) regression (Weltje, et al., 2012)

Once the calibration of the log-ratios has been performed, inversing the operations of log-ratios yields the calibrated concentrations per element. For full description of the method the reader is referred to (Weltje & Tjallingii, 2008).

Applying the calibration to the entire portable XRF dataset enables us to calibrate the measured data and estimate the concentrations of elements that were not measured using the portable XRF device but were measured in the laboratory due to a lower limit of detection. By comparing the calibrated data to the actual measured value in the laboratory an R^2 value can be obtained. This R^2 value represents the degree of certainty of the calibrated value.

The next step involves testing the presence of correlation between elements and gold. For the same reason as listed above log-ratios will be used to compare both data sets to each other. The total number of possible element ratios amounts to 1135. The gold which was measured separately is the only measured element in the fire assay procedure. Total sum constraint is therefore respected by summing up the concentration of gold with the concentration of undefined element. As a results 1 ratio will be used namely: (gold concentrations) / (unity – gold concentration). R^2 values can then be

determined by squaring the Pearson product moment correlation coefficient r between the log-ratios of elements and the belonging log-ratios of gold.

5.2.5.3 Results

Plots have been created displaying the R^2 values of the correlation between log-ratios of gold concentrations and all other possible log-ratios using the calibrated element concentrations. On the X-axis the R^2 values representing the quality of the calibrated ratios are displayed. Several scenarios have been analysed based on subdivisions of het calibrated dataset:

1) All samples
2) All unweathered samples
3) all unweathered volcanic samples
4) all unweathered sedimentary samples
5) The boreholes KHD-508, KHD-566 and KHD-583 have been analysed in several ways. All samples, unweathed samples, weathered samples. For each of these three scenario's data was analysed for each borehole separately and for all three together. As a result 12 scenarios were analyse (Table 5-8).

In a first stage the R^2 value of the correlation between element log-ratios and gold log-ratios will be analysed. To compare the graphs objectively all points are compared to the optimal situation in which both R^2 values would be 1. The distance between a specific data point and point (100,100) (Figure 5-48) is used to quantify the quality of het correlation. The shorter the distance the closer the data point is to the optimum point and therefore the better the log-ratio. This does however mean that log-ratios of elements presenting a good correlation with the gold content but with a poor calibration certainty may still end up as one of the best log-ratios.

The scenario 1 to 4 displays poor results (Table 5-7). Further analysis of these results is deemed to be unnecessary at this stage.

scenario	number of samples	maximum R^2 % of correlation
1 all samples	904	2.9
2 all unweathered samples	639	5.2
3 all unweathered sedimentary samples	565	5
4 all unweathered volcanic samples	79	12.3

Table 5-7, Summary of the scenarios 1 to 4.

The analysis is therefore concentrated on the three boreholes KHD-508, KHD-566 and KHD-583. Boreholes KHD-566 and KHD-583 contain greywacke only while KHD-contains siltstone/mudstone to 122 meters of depth and greywacke from 122 to 222 meters of depth.

Type of Samples	Boreholes	Scenario code	Number of Samples
Weathered and unweathered	all three boreholes	A1	162
	KHD-508	A2	55
	KHD-566	A3	55
	KHD-583	A4	52
Unweathered	all three boreholes	B1	114
	KHD-508	B2	40
	KHD-566	B3	39
	KHD-583	B4	35
Weathered	all three boreholes	C1	48
	KHD-508	C2	15
	KHD-566	C3	16
	KHD-583	C4	17

Table 5-8, Summary of the different scenarios created using data from boreholes KHD-508, KHD-566 and KHD-583.

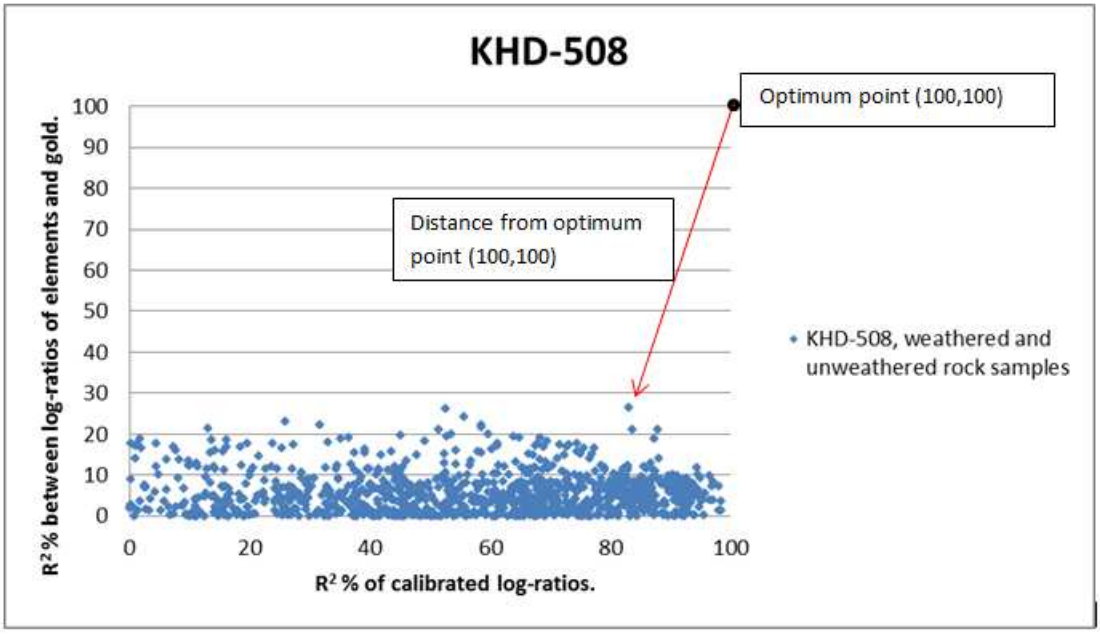

Figure 5-48, Scenario A2 displaying R^2 data in comparison to the optimal point (1,1).

The boreholes KHD-508, KHD-566 and KHD-583 are analysed in more detail. The ten best combinations of R^2 values are presented for each scenario as displayed in appendix Table 10-7, Table 10-8 and Table 10-9.

A t-test was used to test the significance of the correlation coefficients found. The formula used is

$$t = r * \frac{n-2}{\sqrt{(1-r^2)}}$$

Equation 4, t-test formula for testing the significance of the correlations.

t is the t-value

n is number of samples

r is the correlation coefficient.

A significance level of 0.05 was used. Using the significance level and number of samples in each scenario a specific critical value is found against which the t-value is compared. All obtained t-values for the analysis of the three boreholes exceeded the critical value hereby indicating that the correlation is significant and not the result of random values.

A temptation is made to indicate relations between the different scenarios. Table 5-9 summarizes the information from Appendix Table 10-7, Table 10-8 and Table 10-9 by only showing the element ratios and not the values. By comparing the scenario horizontally the different types of rocks (weathered and unweathered) are compared to each other. By comparing the scenarios vertically the influence from each borehole is compared. It must be noted that this analysis does not take into account the number of samples representing each scenario. This is not important when analysing data from one scenario only. However, when analysing the influence of each subset of data compared to the total data set this will be of influence (for example: compare the influence of weathered samples on the data set including weathered and unweathered samples)

The comparison is made by analysing which ratios are present multiple times in the different scenarios. A star "*" indicates ratios that are present multiple time when comparing scenario's within one selection of rock type (apply vertically)

Underlined element ratios written in bold "**example**" apply when comparing scenarios only including samples from a specific borehole or all three borehole (apply horizontally)

Starting with scenario A1 all three boreholes combined and with weathered and unweathered rock samples. It is directly recognized that only one element ratio (Cs/Y) is not present in the results for scenarios B1 and C1. Furthermore scenarios A2 contains three element ratios (Ba/Tl, Ba/Rb, Sn/Y) that also represent three out of the ten best log-ratios in scenario A1. A particular element ratio stands out. Ba/Rb is represented in the scenarios A1, A2, B1 and B2

Borehole KHD-583 seems to display no relation between the three scenarios of A4, B4 and C4. Only one element ratio (Cr/Rb) is also present in the results from other boreholes, namely KHD-508.

According to the information presented in Table 5-9 several suggestions are made.

- The correlation coefficients found prove to be significant at a significance level of 0.05.
- Good correlations between log ratios of elements and gold were obtained using the calibrated data. Several element ratios are present in several scenarios hereby indicating some level of consistency.

- Overall the scenarios in which both weathered and unweathered rock are included (A) seem to be mostly influenced by element ratios which are derived from the unweathered rock (B). This is especially visible in the scenarios A1, B1 and A2, B2. It is suggested to be the result of the difference in number of samples between the unweathered rock samples and weathered rock samples. The effect of correlations derived from the weathered samples will have less influence compared to the correlations derived from the unweathered samples because they are represented by a smaller number of samples.
- Secondly Borehole KHD-508 seems to have the most influence on the overall results when combining all three boreholes together.
- The best correlations with gold are found in the weathered zone. However the element ratios representing the results of weathered rock show only minor correlations to each other and to the rest of the scenarios. The element ratio Cs/Hf is the only one to be present twice in the column for weathered rock (C). As previously stated this may be the result of the limited number of samples, yet a second reason may be the characteristics of the rock. Weathered rock means that mobile elements may have been depleted or brought into the system. This factor would ensure more variance in the chemical composition of the rocks and therefore more variance in the possible correlations.

Boreholes	Rank	Element ratios of weathered and unweathered rock	Rank	Element ratios of unweathered rock	Rank	Element ratios of weathered rock
KHD-508	*1	**Ba/Tl**	**1**	**Tl/Y**	1	Ba/Cs
KHD-566	*2	**Ba/Rb**	**2**	**Ba/Tl**	2	Li/Y
KHD-583	3	Cs/Y	**3**	**Rb/Y**	3	Li/Zr
together	*4	**Sn/Y**	*4	Th/Y	*4	**Cs/Hf**
	5	**Be/Y**	*5	**Ba/Rb**	5	Hf/Li
	6	**Rb/Y**	6	K/Rb	**6**	**Cs/Zr**
	7	**Cs/Zr**	**7**	**Sn/Y**	7	Ca/P
	8	**Cs/Hf**	8	Rb/Zr	8	Cs/Undef
	9	**Ba/K**	9	Tl/Zr	9	Zn/Undef
	10	**Tl/Y**	**10**	**Be/Y**	**10**	**Ba/K**
KHD-508	**1**	**Ba/Cs**	**1**	**Ba/Tl**	1	Cr/Sr
	*2	**Ba/Tl**	**2**	**Ba/K**	2	Fe/Y
	3	**Ba/K**	**3**	**Ba/Cs**	3	Cr/Undef
	*4	**Ba/Rb**	*4	**Ba/Rb**	4	Cr/Na
	*5	Sn/Y	*5	Cr/Cs	5	Al/Cr
	6	Sr/Th	*6	Cr/Rb	6	Cr/Ga
	7	**Cs/Sr**	**7**	**Cs/Sr**	7	Cr/Y
	8	La/Sr	8	Na/Tl	8	Be/Cr
	9	**Be/Sr**	**9**	**Cs/Na**	9	Cr/Hf
	10	**Cs/Na**	**10**	**Be/Sr**	10	Cr/Zr
KHD-566	1	Ca/Zr	1	Cs/Ti	1	Mg/Zr
	2	**Ca/Sn**	2	Ga/Th	2	Cs/Zr
	3	Ca/Y	3	Rb/Sn	3	Hf/Mg
	4	Ca/Hf	4	Ca/Cs	4	Mg/Pb
	5	Ca/U	5	Li/Mn	*5	Cs/Hf
	6	Ca/Ce	*6	Th/Y	6	Mg/Sn
	7	**Ca/Ga**	**7**	**Ca/Sn**	7	Mg/Sc
	8	Ca/Pb	8	Ca/In	8	Ga/Mg
	9	Ca/Ge	9	Mn/Zn	9	Mg/U
	10	Ca/La	**10**	**Ca/Ga**	10	Mg/Th
KHD-583	1	Cs/Zn	1	Cr/K	1	Ni/Rb
	2	Ca/Sn	*2	Cr/Rb	2	Ni/Ti
	3	Sr/Zn	3	Cr/Zn	3	K/Ni
	4	Ca/P	4	Cr/Undef	4	Fe/Tl
	5	Ca/Th	5	Cr/Tl	5	Tl/Zn
	6	Be/Ca	6	Ba/Cr	6	Sc/Tl
	7	Cs/Ni	7	Cr/Cs	7	Ge/Tl
	8	Ni/Sr	8	Cr/Ni	8	Cs/Ni
	9	Be/Zn	9	Cr/Zr	9	Rb/V
	10	Cs/V	10	Al/Cr	10	Cs/Zn

Table 5-9, Summary of the results obtained from analysing boreholes KHD-508, KHD-566 and KHD-583.

5.2.6 Summary

Primary analysis of the different data sets reveals that the data acquired with the portable XRF unit may not reliable for all elements. The plastic bags used in the analyses have greater concentrations of: As, Cd, Ce, La, Nb, P, Sn, U and W compared to the rock pulps. Several elements which should be recorded accurately with the portable XRF unit are not measured quantitatively and qualitatively as is the case for Nickel. Using a linear trend line the elements with R^2 >9 0% were corrected before being used in further analysis.

The use of log-ratios solves

The results from the lithographic differentiation are consistent. The bulk of the volcanic rock is mafic however intermediate and a felsic sample were also encountered. The lithology characterized as greywacke in the pre-existing database has been subdivided into greywacke A which follows the trend of siltstone/mudstone and greywacke B which differs. A relationship between volcanics, conglomerate and greywacke B is suggested by the analysis of the Harker plots.

The lithological differentiation also partially supports the findings of the petrographic study. The major element analysis displaying the CaO content may support the presence of feldspars in the volcanic and conglomerate rock. Both the volcanic rock and conglomerate show the highest CaO values and both are the only ones to contain feldspar which contains calcium. The gradual change in texture of the greywacke from fine grained to coarse grained towards the North is reflected in the major element analysis as is described above.

The results obtained through the application of PLSR are not conclusive. Better correlations are achieved with smaller datasets. The higher R^2 values obtained for the volcanic rock samples are still very low (maximum 34.5% and 27%). Such values cannot effectively be used to predict gold occurrence on the basis of element content in rocks. considering that the calibration method used is mathematically incorrect these results may not be representative.

Secondary analysis of the X-50 Mobile XRF dataset using adequate calibration method using log-ratios respects the constant sum constraint and is therefore thought to be mathematically correct. The results obtained from the correlation analysis of calibrated log-ratios reveal to be difficult to interpret taking into account the geology. Large data sets such as (all unweathered samples, volcanic samples and sedimentary samples) result in poor correlations. The analysis of singular boreholes yields better results yet it must be questioned if these are applicable to the entire mine.

5.3 Spectral analysis

5.3.1 Overview

In this part of the results the totality of the spectral results is displayed. The first part of this chapter is concerned with the data quality of the spectral dataset. The goal is to find a relation between the spectral data and the gold and/or the lithologies present in the Koolhoven pit. Preferably a succession of mineral assemblages vectoring towards the gold deposition would be identified. All spectra used for the analysis can be found in Appendix F.

5.3.2 Data validation

The 10 measurements taken before and after the scratching of the rock can be used in several ways. The total 20 spectra are displayed in Appendix Figure 10-24. First it is clear that all red and all blue spectra display the same shape with absorption features at the same wavelengths. This proves that for homogeneous samples with no specific special feature such as large pyrite grains or veins and of homogeneous composition, the spectra do not change between closely situated measurements locations. This is applicable for homogeneous volcanics as well as sediments with particle sizes up to sand. In the case of conglomerate it is advised to take several measurements because clasts of different composition will have a greater effect on the spectra due to their greater size compared to the probe window.

The two different sets of spectra (red and blue) also indicate that scratching the rock does not affect the location the absorption features and that no absorptions are added/removed.

To quantify the increase in reflectance between all the measurements before and after scratching, the sample was divided into 10 intervals and measured repeatedly. The percentage increase of reflectance for each wavelength per spectrum was calculated. This was then averaged over all the wavelengths of the same spectra (Table 5-10) and later averaged once more for all ten spectra together.

Location	1	2	3	4	5	6	7	8	9	10
Increase in reflectance %	3.25	43.69	27.00	29.88	61.47	50.63	46.05	36.46	30.65	19.94

Table 5-10, Average increase of reflectance for each spectra.

The average increase in reflectance of all the spectra is 34.90 %. The values and spectra in Appendix Figure 10-24 clearly show the importance of minimal preparation (10 second scratching or less by location).

By increasing the level of reflectance the signal to noise ratio increases hereby improving the overall spectra. This is of great importance when using automatic data extraction. Poor spectra of low reflectance do however remain. The issues using automatic data extraction arise for example for the determination of crystallinity values as will be discussed later.

The interpretation by TSA should be regarded as an indication. If we strictly abide by the ranges of absorption for specific minerals it becomes clear that the interpretation is not always correct. For example when determining the white mica composition the wavelength of absorption for the AlOH feature (Appendix Figure 10-26) may not fall within the ranges depicted by Table 5-13 due to mixing

of the responses from different minerals. TSA indicates a specific mineral yet it may be more reliable to look at the position of the wavelength of absorption instead of the specific name given by TSA. For this reason interpretation of the data is a combination of TSA and objective automatic feature extraction.

TSA interpretation of quantities should only be regarded as an indication as well. By default in TSA the mixing percentages are based on two minerals only while in reality more may be present. The level of absorption is not always related to the content of the same mineral. Some minerals may be present in high quantities but only yield shallow absorptions as is the case for carbonate. The intensity of the absorption may also be affected by the crystallinity of the mineral.

5.3.3 Data processing using The Spectral Geologist 7

Three groups of minerals: Kaolinites, White Mica's and Chlorites dominate the overall mineralogy of the deposit (Table 5-11). The percentages displayed should only be regarded as indications as is discussed in the part of data validation 5.1.2.

Mineral group	Mineral	Percentage from TSA
Kaolinites	Kaolinite WX	7.9
	Kaolinite PX	1.9
White Mica's	Muscovite	4.0
	Paragonite	91.4
	Paragonitic illite	3.1
Chlorites	Fe Chlorite	38.7
	Fe Mg Chlorite	5.4

Table 5-11, Mineral groups together with the specific minerals and there percentages of occurrence. WX=high crystalline, PX is low crystalline.

5.3.3.1 Dominant mineral group

Appendix Figure 10-25 illustrating the dominant mineral groups as a function of the wavelength shows four different clusters of absorption. Table 5-12 indicates the relation between the clusters identified in Appendix Figure 10-25 and the feature to which they can be attributed to according to the wavelength position of the absorption.

Cluster	Centre wavelength (nm) of the cluster	Features and their wavelength ranges of absorption (nm)
1	2195	AlOH (2160-2220)
2	2205	AlOH (2160-2220)
3	2255	FeOH (2230-2295)
4	2330	MgOH (2300-2360) and/or CO_3 (2300-2350)

Table 5-12, Approximate centre wavelength of the clusters in relation to the feature it belongs to (nm) according to (AusSpec International, 2008).

5.3.3.2 White mica composition

Two clusters are distinguished in Appendix Figure 10-26. According to Table 5-13 the left cluster concentrated around 2192 nm should be attributed to the presence of paragonite. The cluster concentrated around 2206 nm belongs to muscovite. As can be observed not all data points fit in the ranges depicted by Table 5-13. Several factors may contribute to this. Mixing of different minerals is

due to affect the wavelength position for the AlOH feature (as will be illustrated below). Another cause of inaccuracy could be related to the probe. The spectral device heats up over time. Although regular calibration was performed the heating of the device could have caused a slight shift in wavelength measurement.

Although the absorptions between 2200 and 2208 nm would be attributed to muscovite a closer look at the data reveals that most absorptions in this range contain a double absorption feature and are in fact linked to the presence of kaolinites (Appendix Figure 10-32 & Appendix Figure 10-33). The spectra with an absorption feature between 2208 and 2213 nm were interpreted and associated with muscovite (Appendix Figure 10-34) and penghite (Appendix Figure 10-35). This interpretation does not follow the ranges suggested in Table 5-13. Mixing of minerals is a likely source for this issue. Heating of the ASD machine may also contribute to a shift in wavelength of absorption.

mineral	Wavelength range (nm)
Paragonite white mica	2180-2190
Muscovite white mica	2200-2208
Phenghite white mica	2216-2228

Table 5-13, Interpretation of white mica's in relation to the wavelength position of the AlOH absorption feature (AusSpec International, 2008).

5.3.3.3 White mica crystallinity

The histogram in Appendix Figure 10-27 displaying the white mica crystallinity exhibits two peaks (for calculation procedure of white mica crystallinity see paragraph 4.1). One centred on crystallinity 1 and the second around 4. A closer look at the spectra from which the crystalinity has been determined shows that the majority of the samples resulting in a crystallinity of around 1 are not suitable for accurate analysis. For example, reflectance spectrum KHD-613_00142 shows minimal absorptions (Appendix Figure 10-32 & Appendix Figure 10-36). By applying the Hull quotient corrections these minimal absorptions are exaggerated. Slight inaccuracies in the spectra will also be exaggerated. This is visible in the Hull quotient corrected spectrum (Appendix Figure 10-36) in which the amplitude of noise at both ends of the spectrum are significant. Inaccuracies in the reflectance spectra may also be exaggerated by the Hull quotient correction to the point that they may be interpreted as an absorption feature hereby resulting in wrong interpretation.

5.3.3.4 Relative proportions of: 1. White mica: chlorite and/or carbonate, 2. White mica: Smectite

Both features are calculated by using depths of absorptions. It has been discussed in the part on data validation that these parameters should be used as an indication and not as true value. The values for both parameters are used to define relative changes between different rock samples. In the case of the relative proportion of white mica versus chlorite and/or carbonate, (Appendix Figure 10-29) clearly indicates that the white mica's are dominant (majority of data points have a value > 1). In the case of the relative proportion of smectite, Figure 1016 shows that smectite is not the dominant mineral (majority of data points have a value <1).

5.3.3.5 Composition of Chlorites and Carbonates.

An attempt was made to characterize the composition of chlorites and carbonates throughout the different spectra. The results shown should be used with precaution and even dismissed in the case of carbonates due to the following reason. Quote: " the main problem in the interpretation of spectra of carbonate zone samples is that carbonate is typically weakly absorbing relative to other

minerals such as white mica and chlorite that are strongly absorbing in the SWIR" (AusSpec International, 2008, p.43). The carbonate composition is based on the wavelength position of the MgOH absorption which may also be present in chlorite and white mica's. The analysis of dominant mineral group Appendix Figure 10-25 shows white mica's are the dominant group and especially paragonite is common. Therefore MgOH wavelength position may be the result of a white mica multiple instead of diagnostic for carbonate composition.

In the case of chlorite, the composition is determined on the basis of the wavelength position of the FeOH feature (Appendix Figure 10-31). The results could be affected by other minerals containing FeOH. Following the ranges depicted by (AusSpec international, 2008) (Table 5-14) the FeOH wavelength of absorption can be translated into chlorite composition. The higher the FeOH wavelength of absorption the higher the Fe content. Lower FeOH wavelengths of absorption reflect higher Mg and lower Fe content.

Mineral	Wavelength range FeOH (nm)
Mg chlorite	2240-2249
Intermediate chlorite	2250-2256
Fe chlorite	2257-2265

Table 5-14, Chemical composition interpretation of chlorites in relation to the wavelength position of the FeOH absorption feature (AusSpec international, 2008).

The cluster in the histogram of Appendix Figure 10-31 concentrated around 2243 nm fits in the range belonging to Mg chlorite. According to Appendix Figure 10-31 and Table 5-14 Mg chlorite clearly forms the minority of the chlorite. The Intermediate and Fe chlorites form the bulk of the chlorite compositions. Because the ranges of the FeOH absorption specific to the different types of chlorite have different sizes it is difficult to determine from the histogram if intermediate chlorite or Fe chlorite is more present. The number of spectra within each range depicted by Table 5-14 is counted and displayed in Table 5-15. Because the analysis follows the ranges given by AusSpec international, 2008 the wavelengths between 2249-2250 and 2256-2257 nm are not taken into account. The differentiation results are displayed in Table 5-15.

Chlorite composition	Count	% of specific chlorite composition compared to the total number of chlorites
Mg chlorite	122	13
Intermediate chlorite	349	37
Fe chlorite	478	50

Table 5-15, Number of rock samples with specific chlorite composition.

5.3.3.6 Relation to gold

To relate the extracted parameters to the gold content scatterplots were created for gold against: AlOH wavelength of absorption (Appendix Figure 10-26), white mica crystallinity (Appendix Figure 10-27), relative proportion of white mica against chlorite and carbonate (Appendix Figure 10-28), the relative proportion of smectite (Appendix Figure 10-29), carbonate composition (Appendix Figure 10-30) and chlorite composition (Appendix Figure 10-31). These may enable us to find relations between gold content and minerals active in the SWIR range irrespective of the lithology. In all six

figures gold seems to concentrate in the same ranges as where the most data points are concentrated. No clear correlation or anomaly can therefore be fixed.

5.3.3.7 Lithologies

The spectra were also used to define differences in lithologies. The first separation of lithologies was performed according to the pre-existing drill logs. All samples were classified either as volcanic or sedimentary.

All parameters presented in above were compared to the lithology. Only the white mica shows differences. Separating volcanic rock from sediments and plotting these against the AlOH absorption feature wavelengths reveals that the muscovite is concentrated in the sediments (Figure 5-49). All three degrees of alteration in rocks (saprolite, transitional and fresh rock) contain both paragonite and muscovite (Figure 5-50) however when analysing the dominant mineral group for all three alteration groups it appears that there is a decrease in chlorite and carbonate from fresh rock to transitional rock to saprolite (Figure 5-51). When investigating the AlOH absorption feature wavelength per borehole, it is clear that not all boreholes contain muscovite. However there is only one borehole that contains muscovite only and no paragonite; borehole KHD-593 (Figure 5-52).

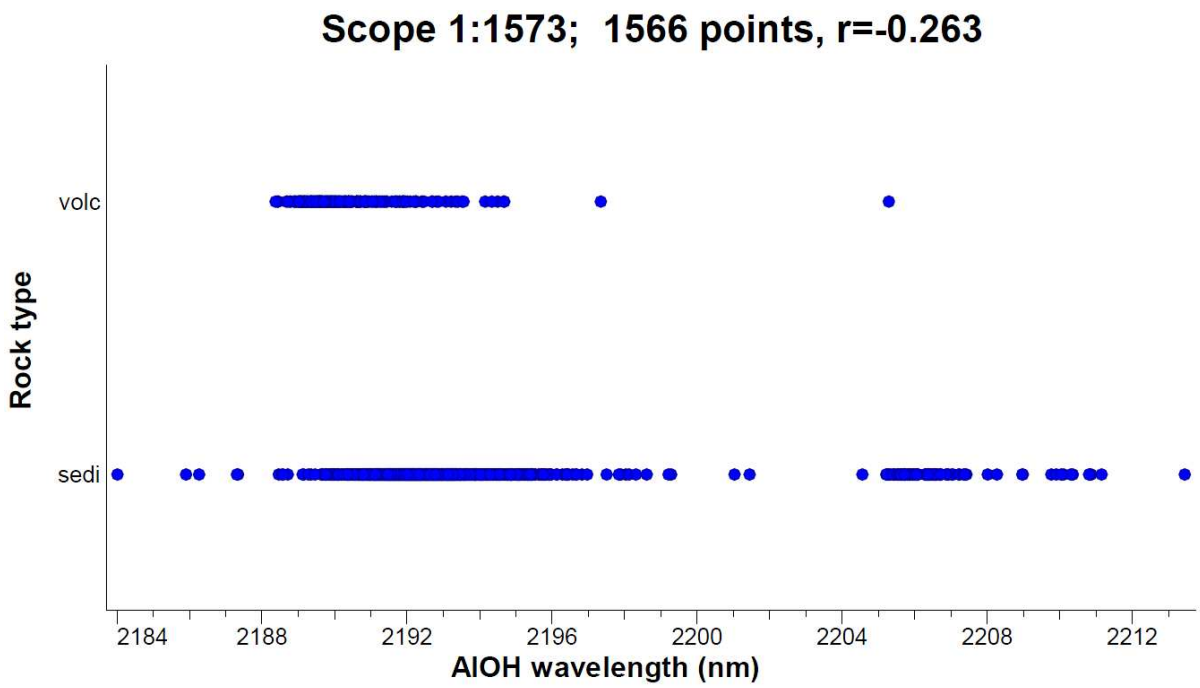

Figure 5-49, Volcanic and sedimentary rock versus the AlOH wavelength of absorption, volc = volcanic and sedi = sediment.

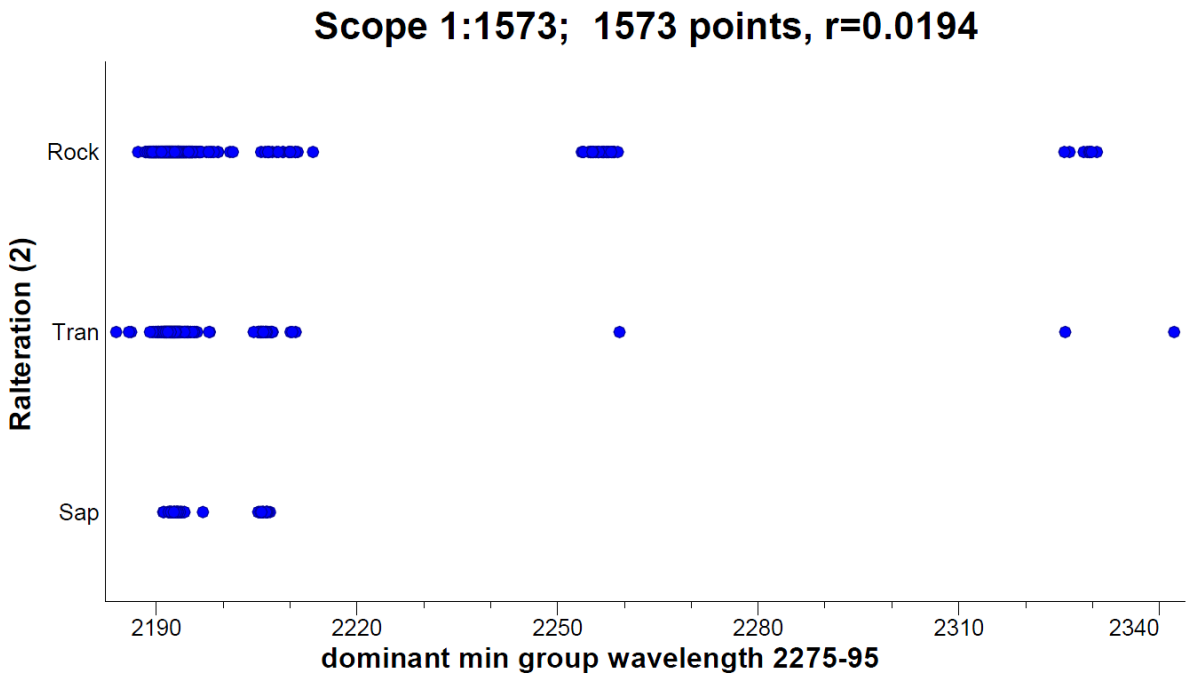

Figure 5-50, Ralteration = rock alteration, versus the dominant mineral group.

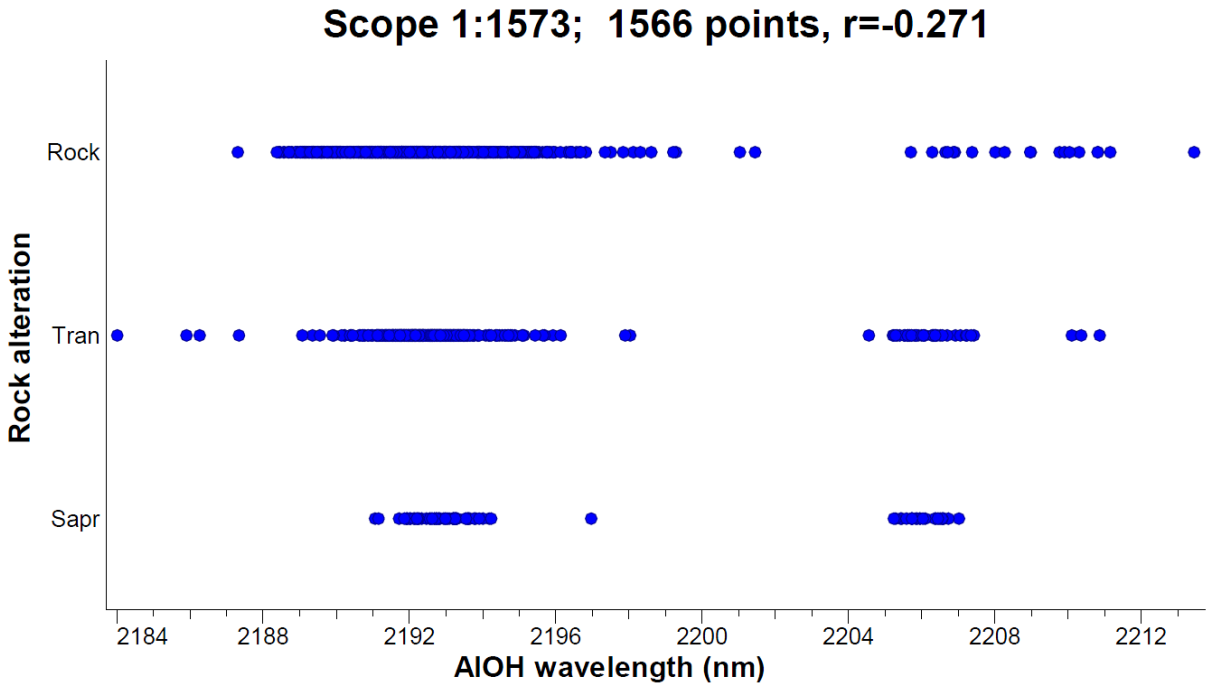

Figure 5-51, Rock (fresh), transitional rock and saprolite are plotted against the AlOH wavelength of absorptions. All three degrees of alteration contain both paragonite and muscovite.

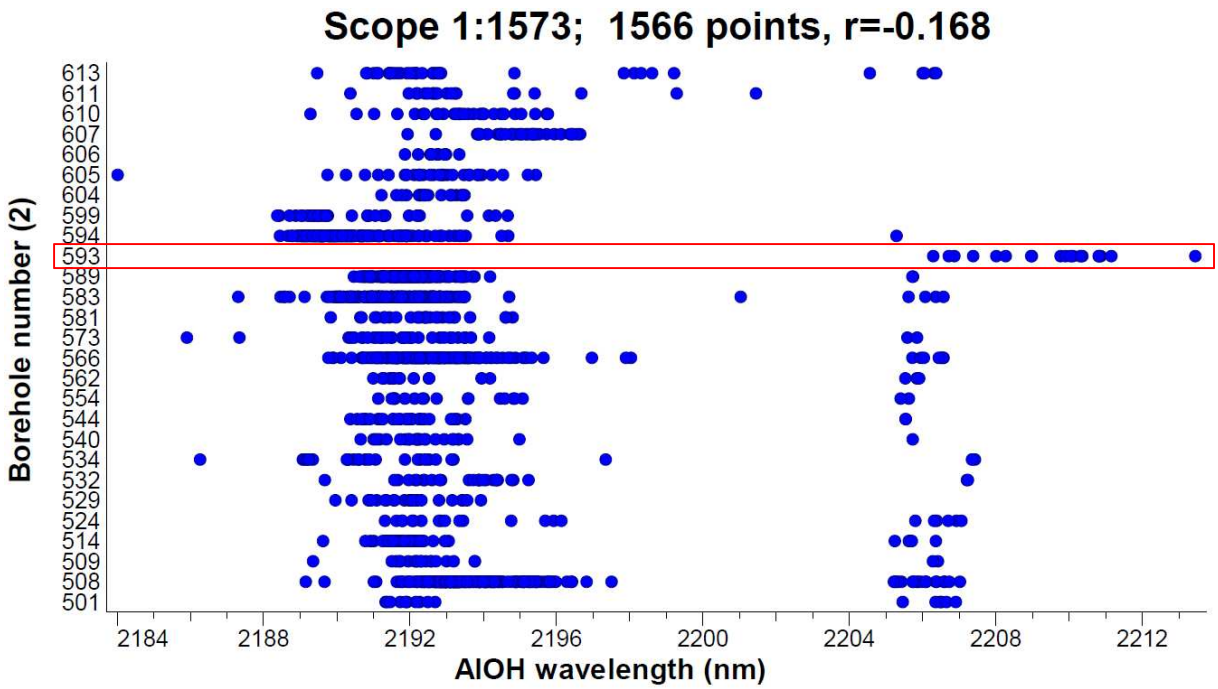

Figure 5-52, AlOH wavelength of absorption per borehole. Borehole KHD-593 is the only borehole to contain no paragonite.

5.3.4 Partial least squares regression

The results from the PLSR simulations are represented in Table 5-16.

Fresh rock only	Simulation	Number of samples	R^2 % for consistency test	R^2 % for cross validation test
All samples	1	750	2.3	1.2
	2	750	8	0
	3	750	2.5	1.6
Sediments	1	565	100	9
	2	565	100	0
	3	565	100	1
Volcanics	1	185	34	27
	2	185	24	12
	3	185	32	26

Table 5-16, Results for the PLSR simulations on the spectra derived from fresh rock.

The R^2 obtained in the consistency test eventually reach 100 % Figure 5-53. Although this may seem good roughly 70 components per simulation are used to achieve this which means that there is no specific variance in the first derivative of the spectra that can be linked to the gold content.

The cross validation procedure clearly indicates that there is no correlation between the spectra and the gold content as well.

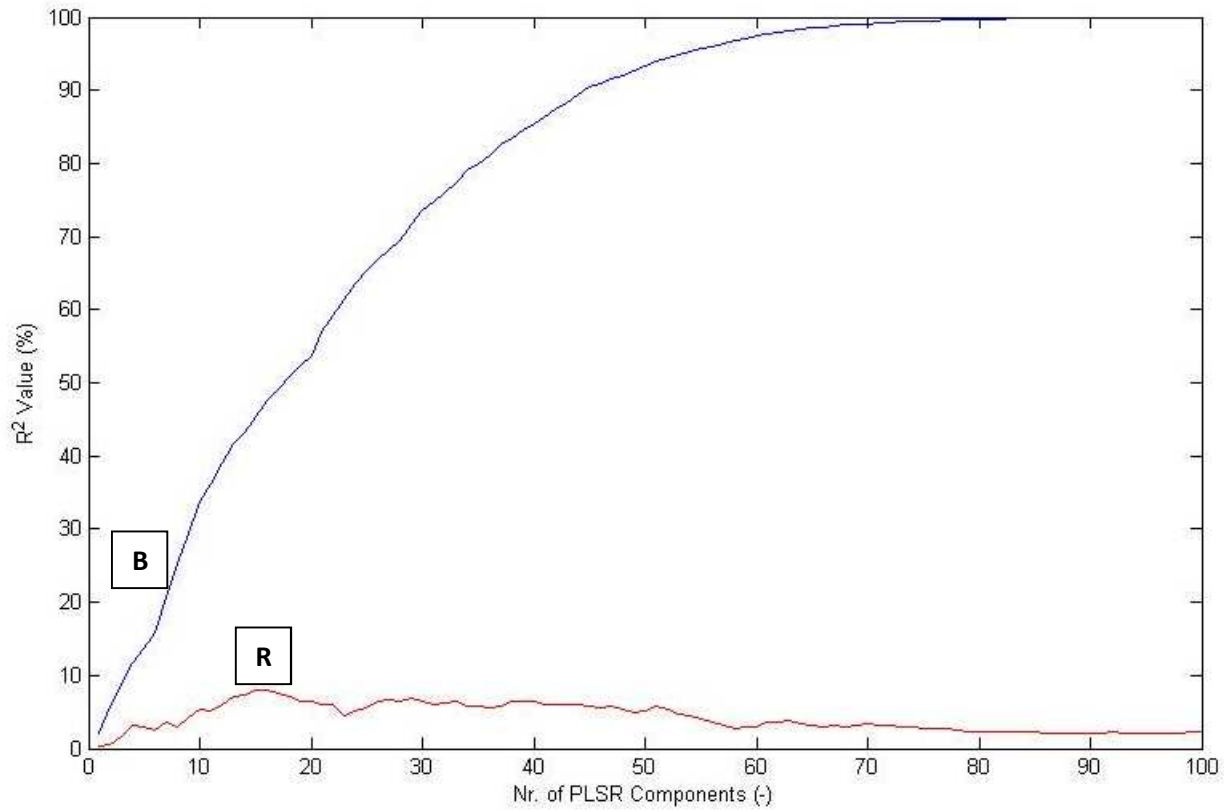

Figure 5-53, R^2 values for simulation 1 of the sediments.

5.3.5 Summary

The dominant mineral observed is paragonite which according to (AusSpec International, 2008) should be regarded as the background signal. No specific link has been found between the spectral data and the gold deposition using visual interpretation of the data processed in TSG7 and by using PLSR simulations. Two particular results deserve attention because they do not follow the general trend. First, the volcanic rock presents only one data point containing muscovite. Secondly borehole KHD-593 which is the furthest away from the mineralized zones is the only borehole which does not contain paragonite. Although this involves only a single borehole this could be an indication of varying white mica composition away from the deposit.

Several results can be related to the petrographic analysis. The VNIR spectral analysis suggested that the carbonate signal was overshadowed by the white mica and chlorite responses. This suggestion is supported by the petrographic analysis which stated that higher concentrations of carbonate were present compared to chlorite. The detected iron feature was attributed to the Fe-chlorite hence the presence of calcite as a carbonate mineral is partially supported.

6 Discussion

By interpreting the various data sets presented in chapter 5 no trend vectoring towards the deposition of gold is suggested. The discussion presented below is divided into three parts. The first part will discuss the forming of the different lithologies present in the Koolhoven deposit and the relations between these. The second part will discuss the alteration characteristics of the Koolhoven deposit. The goal is to relate the results to the geological setting and literature to clarify the geological evolution of the deposit and make a temptation at placing the Koolhoven gold deposit in an alteration system as proposed by chapter 2. The third and last part will focus on the discussion of the data obtained using the X-50 Mobile XRF device.

6.1 Lithology characterization

The lithologies of the Koolhoven deposit include

Volcanic rock:

- The bulk of the measurements indicate mafic composition.
- Intermediate and felsic volcanic rock was also encountered.

Sedimentary rock:

- Siltstone/mudstone.
- Greywacke:
    - Fine greywacke A with an element composition resembling that of siltstone/mudstone.
    - Coarser greywacke B with an element composition closer to that of the conglomerate instead of siltstone/mudstone.
- Sandstone.
- Conglomerate.

The differentiation of lithologies has proven to be possible on the basis of element content for most lithologies. Greywacke A and siltstone/mudstone cannot be differentiated effectively on the basis of their major-element content and should therefore be separated from each other on the basis of visual interpretation. Greywacke A lacks the layering texture of the siltstone/mudstone.

While the report of Rosebel Gold Mines NV (2011) stated that felsic volcanic rock is present in the Koolhoven pit the results obtained in this research project suggest that felsic volcanics make up only a minor part of the volcanics. The samples including volcanic rock were derived from only three boreholes (KHD-534, KHD-594 and KHD-599). The difference between the results presented in this report and the results shown in Rosebel Gold Mines NV (2011) may be related to the sampling location.

The results presented in this report are supported by Watson (2008) and Daoust, et al (2011).

Not only is it possible to differentiate the different lithologies from each other, it is also possible to link them to each other in a geological context. According to the results obtained during the course of this project the forming of the different lithologies in the Koolhoven deposit can be described as such:

The basaltic composition of the rock suggests formation near seafloor margins (Skinner, et al., 2004). The basaltic rock is therefore interpreted to be the result of the Eorhycian oceanic state (Figure 2-3). The sedimentary sequence starts with a distal siltstone/mudstone interval displaying clear turbidite texture (Figure 5-1) conformably overlaying the volcanic rock. The siltstone/mudstone interval gradually changes towards greywacke A which displays the same major element composition. Shallowing of the depositional environment leads to erosion of previously deposited lithologies such as the volcanic rock and shorter transportation distances. The transition from greywacke A to greywacke B illustrates this change in depositional environment. Greywacke B contains coarser clasts than greywacke A (Figure 5-2 & Figure 5-3), supporting the idea of shorter transportation. The element content of greywacke B (paragraph 5.2.3) and the petrographic analysis of the thin-sections support the idea of clasts of volcanic composition being present in greywacke B.

The transition from greywacke B to the conglomerate rock in the North of the Koolhoven pit indicate a further shallowing of the depositional environment. The greywacke B interval is first intercalated by conglomeratic lenses varying from a thickness of tens of centimetres to several meters. Eventually the massive interval of conglomerate rock is deposited. The large size of the clasts indicates a high energy depositional environment such as torrential rivers and short transportation distance. The entire system is then tilted due to tectonic activity, and pull apart basins are created as a result of strike slip movement. The Rosebel sandstone formation is deposited in such a pull-apart basin. A conglomeratic interval of the Rosebel formation was not encountered. The sandstone interval of the Rosebel formation displays typical sandstone characteristics; High SiO_2 content and low Al_2O_3 content. The conglomerates on top of the unconformity between the Armina and Rosebel formation were not intersected.

6.2 Alteration

To describe the alteration superimposed on the geology as illustrated in paragraph 6.1 several sources of information are to be used:

- Visual observations from during the sampling process.
- VNIR spectral analysis results.
- Petrographic analysis of thin sections.

From the visual interpretation of the various datasets and results from the PLSR simulations it can be concluded that no trend has been found vectoring towards gold deposition. The fact that the results presented in chapter 5 do correlate with the background presented in chapter 2 indicates that the Koolhoven pit may still be part of an alteration system.

The similarities between the results obtained in the course of this research project and previously performed research as presented in chapter 2 are summarized below.

- The lithologies identified and the geological evolution suggested are in accordance with (Daoust, et al., 2011) as discussed in paragraph 6.1.
- Field observations yielded the following important findings:
  - A graphite layer is present in the Koolhoven pit.
  - Bleaching near the veins has been observed.
  - Carbonate spots.
  - Sulfide porfyroblasts were found near the veins.
  - Sericitization near the veins has also been detected.

  The above mentioned points are all supported by (Goldfarb, et al., 2012).

- The VNIR spectral analysis revealed that:
  - The dominant minerals throughout the deposit are paragonite, Fe chlorite and carbonate (calcite and dolomite were identified by petrographic analysis of the thin sections).
  - The carbonate response is overshadowed by the chlorite response.

  This is in agreement with the information presented by AusSpec International (2008) and Pontual (2012).

- The petrographic analysis of the thin sections:
  - The mineral composition of het host rock and veins is in accordance with the information presented in chapter 2. The veins contained: quartz, carbonate, chlorite, white mica's and tourmaline which is in accordance with Eilu & groves (2001), Dubé & Gosselin (2007), Robert, et al. (1997,2007) and Daoust, et al. (2011).
  - Due to the lack of deformation the timing of the veins was determined to be late compared to the main deformation stage. This is in accordance with (Daoust, et al., 2011).

As a result, several scenarios are presented to suggest why no alteration halos were found around the Koolhoven gold deposit:

- There are no large scale alteration halos.

  Chapter 2 state: in general no distinct mineral zonation is observed (Robert, et al., 1997; Robert, et al., 2007; Dubé & Gosselin, 2007). If this is true then no mineral zonation should have been found. However, on the small scale close to veins higher concentrations of sericite and pyrite were found.

- The lateral scale of the alteration halo around gold deposition is larger than the scale on which the samples where acquired.

  Scale plays a major role in all geological processes. In this research the scale range is from pit scale to microscopic scale. Alteration halos may however exceed the scale of the sampling area.

- A late overprinting of the alteration characteristics due to one or more hydrothermal events has removed the characteristic features of the alteration halo linked to the gold deposition.

  If this is true the chance is high that the small scale alteration characteristics recognized by field observations would have been overprinted and not be recognized anymore. But they were detected hereby indicating that overprinting must have been minimal. Furthermore the late timing of veining and gold deposition as suggested by the petrographic study reduces the chances of having an overprint simply because there would have been less time for this.

- The gold values are so low that the no clear gold deposit can be located.

  The gold values are indeed low, however, as stated before, gold is only is the product we want to extract but may not be the first characteristics geologist would be looking for to locate it. Gold is not the source of the alteration halo. The veins together with the hydrothermal fluid which carried the gold is the source for creating a thermal gradient around resulting in alteration halo's.

- The coverage of boreholes is not sufficient to capture the variability within the deposit.

  Although the coverage of boreholes is recognized to be sub-optimal if any consistent variation in alteration would be present it should be detectable even with only a few boreholes. The specific investigation of boreholes KHD-508, KHD-566 and KHD-583 covers the shorter ranges around the gold deposition. This ensures that even alteration halo's with a lateral extend smaller than the minimum distance between different boreholes would have been detected. The downhole plotting of elements suggested such small scale halos in the form of a correlation between calcium, arsenic and gold deposition.

- Too many different lithologies are present with each different physical characteristics and geo-chemistry.

  Different lithologies not only contain different elements but will also behave in a different way. The different element compositions of the lithologies (as illustrated in paragraph 5.1.3)

will enable or not certain reactions. The different behaviour of the lithologies has been shown by graph 5.2.3 which clearly indicated the lower content of muscovite in volcanic rock compared to the sediments.

The fact that small scale alteration was found around veins and that the results found show great similarities with previously performed research dismisses the possibility that no mineral zonation is present as suggested in the first scenario. The scenario believed to be the most probable is the second one and will be discussed in more detail below.

Scale plays a major role in all geological research. In this research project the scale varies from pit scale to microscopic scale. The pit which has a maximum length of 1700 meters along the strike of the geological structures is the upper limit of our scale (Figure 6-1). This however, does not need to be the limit for the scale of the gold deposition system present on the Rosebel concession.

If we take the oval perimeter shown in Figure 6-1 with the longest length of 2.5 km and perpendicular width of 1.3 km we observe that 27 out of 28 boreholes fall within the boundaries of the oval. The importance of this perimeter is that it shows how close all the boreholes are to the actual gold deposition.

Borehole KHD-593 suggests a different mineral assemblage may be present away from the deposit according to the results of paragraph 5.2.3. This should be regarded as a clue for further research but should not be accepted as a conclusive result since it is only based on one borehole.

As stated in chapter 2 and 5 the three mineralized zones in Koolhoven are related to shear zones. All three are parallel to the main shear zone which runs south of the volcanic.

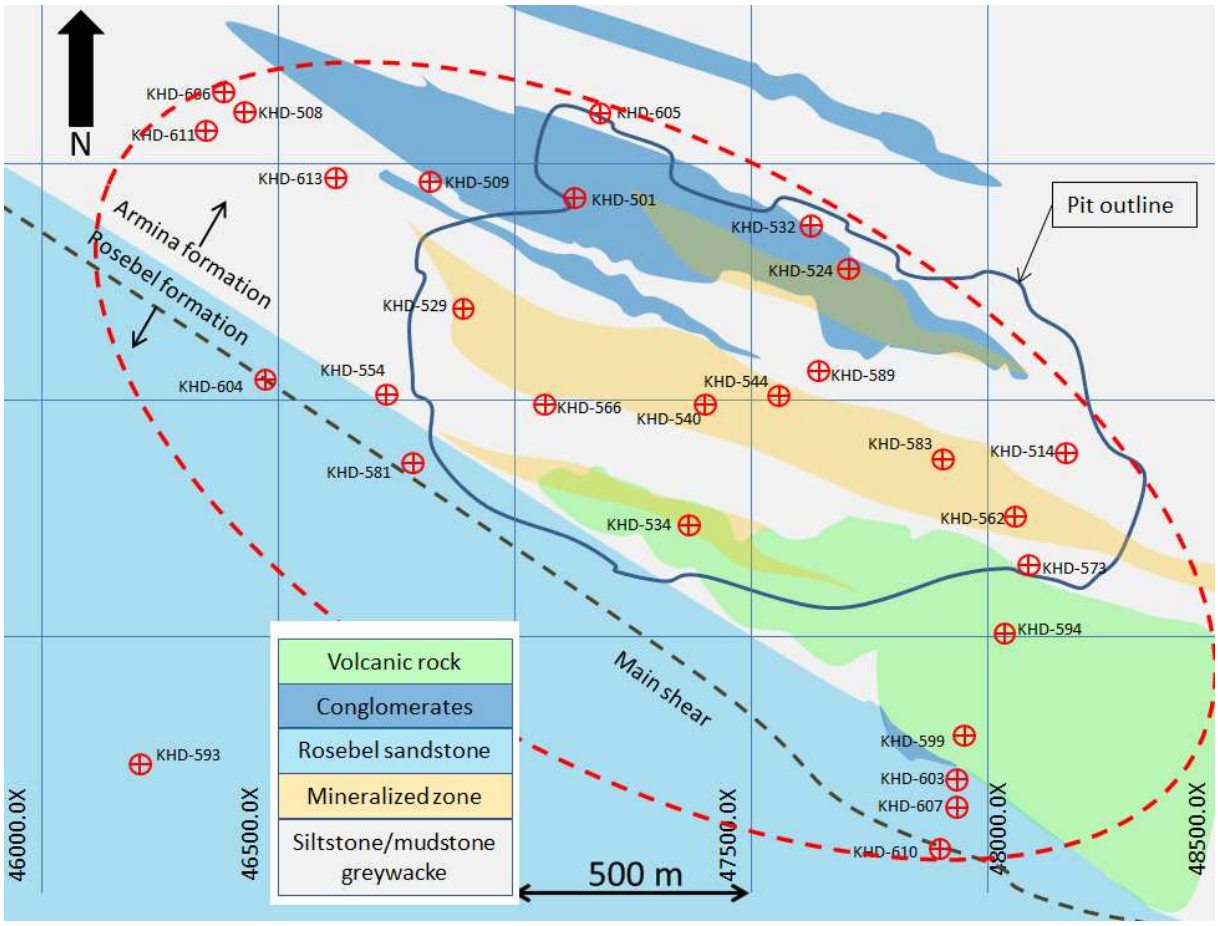

Figure 6-1, Hypothetical oval shape displaying the close proximity of the samples.

From literature it follows that alteration halo's may range from 20 to 200 meters or be greater than 1 to 2 km (Table 2-1). The higher range of alteration halos would by far exceed the size of the area of investigation. Furthermore the Koolhoven deposit should not be regarded as an isolated gold deposit in the Rosebel concession. The deposits J-Zone, Koolhoven, Pay Caro and East Pay Caro are all three concentrated along shear zones related to contact between the volcanic rock and the Armina and Rosebel sedimentological formations. When drawing a second perimeter on the scale of the Rosebel concession including all four deposits it becomes clear that the sampling performed for this research project does not reach outside the gold system.

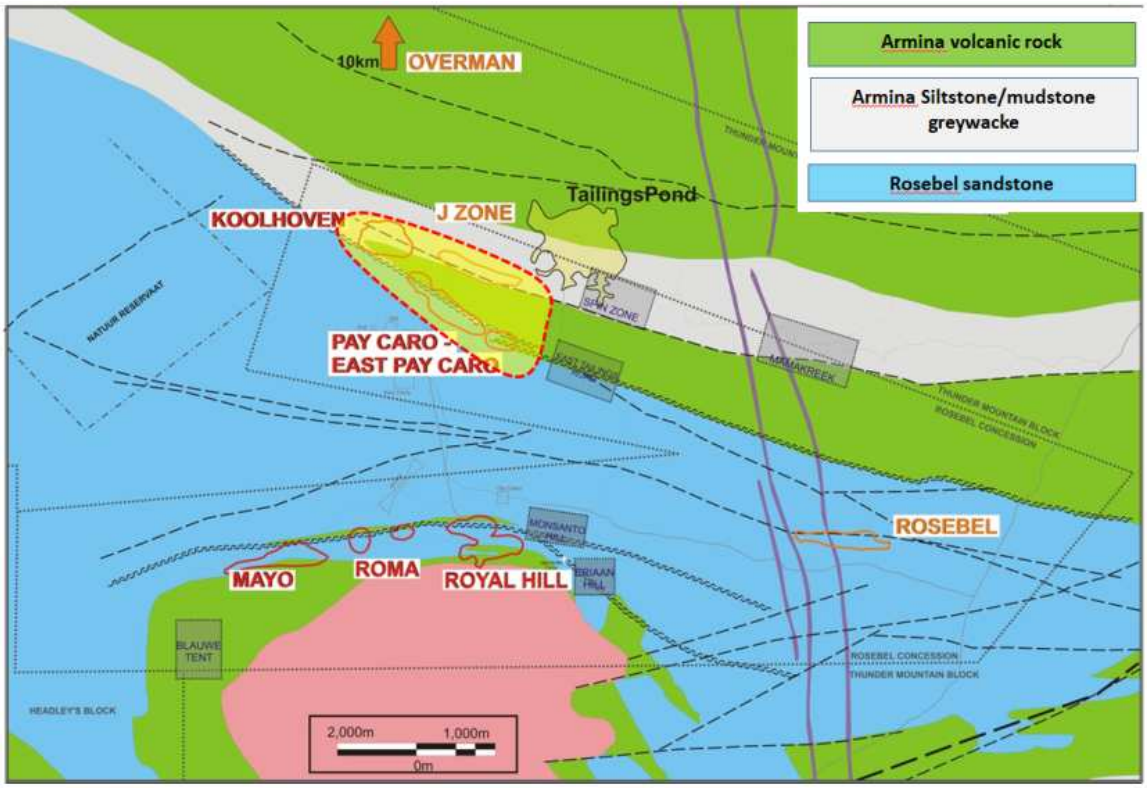

Figure 6-1, Map of the Rosebel concession with a perimeter including the deposits: Jzone, Koolhoven, Pay caro and East Pay caro.

The reason why no large scale alteration halo was found around the Koolhoven gold deposit is therefore believed be the result of a too small sampling area. In chapter 2 it was stated that the halo may envelop an entire deposit (Robert, et al., 1997; Dubé & Gosselin, 2007). This idea implicates that the sampling should therefore reflect the more proximal characteristics of the gold deposit. The presence of a strong carbonate alteration, sericite, sulfide porfyroblasts near the veins, magnetite, hematite, and plagioclase all indicate the proximity to the gold deposition according to the information presented in chapter 2.

6.3 X-50 Mobile XRF dataset

The fact that the direct applications of OLS on the element concentrations one by one does not guarantee to fulfil the constant sum constraint clearly indicates the shortcoming of this method.

The correlation analysis using log-ratios yields stable and objective results. The results obtained from the correlation analysis using log-ratios however, may reveal to be challenging to interpret, especially when taking into account the geology. At this stage the only consideration of geology taken into account is by separating the dataset per lithology and or weathered versus unweathred rock.

Several particularities have been recognized in the results of the correlation analysis using log ratios. The next four particularities may appear dubious yet all four are mathematically sound.

- The best result for the scenario in which all three boreholes are included and only fresh samples are used is obtained with the log-ratio of Tl/Y. Although this log-ratio yields the highest R^2 for correlation it is difficult to accept the result as useful since the R^2 of the element ratio (calibration) is of 0.06. This is purely the results of the criteria which we used

to quantify how good a specific log ratio is. At this stage the only criteria was the distance from the optimal point. Another criteria could be added implicating that only ratios with minimum calibration certainty should be included.

- Some of the higher correlations coefficients are achieved with ratio's using elements that have only been measured in the laboratory and not using the X-50 mobile XRF device. This may seem wrong yet this is also the predictive power of statistics. An objective prediction is made with a certain level of certainty. Furthermore this is the reason why calibration is performed. Element concentration below the detection limit of the X-50 Mobile XRF or elements which could not be measured using the X-50 Mobile XRF are predicted using results from accurate analysis.
- Some log-ratios contain the 'undefined' element. The difficulty arises due to the fact that in reality this undefined element probably consists of more than 1 element. This would imply that in reality while all ratios are the result of combining 2 elements in the ratios using the undefined element more than 2 elements may actually be used. Again although this may seem odd the results obtained remain objective and mathematically sound. The 'undefined' element remains valid because relative changes are analysed and the absolute concentrations of each element which make up the 'undefined' element is not important.
- The use of ratios may suggest correlations between elements present in the ratios while in absolute values these elements may not be related to each other at all even if measured accurately (Rollinson, 1993). This is because one compares absolute changes while the other uses relative changes.

One shortcoming of the procedure used is whether the correct sample is being compared to the correct gold concentration. At this stage samples were selected for analysis using a portable XRF device and compared to a pre-existing data base of gold assay values. As stated in chapter 2 the gold is concentrated in veins. This means that samples selected close to a vein containing gold but in another gold assay interval (sample A) will be compared to low gold values while a sample further away from the vein but in the same gold assay interval will be compared to high gold values (sample B) while the sample itself does not contain more gold than sample. The issue is that zonations around veins containing gold are therefore poorly quantified by the correlation analysis performed in paragraph 3.2.

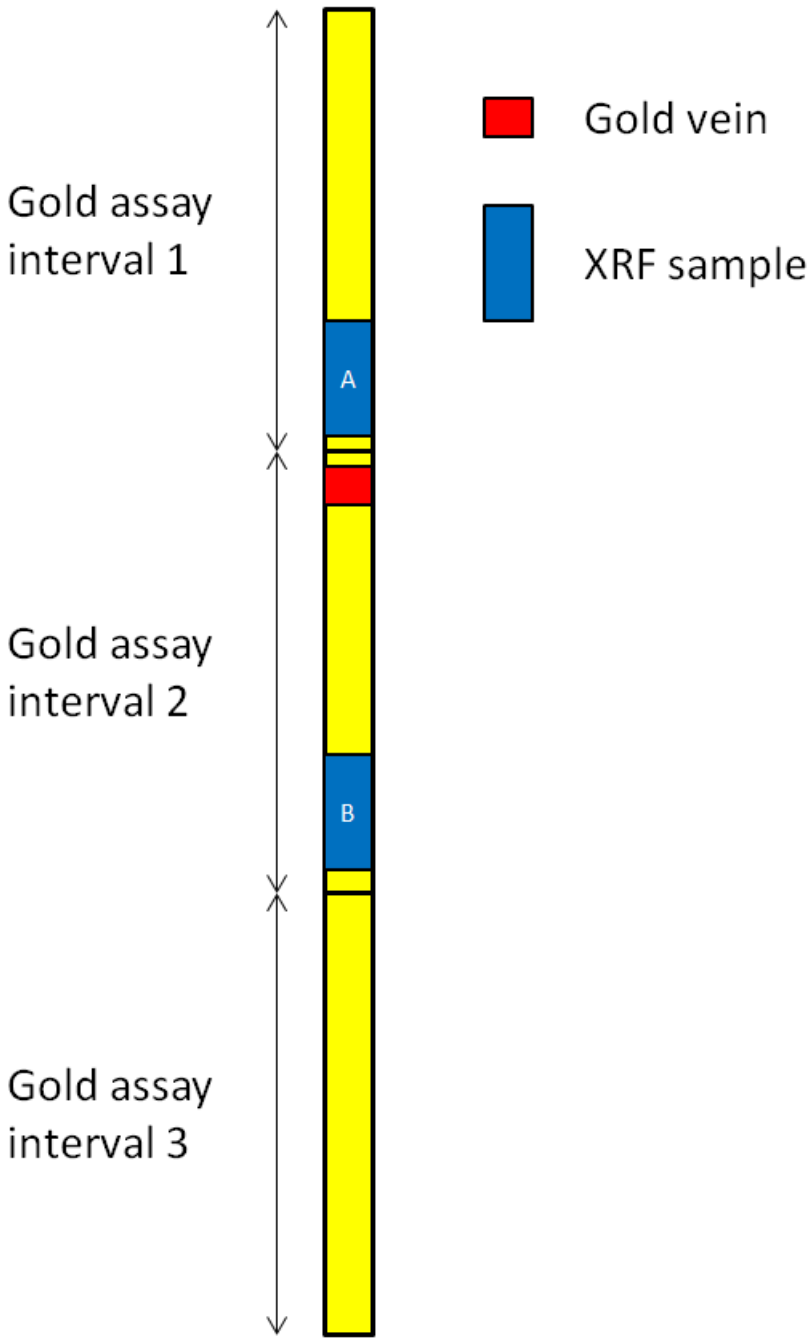

Figure 6-2, Distribution of samples and veins in relation to the gold assay intervals.

7 Conclusions

RQ 1: Is it possible to differentiate the different lithologies in the Koolhoven deposit on the basis of element content?

It is possible to differentiate the different lithologies present in the Koolhoven pit. The bulk of the volcanic rock consists of mafic volcanics. Intermediate and felsic volcanics have also been recognized using their major element content. The sedimentary rocks can be subdivided into siltstone/mudstone, greywacke A and B, sandstone and conglomerate. Greywacke A follows the trend of the siltstone/mudstone and both cannot be differentiated from each other on the on the basis of element content. They can be separated from each other by visual observation because the siltstone/mudstone shows turbiditic textures. Greywacke B follows the trend of the conglomerate in the North. The element content of greywacke B and the conglomerate indicate a relation with the volcanic rock. The petrographic study supports this, clasts of volcanic composition were found in the conglomerate.

RQ 2: Are specific elements related to the gold mineralization?

At this stage it is considered that not enough data is present to take conclusions regarding the correlations between specific elements and gold.

The use of log-ratios applied to boreholes KHD-508, KHD-566 and KHD-583 yielded promising results however more representative samples are needed to test if the correlation also holds for other boreholes and lithologies.

RQ 3: Are alteration mineral halo's detectable in and around the Koolhoven gold deposit?

No alteration mineral halo has been found using the VNIR spectral analysis. Paragonite is the dominant mineral and should be regarded as the background signal. Chlorite overshadows the response from the carbonate minerals. This is supported by the results from the petrographic study which indicate that carbonates are present in higher concentrations than the chlorite. Although no mineral alteration halos were found the findings from the VNIR spectral analysis and petrographic study are in accordance with previous works. The results suggest that the samples are all taken too proximal to the gold deposition to find any large scale alteration halo. On the small scale bleaching, sulfide minerals, carbonate spots and sericitization are associated with veins.

8 Recommendations

Recommendations derived from the results of this research project are divided into three groups

- Recommendations for the continuation of this research project.
- Recommendations specifically focused on the methodology of the analysis.
- Recommendations focussed on the implementation of the recommendations made for this research project on mine site.

8.1 Continuation of the research project:

- Increase the scale. It is believed that the samples selected for this research project are located too close to the actual gold mineralization to find changing alteration patterns. To discover if alteration halos are indeed present the scale of the research area has to increase. Samples further away from the gold mineralization zones should be selected.
- Choose pits with higher gold concentrations and more spatially concentrated gold mineralization. In this research project one issue has been the low gold concentrations encountered in the Koolhoven pit. Higher gold concentrations and especially a better coverage of the higher gold concentrations would allow for better correlation and application of PLSR. Interference between the three different mineralized zones also makes it more challenging to attribute measured characteristics to one specific mineralized zone. A more spatially concentrated gold mineralization would therefore be favourable.
- The choice may be made to extend the research to other producing pits directly or at a later stage. To find out if the results presented in this research project are consistent more pits of the Northern trend and/or Southern trend should be included. Different pits including different lithologies located in different places may yield different results. For the effective use of the information presented in this report in an exploration campaign it is crucial to know if the results are consistent in other gold mineralized zones.
- Choose pits with better borehole coverage. The optimal goal would have been to choose several cross sections throughout the Koolhoven pit to display the different results. Because not all drilled boreholes were available or suitable for the research project because the amount of unweathered rock was too limited. As a result the distance between the used drillholes was too great to make representative cross sections. In the future it is not required to sample the entire pit but it is recommended to select a few cross sections with good quality boreholes and good lateral coverage. Extra boreholes may be sampled to ensure enough data is gathered for each lithology. Choosing cross-sections may be done at two stages. First prior to any sampling or secondly after a 3D model has been created on the basis of major element analysis defining the different lighologies present in the pit (paragraph 8.2.2.1).
- Extend the research of vein characterization. In this project veins have been characterized by optical analysis. Because the gold is concentrated in the veins it is recommended that in the future veins should be analysed in more detail using multi-element analysis. Sample spacing around veins should be reduced to capture the small scale changes. The capacity to

differentiate between mineralized and non-mineralized veins on the basis of multi-element analysis would be a great asset.

8.2 Methods of analysis

8.2.1 Petrographic analysis:

- It is recommended to concentrate the petrographic study on the characterizations of veins and their surrounding area. A more precise timing of gold mineralization may be obtained on the basis of rock textures.
- Bleeching of the vein selvages should be investigated in more detail. An important part of this study may be directly performed on boreholes. Thins sections should be used as a control method.

8.2.2 Element analysis general:

- Samples were only sent to one laboratory. In the future and as is conventional samples should be sent to two laboratories. In the case of the ICP-MS and ICP-AES analysis this is important because they are used as reference for the calibration for the X-50 Mobile XRF data.

8.2.2.1 Major element analysis:

- The results presented in this project have proven that visual interpretation of the different lithologies is not sufficient. Clear differences in chemical content were observed where visual interpretation did not record differences. Since the varying chemical composition is due to affect alteration patterns and correlation analysis it is recommended to clearly define all different lithologies present in the area of research on the basis of chemistry.
- Several cases deserve special attention:
  - Only three samples from the same borehole represent the conglomerates. More samples containing conglomerates from different boreholes should therefore be selected.
  - The literature (give reference) and data in this report confirm the presence of volcanic rock ranging from mafic to felsic composition. No agreement is found however on the relative abundance of each composition.
- The results should be imported in a 3D model or 2D cross sections and be used as new geological model.

8.2.2.2 X-50 Mobile XRF device:

- Evaluate the use of the X-50 Mobile XRF with more samples. The X-50 Mobile XRF device should be used with care and always with quantitative analysis performed in parallel to allow for cross validation. Considering the low gold grades in the deposits of the Rosebel concession accurate quantitative analysis is required. The other setups of the desktop XRF should also be tested and used.

- Various plastic bags should be tested for their chemical content and varying interference due to their thickness. The emphasis would be to select the plastic bag with the least varying chemical composition and interference.

- Sampling should be conducted such to contain enough samples from each lithology (as defined by the major element analysis). At a first stage analysing samples randomly distributed throughout one lithology could be used to define if a correlation between specific elements and/or element ratios and gold exists irrespectively of the geology. Secondly samples selected on regular intervals and along a cross section would be appropriate to link the results to a geological context. For these reasons it is recommended to sample along the cross sections and sample extra boreholes to ensure a representative population of samples. Perhaps the most important criteria according to which the samples should be selected is the actual presence of gold.
- Regular repeated measurements of specific samples should be performed to quantify the variance resulting from the device itself.
- Building on the techniques of calibration proposed by (Weltje & Tjallingii, 2008) element concentrations may not be needed. Instead recorded intensities could be used and calibrated with proven methods of analysis performed in a controlled environment (laboratory). The benefit of this would be that other setups of the X-50 Mobile XRF device (using different KV) could readily be used hereby measuring other elements which were not recorded using the 3-beam setup. This would reduce the amount of undefined material in a sample and improve the calibration.
- To improve the correlation analysis it is suggested to eliminate all the samples with a gold concentration of 0.01 and 0.02 ppm. Since both these concentrations make up the bulk of the gold concentration (Figure 2-5) this group of samples is due to have a large influence on the correlation analysis while not being the most important. We are interested in the relations linked to high gold grades.

8.2.3 Visible and near infrared analysis:

- It is recommended to perform this analysis after the major element analysis has been finalized.
- Samples should be taken on meter intervals along all selected boreholes.
- X-ray diffraction (XRD) analysis should be used in parallel to cross validate the VNIR analysis. The use of XRD may prove to be useful to determine the reason of scattering of the ALOH wavelength of absorption and why these do not follow the ranges as depicted in table Table 5-13.
- The effect of finely dispersed sulfides should be analysed in more detail.
- Partial least squares regression was performed on the first derivative of the spectra based on an interval of four nm. Although this method is deemed to be more stable because it partially reduces the effect of noise and no longer depends on the signal strength this method does not capture the effect of varying amounts of minerals based on the depth of absorption. In the future it is recommended test the possibility of including these characteristics by applying partial least squares regression on the hull quotient spectra.
- In the course of this project automatic feature extraction has been used extensively to compare different characteristics. It is recommended to keep using this method since it is objective and not dependent on the geologist interpreting the data. This method does however have its limitation as has been illustrated in paragraph 5.3.3. It is therefore recommended to analyse a selection of spectra in more detail to capture the small differences.

8.3 Implementation of the recommendations

The future of this research project will be strongly influenced by the level of collaboration and communication of the Regional Exploration and Mine Exploration department. This project was initiated and performed for the Regional Exploration department but data was obtained from the Mine Exploration department. Several recommendations are made to improve the efficiency and quality of the data gathering and processing stage.

- To be efficient in the gathering of a representative and complete dataset it is recommended to choose specific cross sections across producing pits. Drilling in the mine should be organized such that they optimize the coverage of these cross sections. Small changes in positioning and orientation of the boreholes would greatly improve the quality of the cross sections. Boreholes should also be drilled outside the mine along the cross sections. These boreholes may not intersect gold but yield more valuable information that could be used to differentiate between mineralized and non-mineralized rock.

- Changes are needed in the processing of boreholes to make further research possible and valuable. A large amount of data is not recorded while the instruments are available. It is recommended to train staff to use the different analysis methods and include both the VNIR spectral analysis and multi-element analysis (using the X-50 Mobile XRF device) in the process of logging directly after the borehole has been drilled. This process should be performed on all boreholes selected to form the cross sections in the producing pits and on all boreholes from regional exploration campaigns. It is important to perform these analysis on the boreholes from regional exploration campaigns since otherwise even if we have found trends in the producing pits the data from the regional exploration projects will not be available

- Condemnation boreholes which are drilled to confirm that an area contains no gold and therefore can be used to build on should be preserved. As mentioned previously to boreholes outside the gold deposition area are needed as reference. Condemnation boreholes would be ideal to use as a reference however at this stage they are not preserved once the gold assay has revealed that they contain no gold.

- At the stage of the research project the Regional Exploration department did not use the same software version as the Mine Exploration department. In the future, to be efficient it is vital that one can directly access the information and geological models created by the Mine Geology and Mine Exploration department. The results obtained by using the instruments from the Regional Exploration department should directly be imported into the geological models supplied by the Mine Geology and Mine Exploration department. To allow this, data sharing should be made easier and software versions between different departments should be adapted to each other.

9 List of references

Abdi, H., 2007. Partial least squares regression. In: *Encyclopedia of Measurement and Statistics.* s.l.:Thousand Oaks (CA): Sage.

Allen, R. et al., 1996. *Atlas of alteration.* s.l.:Geological Association of Canada.

Anon., 2012. *http://www.iamgold.com.* [Online].

Anon., n.d. *http://speclab.cr.usgs.gov.* [Online].

AusSpec International, 2008. *GMEX2, Practical applications handbook.* s.l.:Ausspec International Ltd.

AusSpec International, 2008. *GMEX6, Archean greenstone gold.* s.l.:s.n.

Balaram, V., 1996. Recent trends in the instrumental analysis of rare earth elements in geological and industrial materials..

Condie, K. C. & Wronkiewicz, D., 1990. The Cr/Th ratio in Precambrian pelites from the Kaapvaal Craton as an index of craton evolution.. *Earth and Planetary Science Letters,* Volume 97, pp. 256-267.

Crosta, A. P., 2010. *Unveiling mineralogical informatin in ore deposits: the use of reflectance spectroscopy for mineral exploration in South-america,* s.l.: s.n.

Dalm, M., 2011. Applicability of near-infrared spectroscopy for sensor based sorting of mill pebbles from the Los Bronces copper mine, Chile..

Dalm, M., 2012. *Discussion on partial least squares regression applied on spectral data.* s.l.:s.n.

Daoust, C., Voicu, G., Brisson, H. & Gauthier, M., 2011. Geological setting of the Paleoproterozoic Rosebel gold district, Guiana Shield, Suriname. *Journal of South Americal Earth Sciences,* Issue 32, pp. 222-245.

Delor, C. et al., 2003. The Bakhuis ultrahigh-temperature granulite belt (Suriname): II. implications for late Transamazonian crustal stretching in a revised Guiana Shield framework. *Geologie de la France,* Issue 2-3-4, pp. 207-230.

Dubé, B. & Gosselin, P., 2007. Greenstone-hosted quartz-carbonate vein deposits. Volume 5, pp. 49-73.

Eilu, P. & Groves, D., 2001. Primary alteration and geochemical dispersion haloes of Archaen orogenic gold deposits in teh Yilgarn Craton: the pre-weathering scenario. *Gechemistry: Exploration, Environment, Analysis,* Volume 1, pp. 183-200.

Gill, R., 1997. *Modern analytical geochemistry.* s.l.:Longman limited.

Goldfarb, R. J., Hart, C. & White, N., 2012. *SEG gold deposit workshop.* Cape Town, South Africa, Society of Economic Geologists.

Hutton, J. & Elliott, S., 1980. An accurate XRF method for the analysis of geochemical exploration samples for major and trace elements using one glass disc.. *Chemical Geology*, Issue 29, pp. 1-11.

Jenner, G., Longerich, H., Jackson, S. & Fryer, B., 1990. ICP-MS A powerful tool for high-precision trace-element analysis in Earth sciences: Evidence from analysis of selected U.S.G.S. reference samples. *Chemical Geology*, Issue 83, pp. 133-148.

Kroonenberg, S. B. & de Roever, E. W., 2010. *Geological evolution of the Amazonian Craton,* s.l.: Blackwell Publishing.

Ledru, P., Lasserre, J., Manier, E. & Mercier, E., 1991. Revision de la lithologie du Paleoproterozoique du craton guyanais. Tectonique transcurrente et dynamique des bassins sedimentaires.. *Societe geoloquique de France,* Issue 162, pp. 627-636.

Pontual, S., 2012. *Discussion on the aquired VNIR spectral data of the Koolhoven gold deposit..* s.l.:s.n.

Pontual, S., Merry, N. & Gamson, P., 1997. *Spectral interpretation field manual.* s.l.:Ausspec International.

Potts, P. J. & Webb, P. C., 1992. X-ray fluorecense spectrometery. *Journal of Geochemical Exploration,* Issue 44, pp. 251-296.

Rafferty, J. P., 2012. *http://www.britannica.com/.* [Online].

Ramsey, M. H. et al., 1995. An objective assessment of analytical method precision: comparison of ICP-AES and XRF for the analysis of silicate rocks.. *Chemical Geology*, Issue 124, pp. 1-19.

Robert, F. et al., 2007. Models and exploration methods for major gold deposit types. *Ore deposits and exploration technology,* Issue 48, pp. 691-711.

Robert, F., Poulsen, K. & Dubé, B., 1997. Gold deposits and their geological classification. *Exploration geochemistry,* pp. 209-220.

Robert, F., Poulsen, K. & Dubé, B., 1997. Gold deposits and their geological classification. *Proceedings of exploration,* pp. 209-220.

Rollinson, H., 1993. *Using geochemical data: evaluation, presentation, interpretation.* s.l.:Longman Group UK Ltd.

Rosebel Gold Mines NV, 2011. *Rosebel Mine, Suriname, Mineral reseves report December 31st 2011,* s.l.: IAMGold.

Skinner, B. j., Porter, S. C. & Park, J., 2004. *Dynamic Earth, an introduction to physical geology.* Fifth ed. s.l.:John Wiley & Sons.

Thomas, I. & Haukka, M., 1976. XRF determination of tace and major elements usings a singele-fused disc.. *Chemical geology*, Issue 21, pp. 39-50.

Thompson, A. J., Hauf, P. L. & Robitaille, A. J., 1999. Alteration mapping in exploration: application of short-wave infrared (SWIR) spectroscopy. *SEG newsletter,* Issue 39, pp. 15-27.

tie Jong, S., 1992. SIMPLS: an alternative approach to partial least squares regression. *Chemometrics and Intelligent Laboratory Systems,* pp. 251-263.

Voncken, J., 2012. *Discussion on standard deviation as a criteria for data quality.* s.l.:s.n.

Watson, T., 2008. *Volcanism and sedimentation: new insight into Arc-related Volcanism and sediment deposition in sykinematic Paleoproterozoic basin: Rosebel Gold Mine, Northeastenr Suriname,* Chapel Hill: s.n.

Weltje, G. et al., 2012. *Prediction of geochemcial composion from XRF-core-scanner data: A new multivariate approach into filtering, sample selection, and quantificaion of uncertainties.,* s.l.: s.n.

Weltje, G. J. & Tjallingii, R., 2008. Calibration of XRF core scanners for quantitative geochemical logging of sediment cores; Theory and application. *Earth and Planetary Science Letters,* Issue 274, pp. 423-438.

Yeats, C. J. & Vanderhor, F., 1998. Archaean lode-gold deposits. *AGSO Journal of Australian geology & Geophysics*, Issue 17, pp. 253-258.

10 Appendix A

10.1 Background

Milestones:

1992	Mineral Agreement between the Government of Suriname, Grassalco and Golden Star.
1994	Earn-in agreement between Cambior and Golden Star.
1997	Grassroots exploration and Feasibility Study
2001	Cambior purchases remaining 50% interest from Golden Star
2002	Final Feasibility Study
2003	Phase I construction (Design 4.8 Mpa)
2004	Commercial production (February)
2005	Completion of Phase II expansion (Design 5.8 Mpa)
2006	IAMGOLD acquires Rosebel through acquisition of Cambior (November)
2008	Record mine throughput and gold production. IAMGOLD acquires 86% of Euro Ressources S.A. which holds a royalty interest in Rosebel.
2009	Phase III mill expansion & optimization increases nameplate capacity to 11 Mtpa.
2010	Production at Rosebel of 395,000 attributable ounces at a cash cost of $484 per ounce

Figure 10-1 Milestones of the Rosebel Gold Mine (Rosebel Gold Mines NV, 2011).

Rosebel Gold Mine, Suriname

LOCATION: Suriname, South America

OWNERSHIP: 95% IAMGOLD, 5% Government of Suriname

ATTRIBUTABLE GOLD PRODUCTION: 2011 - 385,000 ounces

TOTAL CASH COST: 2011 - $616 per ounce

MINE LIFE(E): 14 years

RESERVES & RESOURCES* (as at December 31, 2011):

Proven and Probable Reserves			Measured and Indicated Resources			Inferred Resources		
Tonnes (000)	Grade (g/t)	Attributable Contained Ounces (000)	Tonnes (000)	Grade (g/t)	Attributable Contained Ounces (000)	Tonnes (000)	Grade (g/t)	Attributable Contained Ounces (000)
186,381	1.0	5,730	263,115	1.0	7,719	13,876	0.7	278

*Cautionary Note to U.S. Investors: The United States Securities and Exchange Commission limits disclosure for U.S. reporting purposes to mineral deposits that a company can economically and legally extract or produce. IAMGOLD uses certain terms on this website, such as "measured," "indicated," or "inferred," which may not be consistent with the reserve definitions established by the SEC. U.S. investors are urged to consider closely the disclosure in the IAMGOLD Annual Reports on Forms 40-F. You can review and obtain copies of these filings from the SEC's website at http://www.sec.gov/edgar.shtml or by contacting the Investor Relations department.

MINING & PROCESSING: Open pit; gravity separation & carbon-in-leach

TECHNICAL REPORT: "Rosebel Technical Report, Suriname, South America", March 2010

Figure 10-2, Rosebel Gold Mine general information (Anon., 2012).

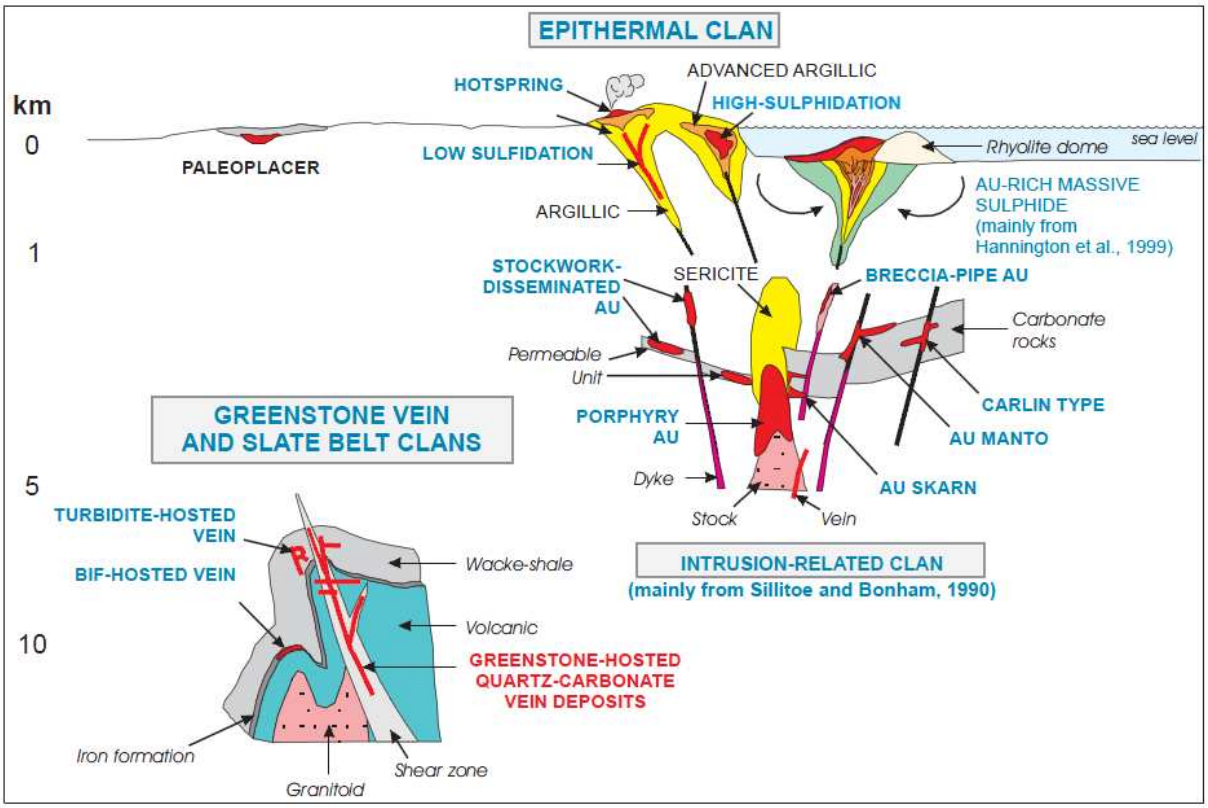

Figure 10-3, Different types of gold deposits in relation to inferred crustal levels (Dubé & Gosselin, 2007).

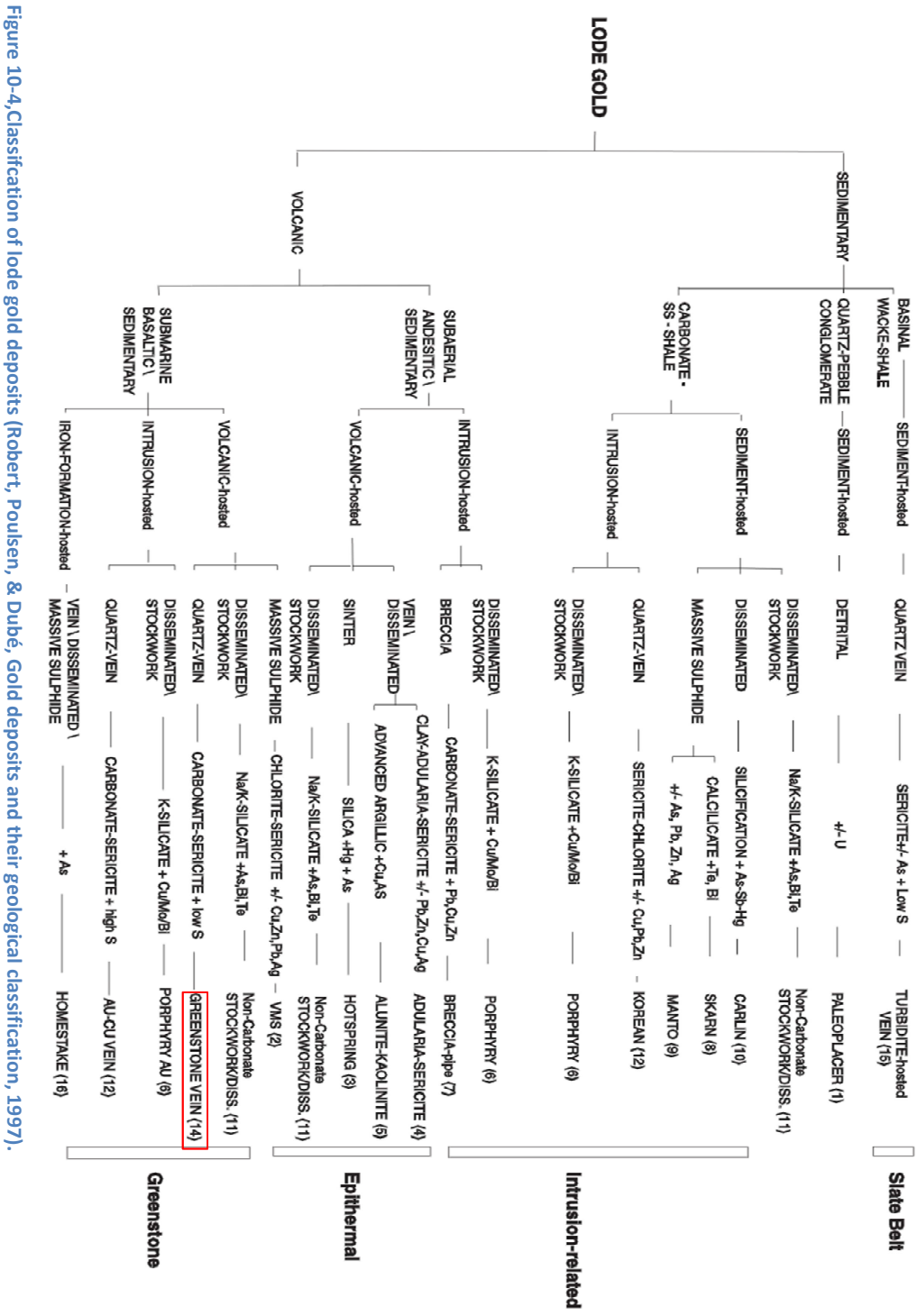

Figure 10-4,Classification of lode gold deposits (Robert, Poulsen, & Dubé, Gold deposits and their geological classification, 1997).

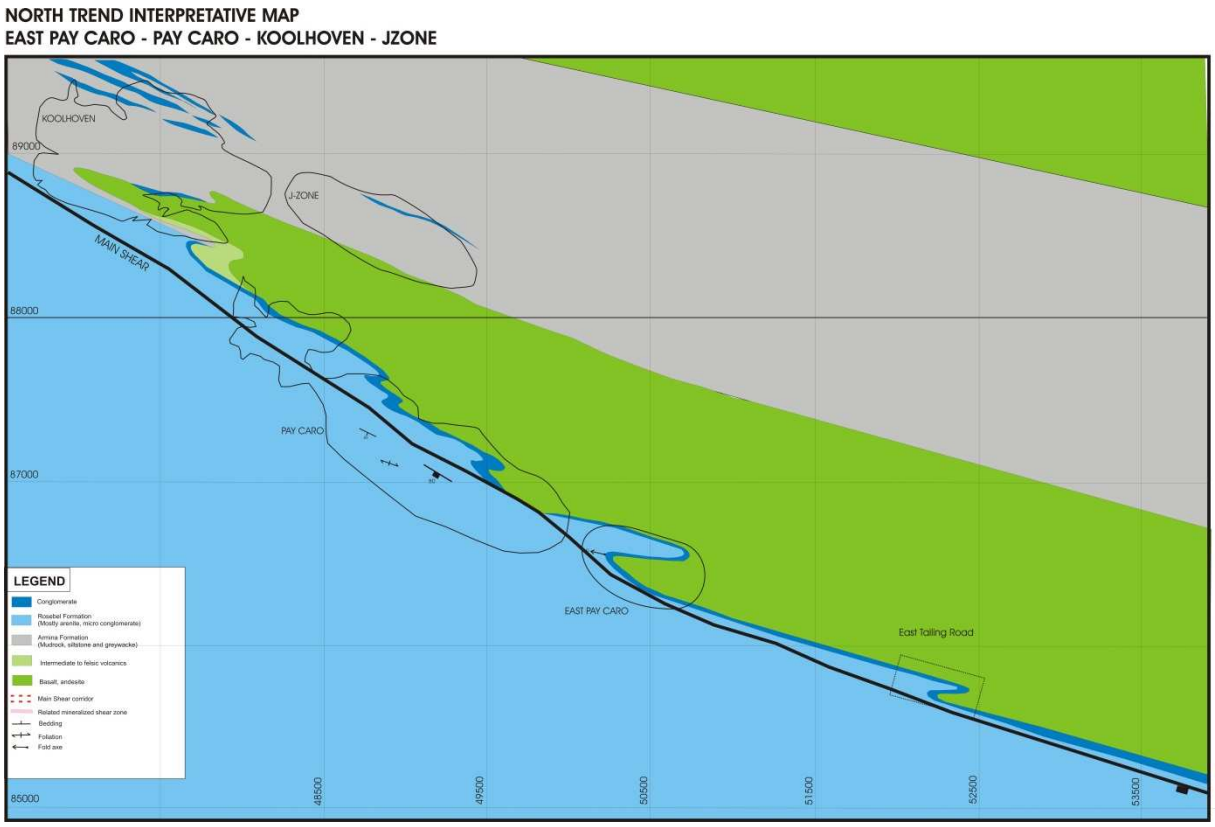

Figure 10-5, North trend interprative map (Rosebel Gold Mines NV, 2011).

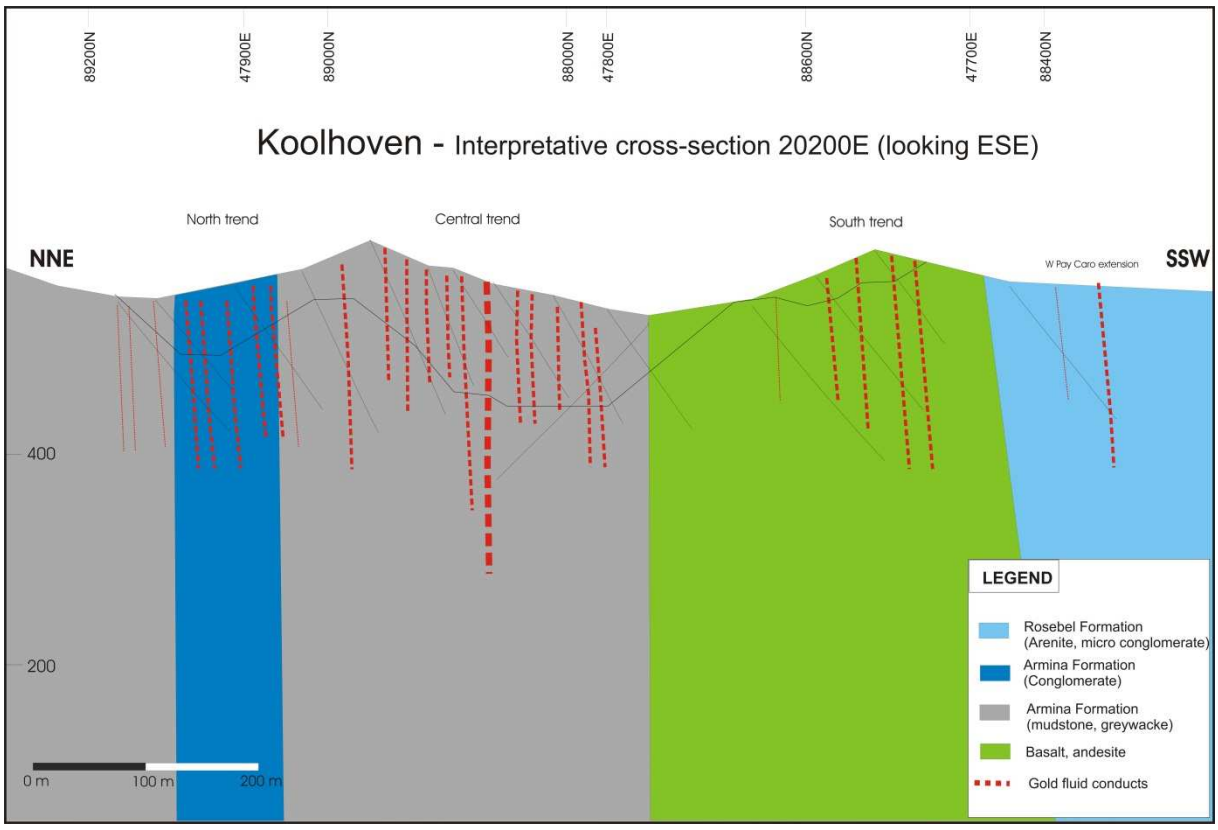

Figure 10-6, Koolhoven interpretive cross section (looking ESE). The three mineralized zones are in the: Armina conglomerate, Armina mudstone & greywacke and in the basalt & andesite interval to the SSW (Rosebel Gold Mines NV, 2011).

10.2 Data acquisition and methodology

ALS laboratory in Lima (Peru)

Certifications

ISO 9001:2008, ISO 17025:2005, IQNet

Address:
Calle 1 LT-1A Mz-D Esq. Con Calle A
Urb. Industrial Bocanegra Callao 1
Lima
Perú

Phone:
+51 1 574 5700

Figure 10-7, ALS laboratory in Lima, contact information and certifications.

vanPetro

8080 Glover Road,

Langley, British Columbia

Canada

Tel: 6048881323

Figure 10-8, vanPetro Canada, contact information.

Mobile X-50 LOD Table

Application	X-50 LOD (ppm)
RoHS Polymer or Plastic (Non PVC)	
Cd	1
Cr	5-10
Pb	2
Hg	2
Br	2
PVC (40% or more Cl)	
Cd	1
Cr	15
Pb	7
Hg	7
Br	6
RoHS Packaging Directive	
Sum Cd + Cr + Pb + Hg	< 20
EPA RCRA and Priority Pollutant Metals, (Soil Ranging from SiO2 to 3-5% Fe-content,) Many Liquids, Oil or Fuels, Aluminum Alloys	
Cr	5-10
Cd	1-2
Ag	1
Sn	4-5
Sb	4-5
Ba	20
Pb	3-5
As	3-5
Hg	3-5
Tl	3-5
Se	3-5
Cu	5-8
Ni	5-8
Zn	5-8
Sn-based Solders (RoHS)	
Cd	<80
Precious Metals Exploration and Mining	
Gold (Au) in soil, sediment	3-5
Silver (Ag) in soil, sediment	1-2
Platinum Metals Group I: Pd, Rh, Ru	1-2
Platinum Metals Group 2: Pt, Ir, Os	3-5
Some Rare Earth Elements (non alloys only)	
La, Ce, Pr, Nd	15-25

Figure 10-9, Limit Of Detection (LOD) for hte Mobile X-50 XRF unit.

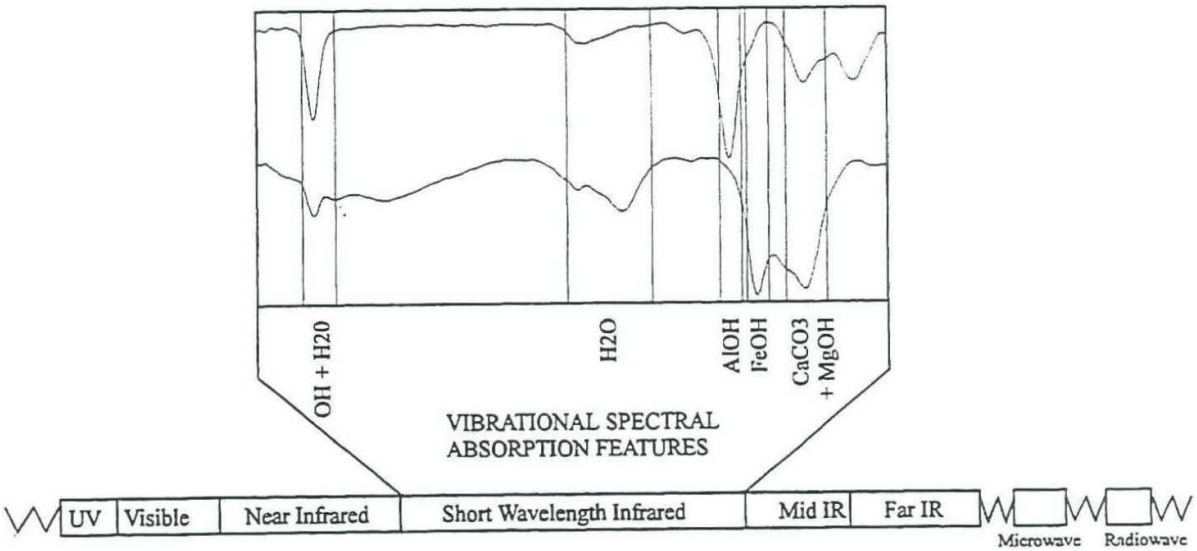

Figure 10-10, SWIR position in the electromagnetic spectrum (AusSpec International, 2008).

10.3 Results

10.3.1 Fusion XRF data and lithology differentiation

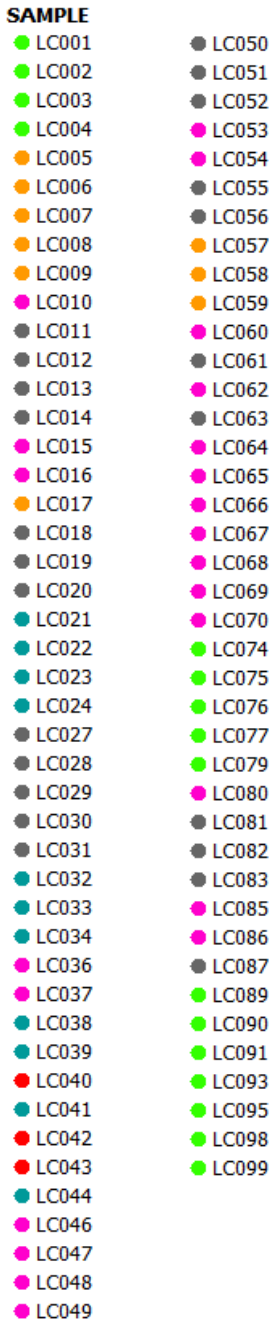

Figure 10-11, All sample ID numbers for the samples sent to ALS laboratory together with the colour coding used in the display of the fusion XRF results.

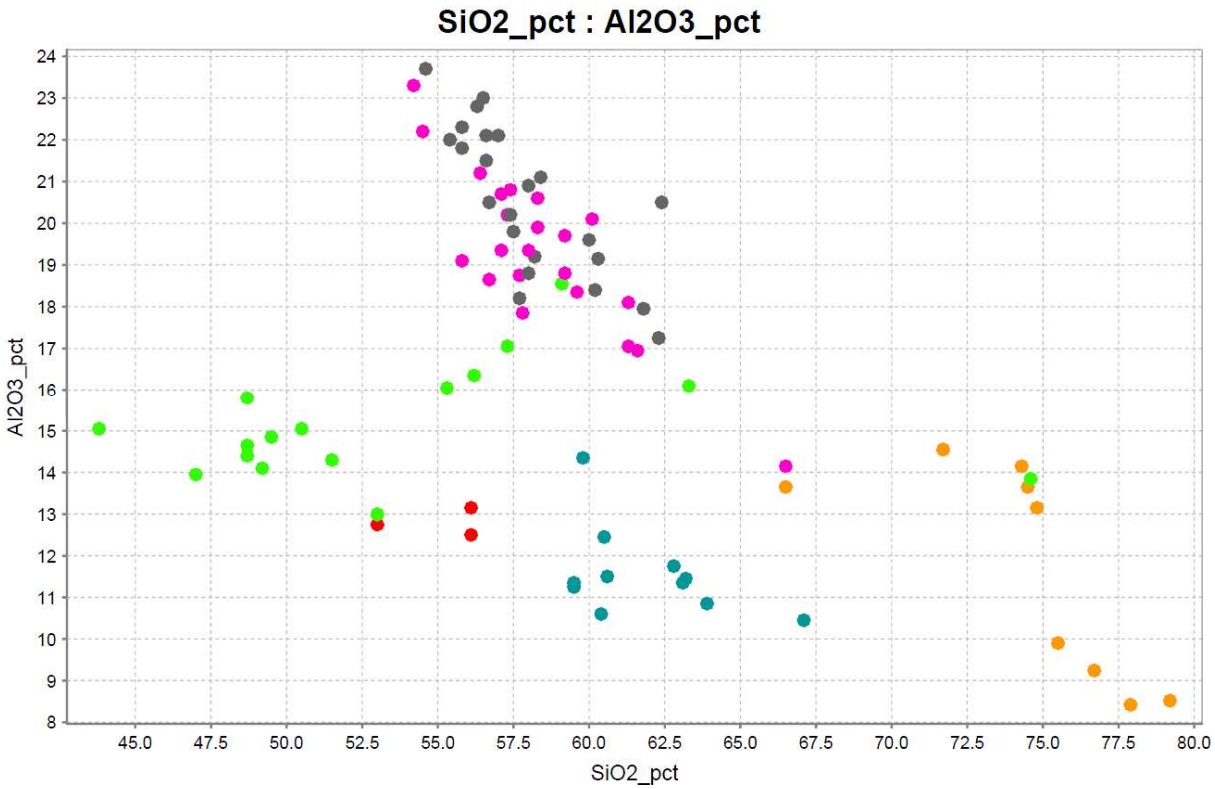

Figure 10-12, Data points obtained by fusion XRF, AL_2O_3 vs SiO.

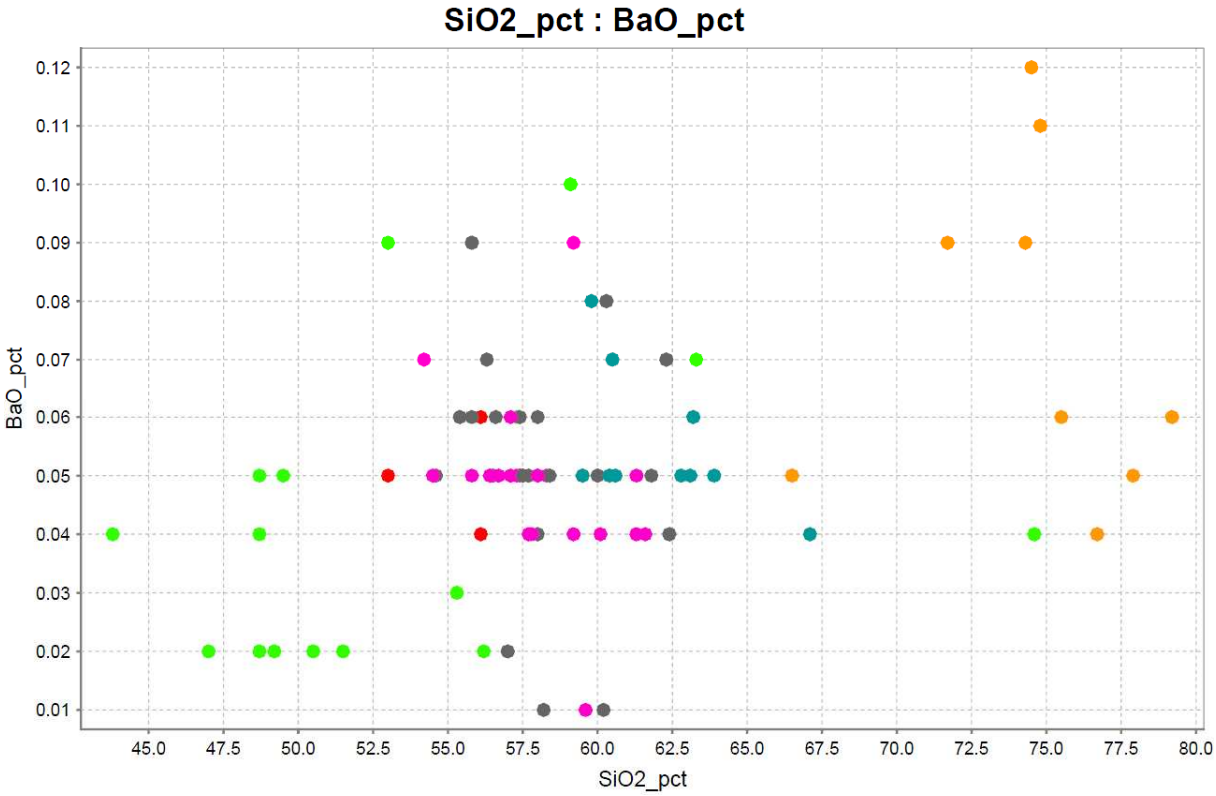

Figure 10-13, Data points obtained by fusion XRF, BaO vs SiO

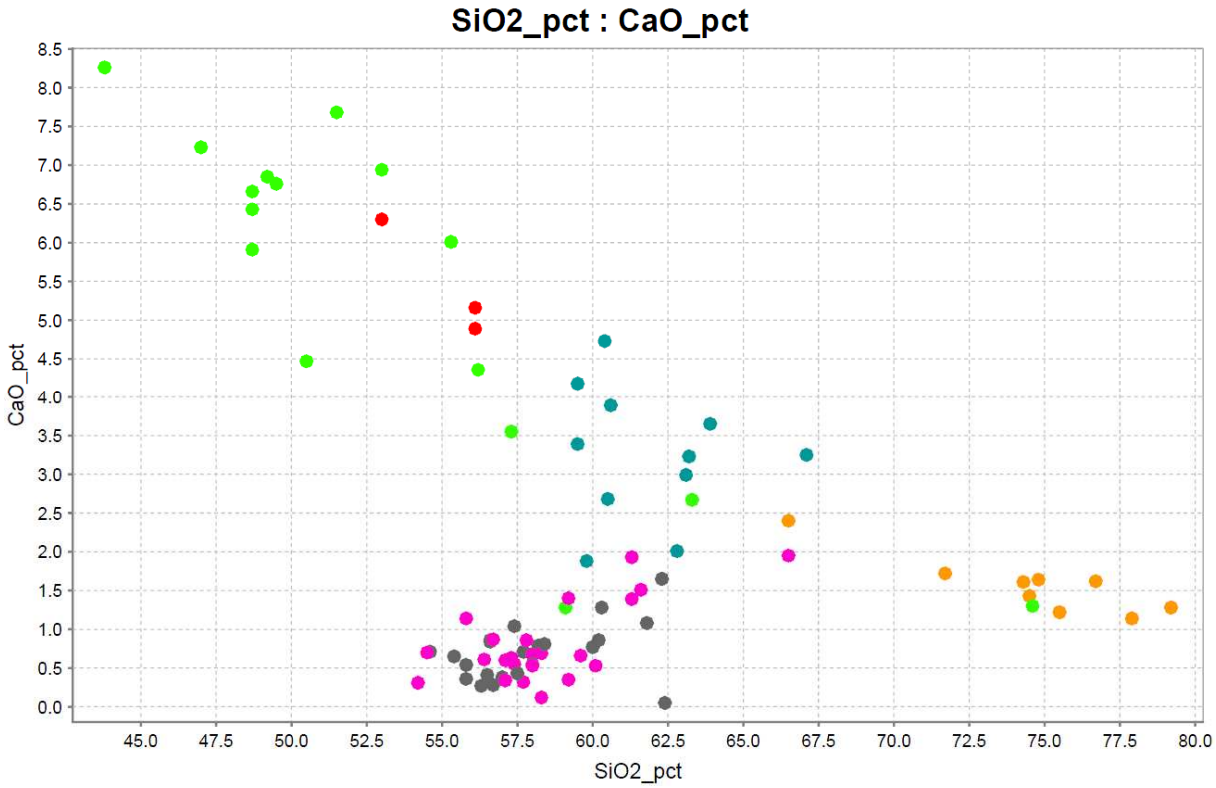

Figure 10-14, Data points obtained by fusion XRF, CaO vs SiO

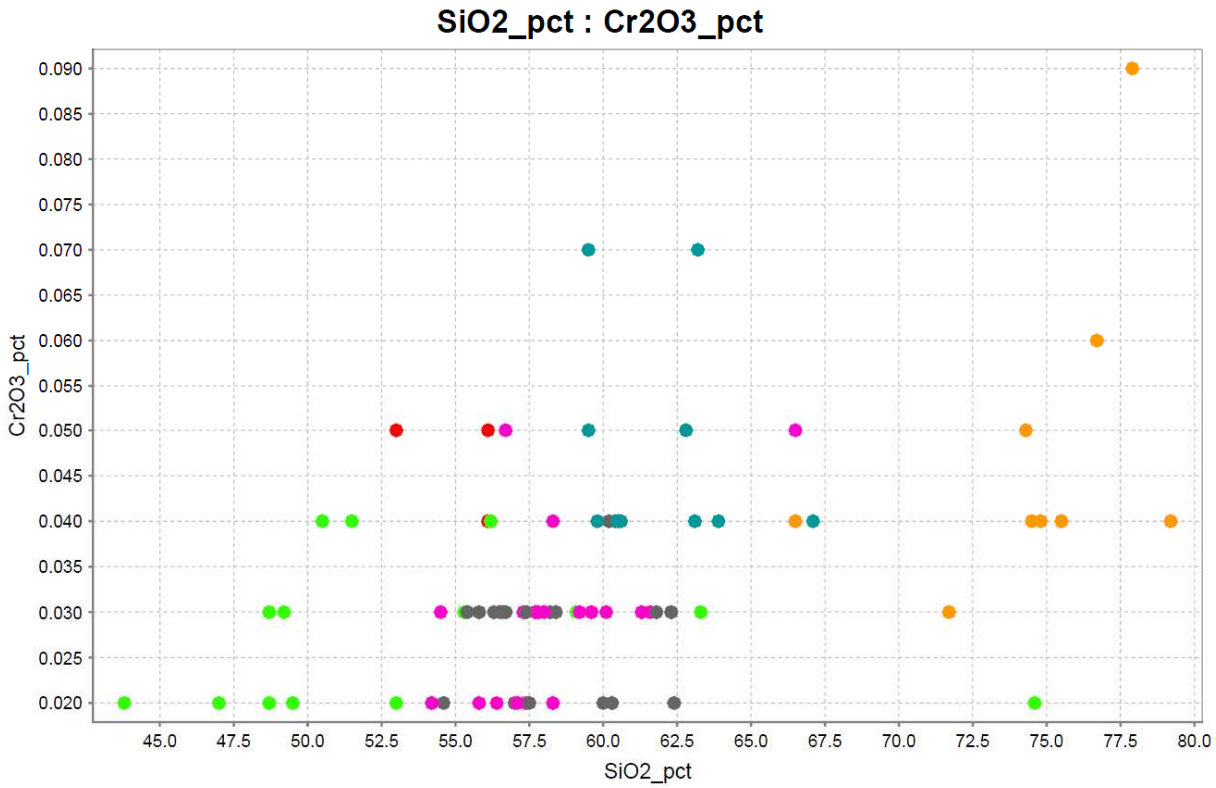

Figure 10-15, Data points obtained by fusion XRF, Cr_2O_3 vs SiO

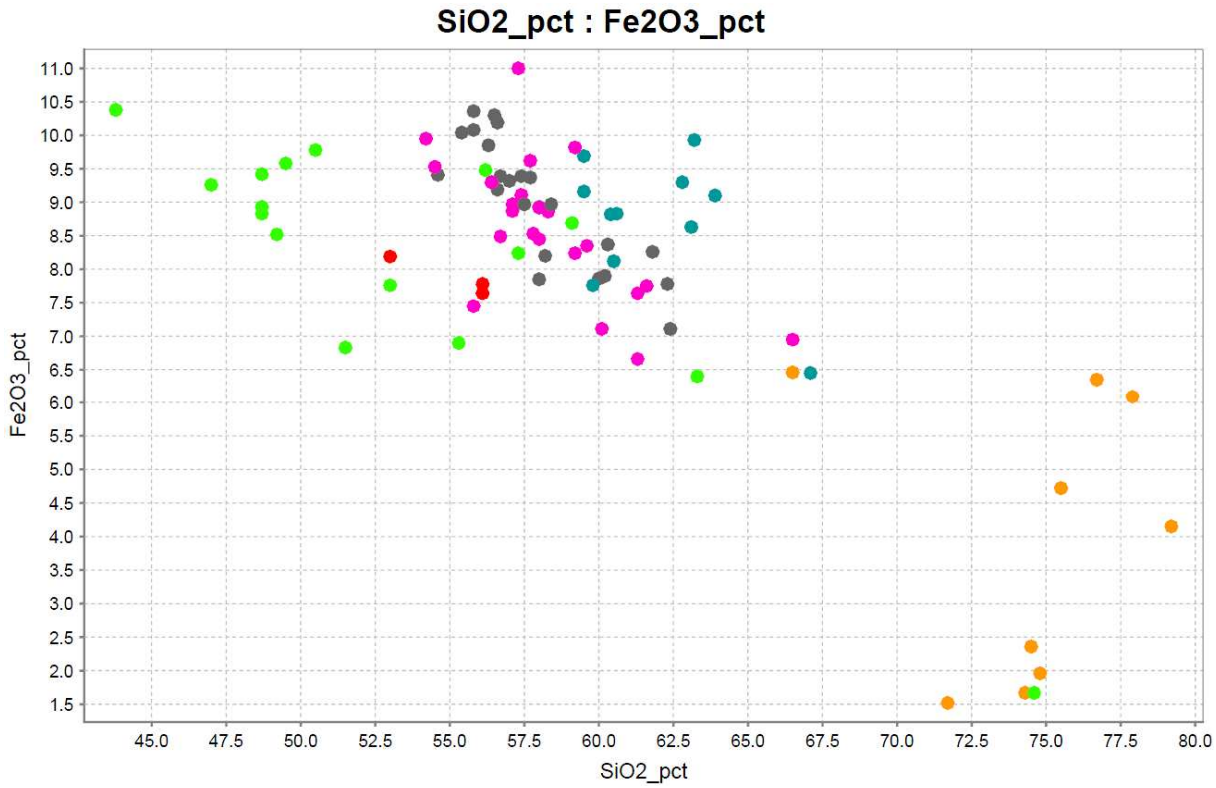

Figure 10-16, Data points obtained by fusion XRF, Fe_2O_3 vs SiO

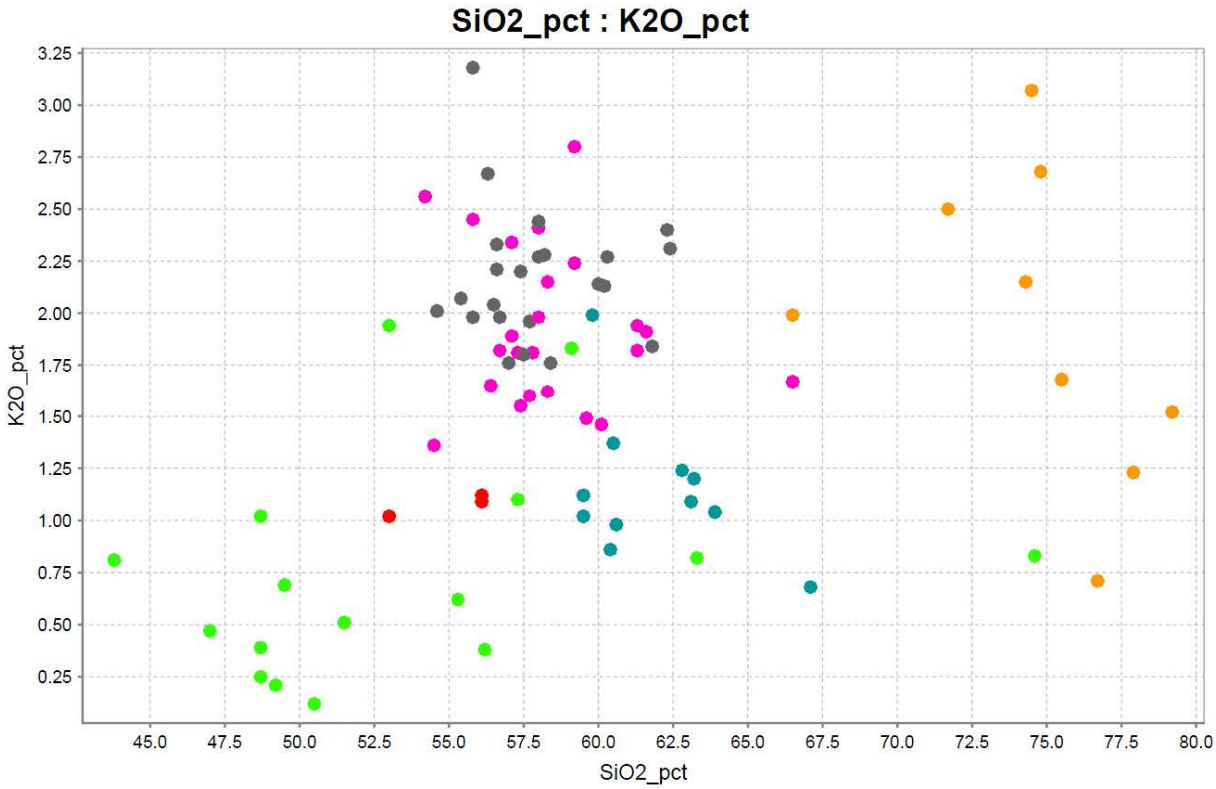

Figure 10-17, Data points obtained by fusion XRF, K_2O vs SiO

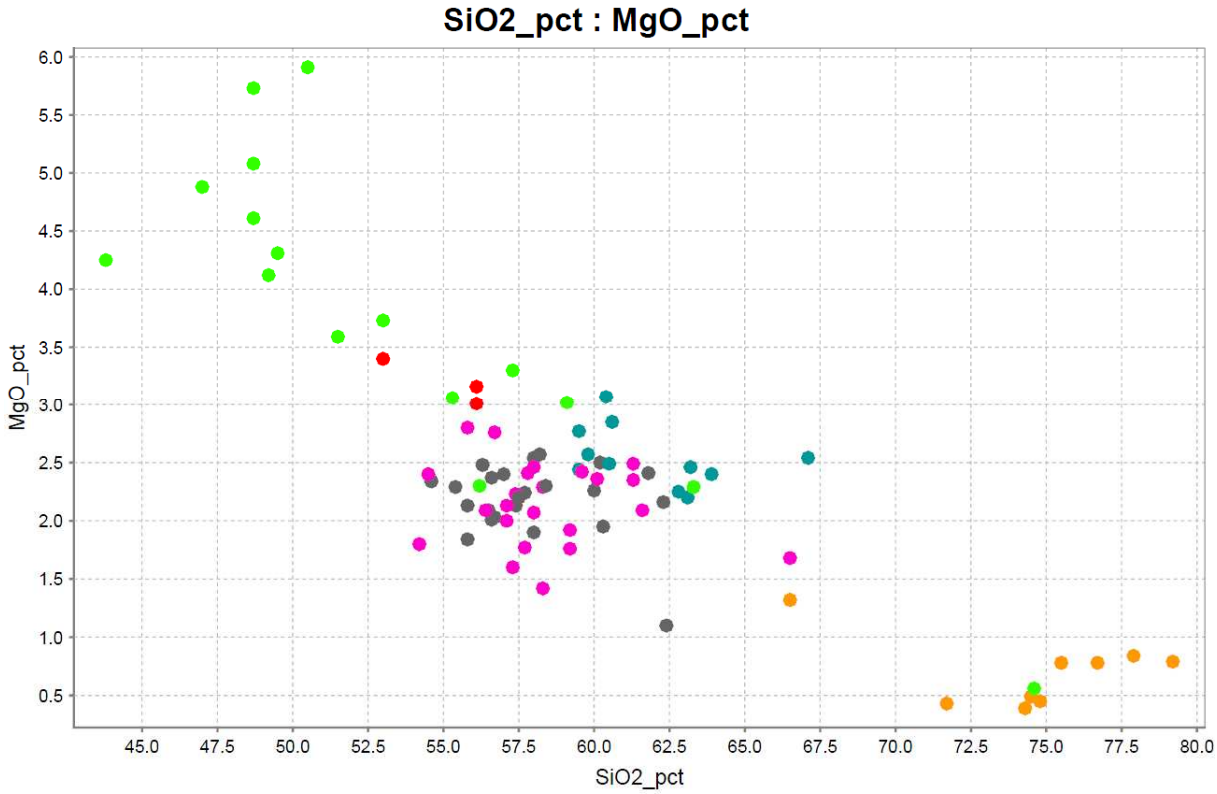

Figure 10-18, Data points obtained by fusion XRF, MgO vs SiO

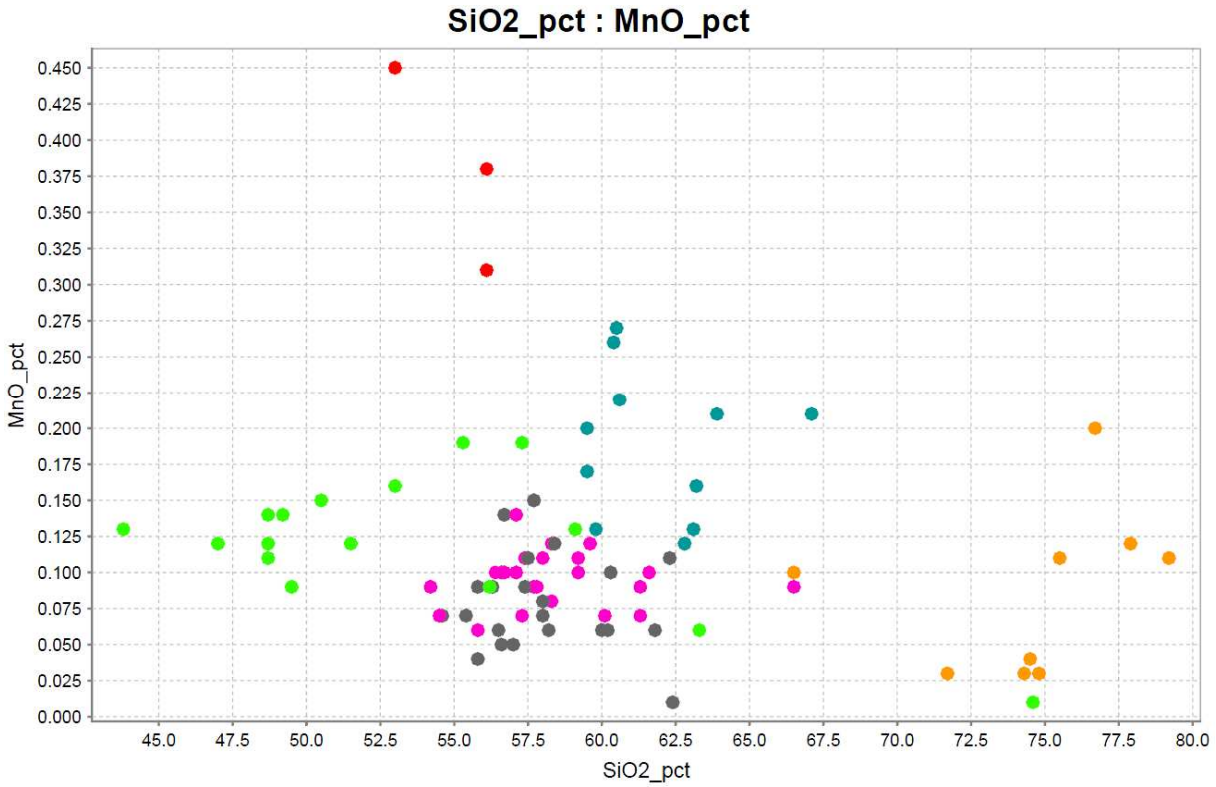

Figure 10-19, Data points obtained by fusion XRF, MnO vs SiO

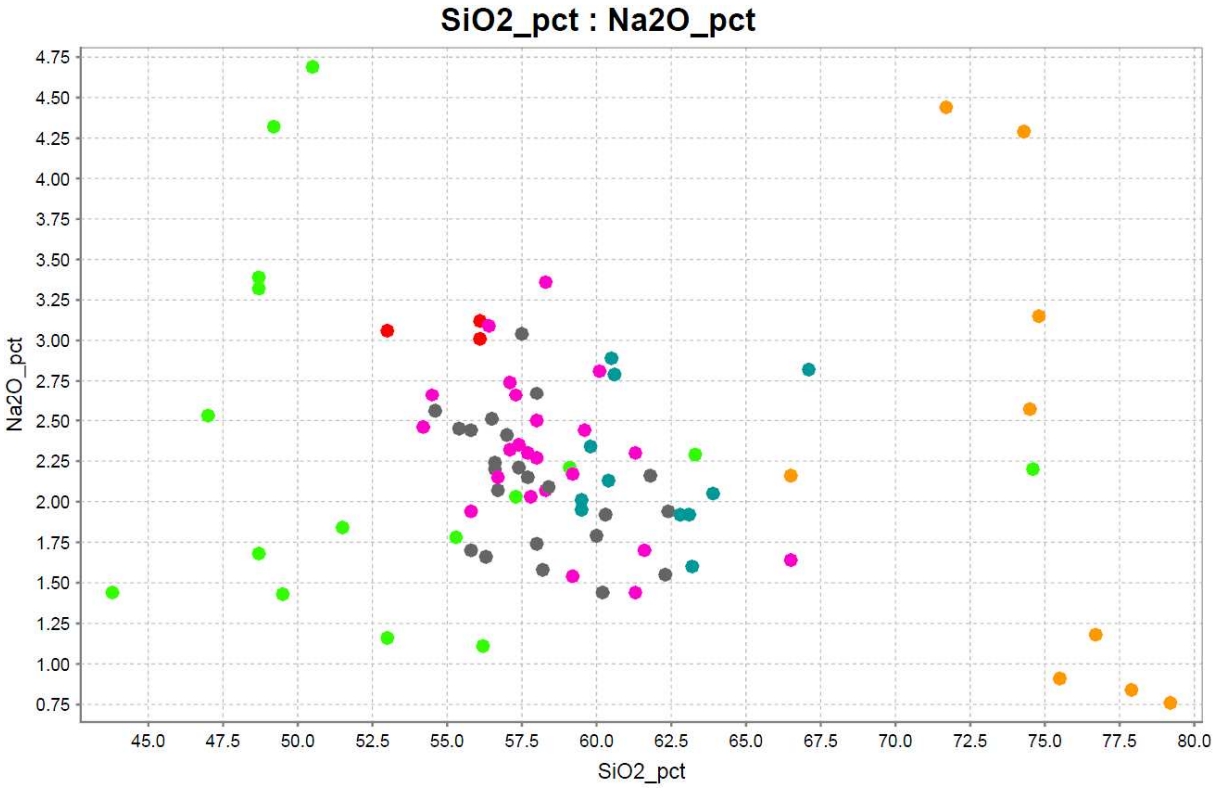

Figure 10-20, Data points obtained by fusion XRF, Na_2O vs SiO

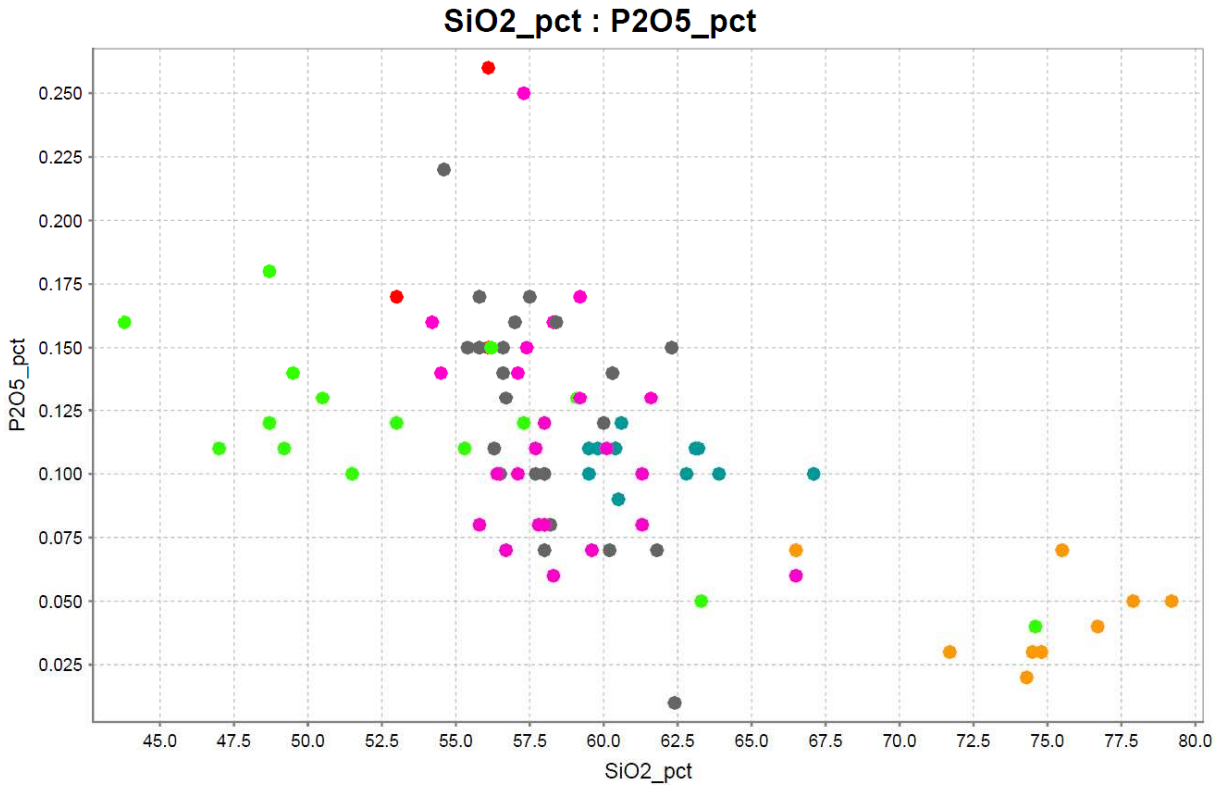

Figure 10-21, Data points obtained by fusion XRF, P_2O_5 vs SiO

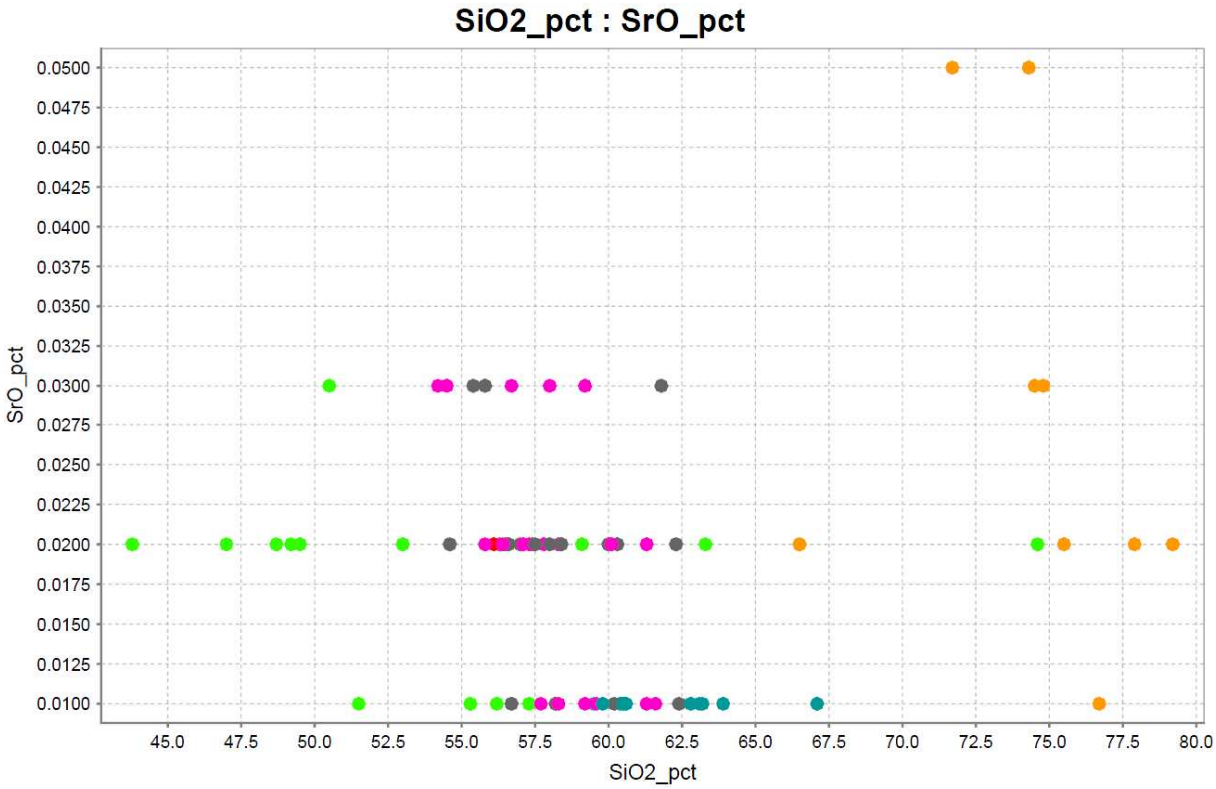

Figure 10-22, Data points obtained by fusion XRF, SrO vs SiO

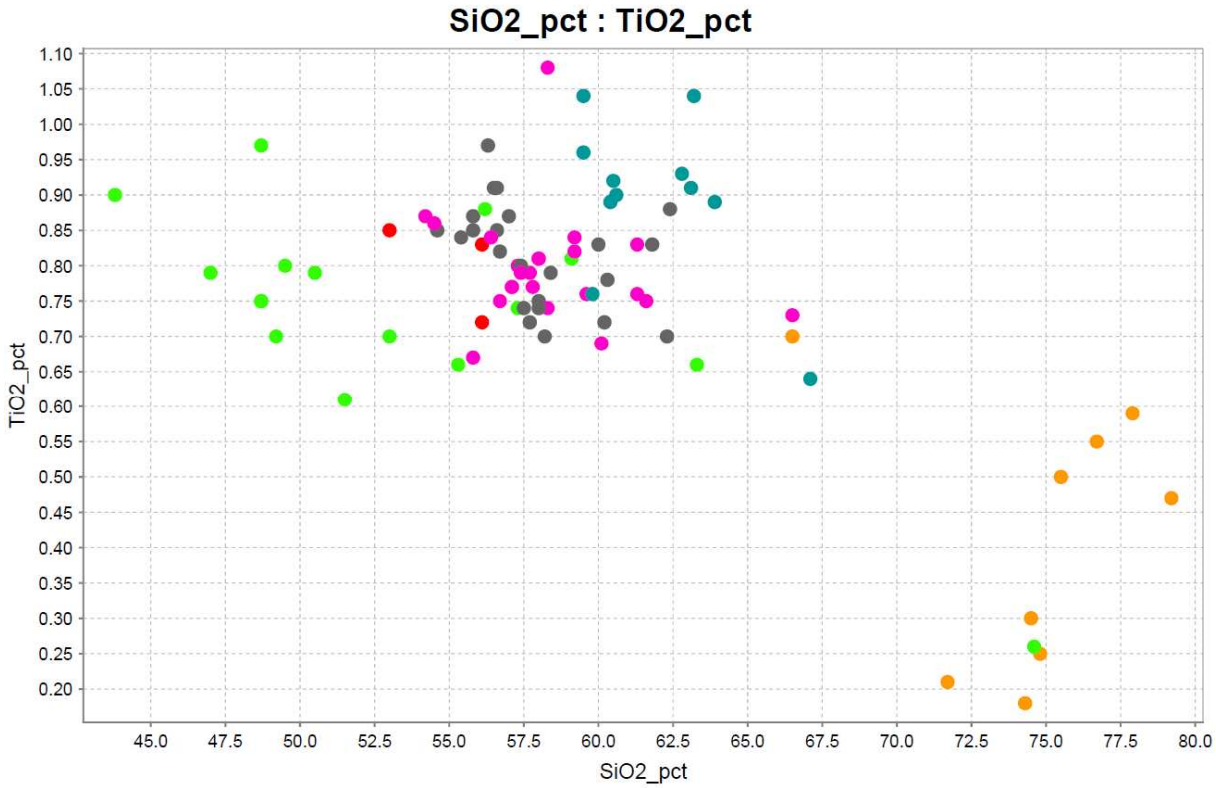

Figure 10-23, Data points obtained by fusion XRF, TiO_2 vs SiO

10.4 X-50 Mobile XRF data quality

	standard deviation	Average of measured values	Percentage of standard deviation compared to the average of the measured values
Ag	53	122	44
As	ND	ND	ND
Ba	16	80	20
Bi	607	3383	18
Ca	ND	ND	ND
Cd	15	18	86
Ce	199	274	73
Cl	648	16606	4
Co	12	330	4
Cr	1549	79654	2
Cu	73	2897	3
Fe	9749	710809	1
Hg	16	91	17
K	114	2893	4
La	9	24	37
Mn	234	9830	2
Mo	238	6732	4
Nb	ND	ND	ND
Ni	3119	202663	2
P	7699	9753	79
Pb	17	146	12
Rb	1	1	63
S	9575	131441	7
Sb	14	29	47
Sc	1	8	17
Se	1	20	7
Sn	54	596	9
Sr	ND	ND	ND
Ti	30	1366	2
U	7	238	3
V	42	353	12
W	31	382	8
Zn	12	780	2
Zr	ND	ND	ND

Table 10-1, Portable XRF test, measurements on the same spot of the calibration disc. Results are based on 10 measurements.

	standard deviation	Average of measured values	Percentage of standard deviation compared to the average of the measured values
Ag	45	130	35
As	ND	ND	ND
Ba	25	93	27
Bi	330	3226	10
Ca	ND	ND	ND
Cd	7	5	141
Ce	159	190	83
Cl	903	16423	6
Co	15	351	4
Cr	1765	79550	2
Cu	99	2865	3
Fe	8801	703984	1
Hg	12	82	15
K	117	2929	4
La	12	17	72
Mn	289	9778	3
Mo	232	6745	3
Nb	ND	ND	ND
Ni	2233	199843	1
P	4399	8146	54
Pb	5	148	4
Rb	1	1	104
S	12794	129592	10
Sb	7	31	23
Sc	2	7	30
Se	1	20	7
Sn	41	602	7
Sr	ND	ND	ND
Ti	34	1331	3
U	21	243	9
V	35	335	10
W	34	387	9
Zn	21	777	3
Zr	ND	ND	ND

Table 10-2, Portable XRF test, measurements on different locations of the calibration disc. Results are based on 10 measurements.

	Standard deviation	Average of measured values	Percentage of standard deviation compared to the average of the measured values
Ag	ND	ND	ND
As	3	10	30
Ba	16	292	6
Bi	ND	ND	ND
Ca	437	10362	4
Cd	2	2	83
Ce	55	134	41
Cl	224	1964	11
Co	1	23	4
Cr	7	117	6
Cu	2	171	1
Fe	541	49533	1
Hg	1	3	32
K	375	10099	4
La	6	8	70
Mn	30	848	4
Mo	1	5	11
Nb	1	5	26
Ni	ND	ND	ND
P	ND	ND	ND
Pb	ND	ND	ND
Rb	0	9	0
S	2951	18409	16
Sb	5	7	74
Sc	1	11	11
Se	0	7	0
Sn	6	4	141
Sr	3	105	3
Ti	54	3124	2
U	ND	ND	ND
V	8	138	6
W	ND	ND	ND
Zn	2	750	0
Zr	3	83	4

Table 10-3, Portable XRF test, results based on ten measurements of sample LC1153 on different spots.

	Standard deviation	Average of measured values	Percentage of standard deviation compared to the average of the measured values
Ag	ND	ND	ND
As	26	463	6
Ba	15	353	4
Bi	ND	ND	ND
Ca	509	15954	3
Cd	2	2	79
Ce	44	166	26
Cl	276	2417	11
Co	1	28	3
Cr	10	250	4
Cu	2	172	1
Fe	342	55435	1
Hg	1	4	35
K	363	12486	3
La	10	12	86
Mn	26	755	3
Mo	1	5	12
Nb	1	4	15
Ni	ND	ND	ND
P	2162	1685	128
Pb	ND	ND	ND
Rb	1	10	5
S	2551	10753	24
Sb	2	2	114
Sc	2	11	13
Se	0	7	0
Sn	9	15	61
Sr	2	50	5
Ti	56	2993	2
U	ND	ND	ND
V	18	147	12
W	ND	ND	ND
Zn	3	768	0
Zr	3	83	3

Table 10-4, Portable XRF test, results based on ten measurements of sample LC1143 on different spots.

Plastic bag number →	1	2	3	4	5	standard deviation of the bags	average content of the bags	average content of all samples	difference
Ag	ND	ND	ND	ND	ND				0
As	8	13	13	47	16	16	19	22	3
Ba	217	267	153	34	83	95	151	378	228
Bi	ND	ND	ND	ND	ND			197	197
Ca	ND	ND	ND	ND	ND			22672	22672
Cd	92	37	ND	ND	ND	39	65	4	-60
Ce	87	ND	ND	784	773	399	548	132	-416
Cl	ND	ND	ND	ND	ND			1962	1962
Co	2	2	1	1	2	1	2	22	21
Cr	7	16	23	4	19	8	14	183	169
Cu	52	55	63	49	51	5	54	173	119
Fe	27360	27420	27501	27386	27309	72	27395	48965	21569
Hg	ND	1	ND	3	ND	1	2	4	2
K	506	511	184	188	ND	186	347	9389	9041
La	ND	152	ND	ND	ND		152	15	-137
Mn	127	133	182	129	119	25	138	816	678
Mo	4	3	ND	ND	4	1	4	4	1
Nb	58	54	52	60	58	3	56	4	-53
Ni	46	43	51	66	90	19	59	73	14
P	3804	1014	8158	ND	ND	3600	4325	608	-3717
Pb	ND	ND	ND	ND	ND			4	4
Rb	2	2	2	2	1	0	2	7	6
S	ND	4509	11756	ND	3760	4416	6675	11763	5088
Sb	2	ND	ND	ND	25	16	14	5	-9
Sc	8	7	8	9	8	1	8	11	3
Se	7	6	6	8	7	1	7	7	0
Sn	ND	ND	ND	ND	48		48	11	-37
Sr	ND	ND	1	1	ND	0	1	95	94
Ti	1117	1112	1122	1122	1095	11	1114	3263	2149
U	18	2	3	ND	26	12	12	2	-10
V	ND	ND	ND	ND	ND			167	167
W	36	24	44	36	47	9	37	6	-31
Zn	598	603	597	586	593	6	595	748	153
Zr	1	6	15	6	3	5	6	90	84

Table 10-5, Results for the testing of plastic bags.

Sample #	portable XRF	laboratory	Sample #	portable XRF	laboratory
LC001	75	94.7	LC048	ND	58.2
LC002	41	71	LC049	ND	67.7
LC003	80	105.5	LC050	ND	82.4
LC004	35	95.9	LC051	ND	88.5
LC005	7	45.4	LC052	ND	90.4
LC006	36	13.5	LC053	ND	79.2
LC007	37	11.2	LC054	ND	80.6
LC008	38	11.2	LC055	ND	72.9
LC009	46	10	LC056	31	58.4
LC010	ND	74.3	LC057	21	22.9
LC011	ND	88.4	LC058	0	38.9
LC012	ND	88.5	LC059	29	23.5
LC013	ND	91.6	LC060	ND	43.5
LC014	ND	83.7	LC061	ND	62.9
LC015	7	61.4	LC062	ND	73.6
LC016	ND	52	LC063	ND	80.7
LC017	ND	41	LC064	ND	76.8
LC018	ND	95.9	LC065	ND	57.5
LC019	ND	78.5	LC066	ND	59.7
LC020	ND	74.6	LC067	58	64.2
LC021	ND	63.1	LC068	ND	71.8
LC022	ND	69.2	LC069	ND	72.9
LC023	ND	70.3	LC070	ND	64.2
LC024	ND	65.1	LC074	ND	84.5
LC027	ND	81.8	LC075	42	82.5
LC028	ND	92.9	LC076	15	85.1
LC029	16	61.7	LC077	53	73.9
LC030	22	91	LC079	75	88.6
LC031	5	74.5	LC080	17	74.9
LC032	ND	71.8	LC081	5	58.8
LC033	ND	69.2	LC082	14	46.1
LC036	0	87.3	LC083	20	61.9
LC037	8	108	LC085	41	73.4
LC038	ND	59.6	LC086	17	74
LC039	ND	63.2	LC087	23	69.9
LC040	31	65	LC089		68.8
LC041	ND	52.9	LC090	51	95
LC042	13	67.2	LC091	58	86.3
LC043	38	66.1	LC093	ND	79.1
LC044	ND	61.7	LC095	39	92.3
LC046	ND	68.4	LC098	72	65
LC047	ND	67.7	LC099	56	7.3

Table 10-6, Ni concentrations obtained with the portable XRF unit and four-acids ICP-MS and ICP-AES in the laboratory.

10.5 Results using calibrated X-50 Mobile XRF data following the procedure of (Weltje & Tjallingii, 2008).

Boreholes	Rank	Element ratio	R^2% of element ratio	r correlation	R^2% correlation	Distance from optimum
all three	1	Ba/Tl	87.9	-0.331	10.9	89.9
	2	Ba/Rb	87.4	-0.326	10.6	90.2
	3	Cs/Y	78.6	0.344	11.8	90.7
	4	Sn/Y	74.5	0.359	12.9	90.8
	5	Be/Y	66.6	0.384	14.7	91.6
	6	Rb/Y	88.2	0.300	9	91.8
	7	Cs/Zr	79.1	0.325	10.5	91.9
	8	Cs/Hf	82.1	0.312	9.7	92
	9	Ba/K	83.8	-0.306	9.4	92.1
	10	Tl/Y	86	0.298	8.9	92.2
					0	0
KHD-508	1	Ba/Cs	90.8	-0.513	26.3	75.6
	2	Ba/Tl	90	-0.459	21	79.9
	3	Ba/K	80.6	-0.461	21.2	80.4
	4	Ba/Rb	91.3	-0.432	18.7	82.3
	5	Sn/Y	14.9	0.422	17.8	86.1
	6	Sr/Th	18.9	-0.406	16.4	86.6
	7	Cs/Sr	71.8	0.374	14	86.9
	8	La/Sr	41.1	0.436	19.1	86.9
	9	Be/Sr	85.1	0.416	17.3	87
	10	Cs/Na	61.3	0.406	16.5	87
					0	0
KHD-566	1	Ca/Zr	94.7	0.372	13.9	87.3
	2	Ca/Sn	92.9	0.364	13.2	87.8
	3	Ca/Y	94.9	0.388	15	87.8
	4	Ca/Hf	87	0.362	13.1	88
	5	Ca/U	58.7	0.350	12.3	88.3
	6	Ca/Ce	85.1	0.352	12.4	88.4
	7	Ca/Ga	70.5	0.352	12.4	88.4
	8	Ca/Pb	89.6	0.347	12	88.4
	9	Ca/Ge	90.8	0.360	13	88.5
	10	Ca/La	87.5	0.351	12.4	88.5
					0	0
KHD-583	1	Cs/Zn	62.9	0.370	13.7	87.6
	2	Ca/Sn	92.2	-0.368	13.5	87.9
	3	Sr/Zn	9.7	0.355	12.6	88
	4	Ca/P	66.9	-0.356	12.7	88.3
	5	Ca/Th	68.9	-0.337	11.4	89.1
	6	Be/Ca	82.6	0.340	11.5	89.1
	7	Cs/Ni	62.4	0.347	12	89.4
	8	Ni/Sr	34.8	-0.325	10.6	89.9
	9	Be/Zn	94.4	0.379	14.4	90.3
	10	Cs/V	73.9	0.329	10.8	90.4

Table 10-7, Log-ratio correlation results for weathered and unweathered rock samples using samples form boreholes: KHD-508 KHD-566 and KHD-583.

Boreholes	Rank	Element ratio	R^2% of element ratio	r correlation	R^2% correlation	Distance from optimum
all three	1	Tl/Y	6	0.353	12.5	88.6
	2	Ba/Tl	81.5	-0.347	12.1	88.8
	3	Rb/Y	24.3	0.343	11.8	89
	4	Th/Y	9.8	0.407	16.5	89.3
	5	Ba/Rb	82.1	-0.331	11	89.9
	6	K/Rb	42.3	-0.357	12.7	90.2
	7	Sn/Y	14.2	0.365	13.3	90.4
	8	Rb/Zr	22.6	0.314	9.9	90.6
	9	Tl/Zr	3.4	0.313	9.8	90.7
	10	Be/Y	77.8	0.394	15.5	90.9
			0		0	0
KHD-508	1	Ba/Tl	92.4	-0.650	42.2	59
	2	Ba/K	89.9	-0.646	41.7	60.5
	3	Ba/Cs	67.7	-0.621	38.5	63.8
	4	Ba/Rb	91.2	-0.595	35.4	65.8
	5	Cr/Cs	92.2	-0.572	32.8	68
	6	Cr/Rb	39.5	-0.558	31.1	69.1
	7	Cs/Sr	52.9	0.563	31.7	69.4
	8	Na/Tl	25.5	-0.571	32.6	69.5
	9	Cs/Na	53	0.590	34.8	69.6
	10	Be/Sr	78.3	0.596	35.5	69.9
			0		0	0
KHD-566	1	Cs/Ti	74.5	-0.412	17	87.7
	2	Ga/Th	63.4	-0.391	15.3	88.1
	3	Rb/Sn	23.7	0.351	12.3	88.9
	4	Ca/Cs	58.4	0.326	10.6	89.9
	5	Li/Mn	45.5	-0.344	11.8	89.9
	6	Th/Y	14.9	0.399	15.9	89.9
	7	Ca/Sn	93.8	0.333	11.1	89.9
	8	Ca/In	60.7	0.344	11.8	90
	9	Mn/Zn	43.7	0.319	10.2	90
	10	Ca/Ga	92.7	0.326	10.6	90.1
			0		0	0
KHD-583	1	Cr/K	66.6	0.364	13.3	86.9
	2	Cr/Rb	68.9	0.356	12.7	87.5
	3	Cr/Zn	68.2	0.356	12.7	87.7
	4	Cr/Undef	66.7	0.328	10.7	89.7
	5	Cr/Tl	67.6	0.318	10.1	90.1
	6	Ba/Cr	91.1	-0.325	10.6	90.3
	7	Cr/Cs	71.6	0.321	10.3	90.3
	8	Cr/Ni	59.3	0.293	8.6	91.8
	9	Cr/Zr	61.5	0.311	9.7	91.8
	10	Al/Cr	86.6	-0.293	8.6	92

Table 10-8, Log-ratio correlation results for unweathered rock samples using samples form boreholes: KHD-508 KHD-566 and KHD-583.

Boreholes	Rank	Element ratio	R^2% of element ratio	r correlation	R^2% correlation	Distance from optimum
all three	1	Ba/Cs	83.1	-0.482	23.2	78.6
	2	Li/Y	67.2	0.493	24.3	82.5
	3	Li/Zr	65.3	0.452	20.4	86.8
	4	Cs/Hf	82.1	0.386	14.9	87
	5	Hf/Li	67.5	-0.437	19.1	87.2
	6	Cs/Zr	79.1	0.391	15.3	87.3
	7	Ca/P	86.8	-0.363	13.2	87.8
	8	Cs/Undef	86.1	0.362	13.1	88
	9	Zn/Undef	86.5	0.352	12.4	88.6
	10	Ba/K	83.8	-0.351	12.3	89.2
			0		0	0
KHD-508	1	Cr/Sr	92.2	0.794	63.1	37.8
	2	Fe/Y	61.4	0.767	58.8	56.5
	3	Cr/Undef	90.7	0.664	44.1	56.7
	4	Cr/Na	64.6	0.691	47.8	63.1
	5	Al/Cr	89.7	-0.608	37	63.8
	6	Cr/Ga	89.3	0.590	34.8	66.1
	7	Cr/Y	61.5	0.674	45.4	66.9
	8	Be/Cr	79.6	-0.569	32.4	70.6
	9	Cr/Hf	84.4	0.550	30.3	71.4
	10	Cr/Zr	83.3	0.552	30.4	71.5
			0		0	0
KHD-566	1	Mg/Zr	84.8	0.721	52.1	50.3
	2	Cs/Zr	79.1	0.736	54.2	50.3
	3	Hf/Mg	85.7	-0.714	50.9	51.1
	4	Mg/Pb	85.2	0.710	50.4	51.8
	5	Cs/Hf	82.1	0.703	49.4	53.7
	6	Mg/Sn	81	0.699	48.9	54.5
	7	Mg/Sc	60.7	0.789	62.2	54.5
	8	Ga/Mg	79.8	-0.697	48.5	55.3
	9	Mg/U	82.6	0.689	47.4	55.4
	10	Mg/Th	85.4	0.682	46.5	55.5
			0		0	0
KHD-583	1	Ni/Rb	92.4	-0.689	47.5	53.1
	2	Ni/Ti	93.5	-0.680	46.3	54.1
	3	K/Ni	92.9	0.671	45.1	55.4
	4	Fe/Tl	94.6	-0.657	43.1	57.1
	5	Tl/Zn	92.9	0.655	42.9	57.5
	6	Sc/Tl	92.8	-0.648	42	58.4
	7	Ge/Tl	82.3	-0.665	44.2	58.6
	8	Cs/Ni	84.1	0.656	43	59.1
	9	Rb/V	92.6	0.638	40.7	59.8
	10	Cs/Zn	85.2	0.649	42.1	59.8

Table 10-9, Log-ratio correlation results for weathered rock samples using samples form boreholes: KHD-508 KHD-566 and KHD-583.

10.5.1 Spectral analysis

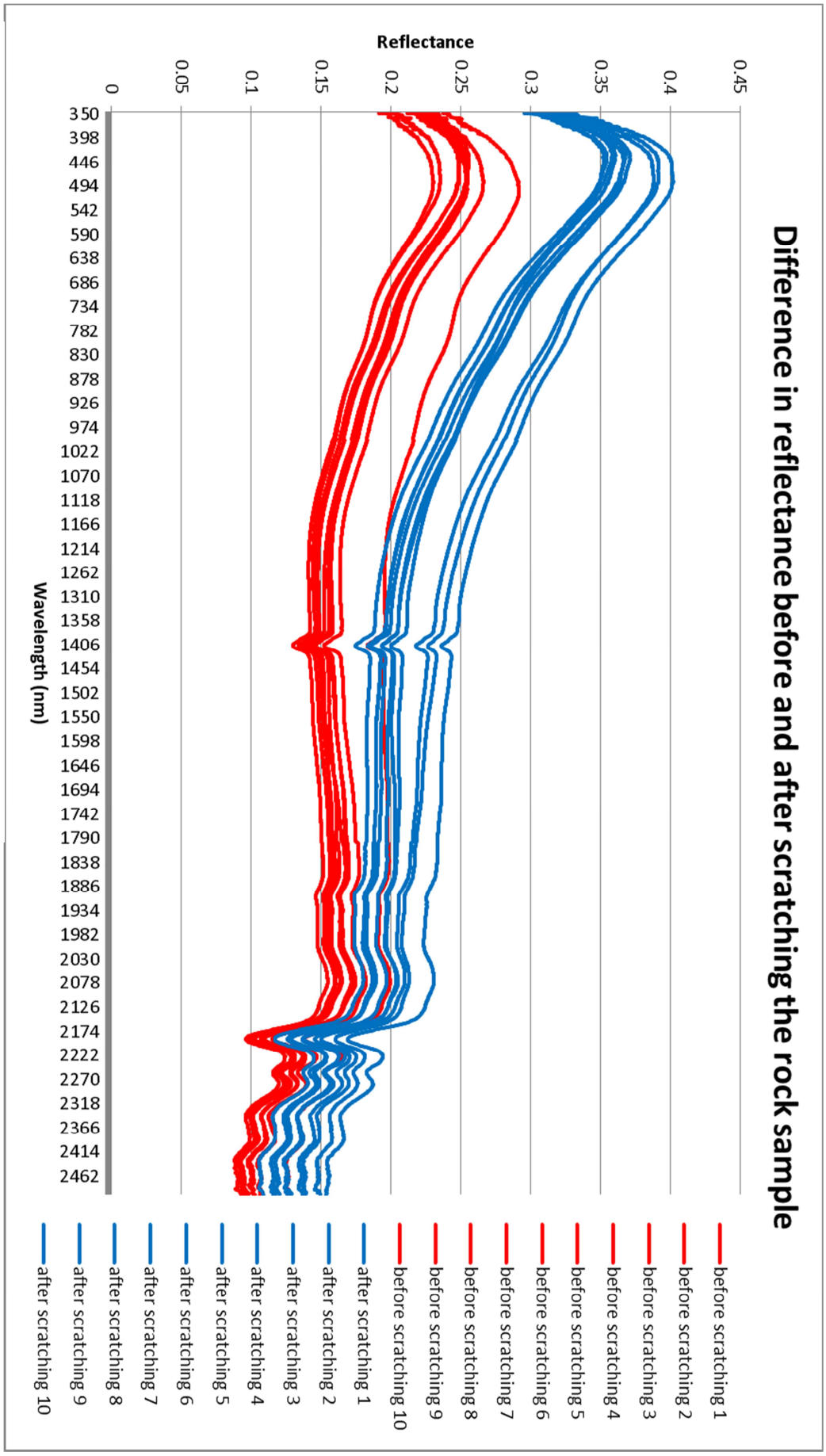

Figure 10-24, spectra displaying the difference between non-scratched rock (red) and scratched rock (blue).

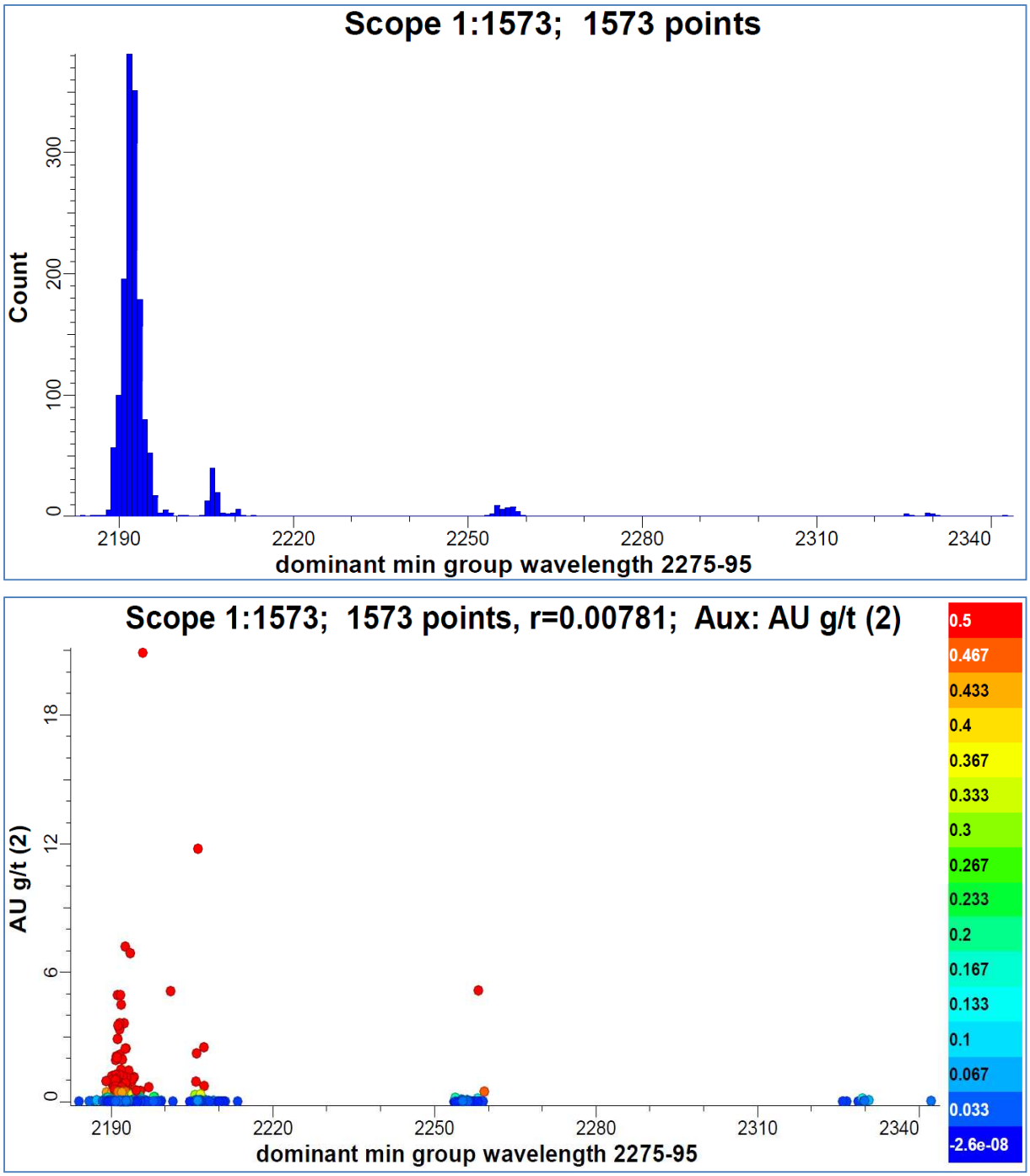

Figure 10-25, dominant mineral groups. Four concentrations of datapoints are recognisable in the histogram (gold grade g/t scale is indicated on the right).

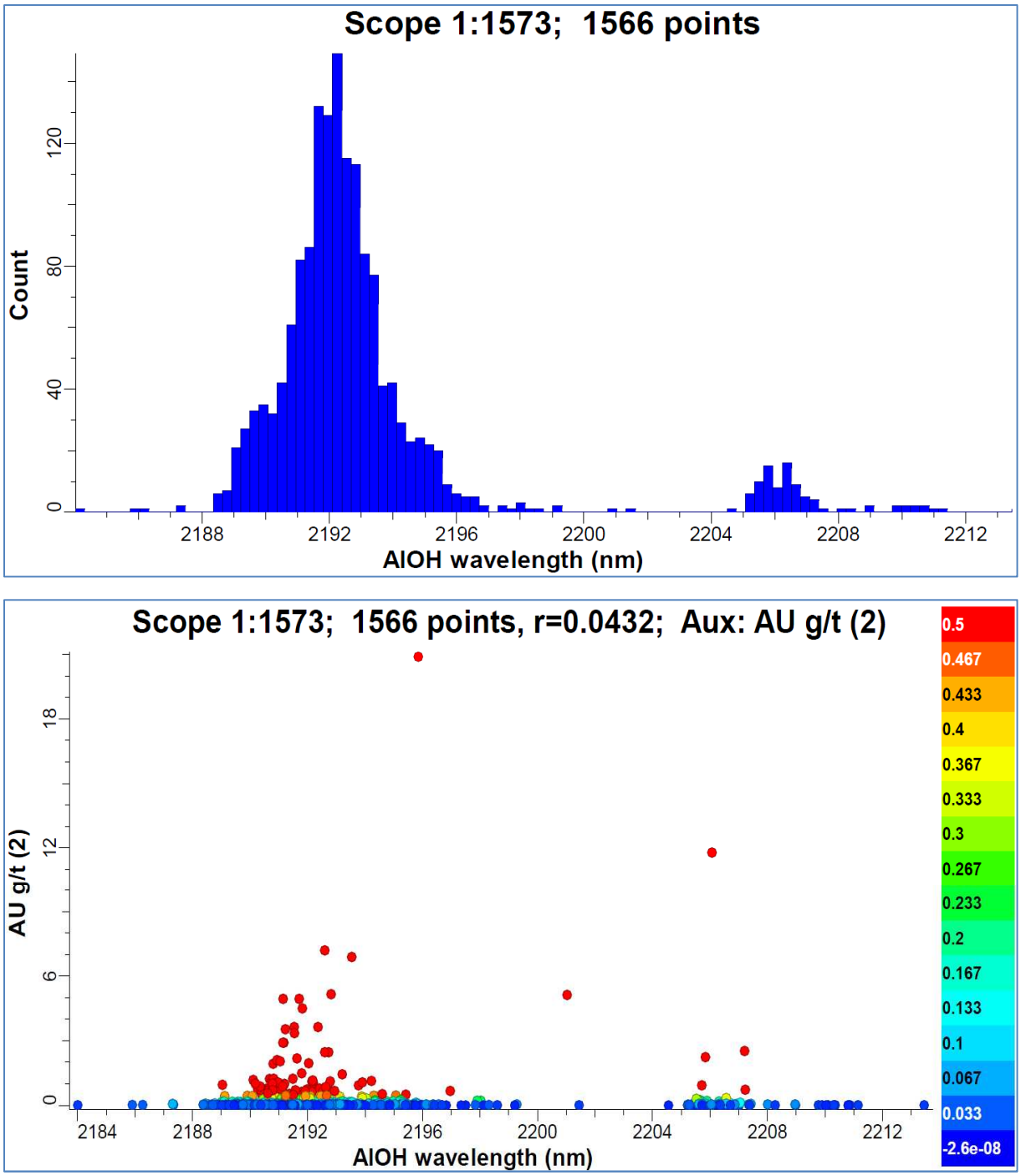

Figure 10-26, AlOH feature wavelengt of absorption. The top histogram shows two clusters. The left one centred around 2192 nm belongs to the paragonite while the cluster centred around 2206 nm should be attributed to muscovite (gold grade g/t scale is indicated on the right).

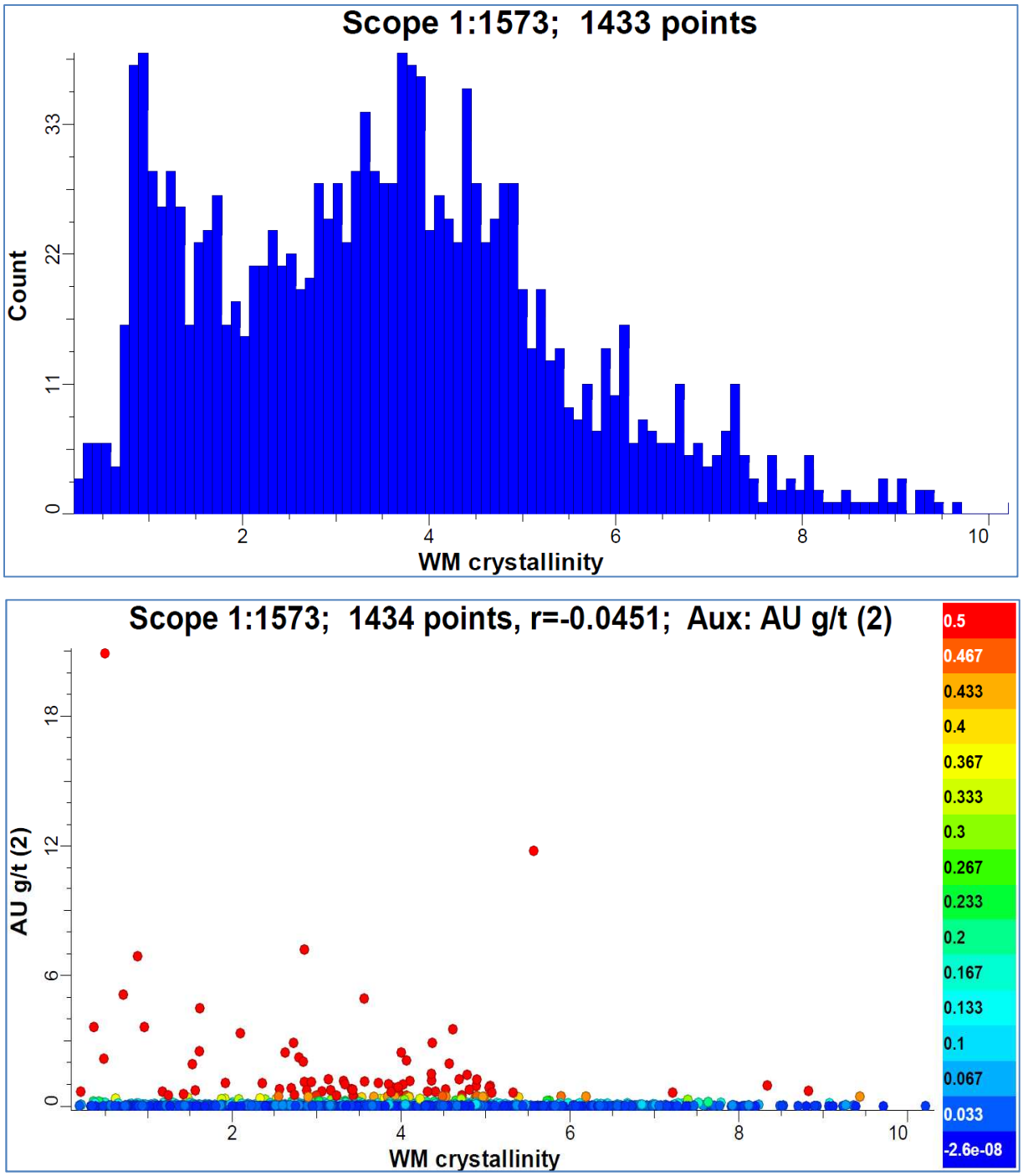

Figure 10-27, White mica crystallinity. Values < 1 imply that the white mica is of low crystallinity. Values > 1 indicate the the white mica is of moderate to high crystallinity (gold grade g/t scale is indicated on the right).

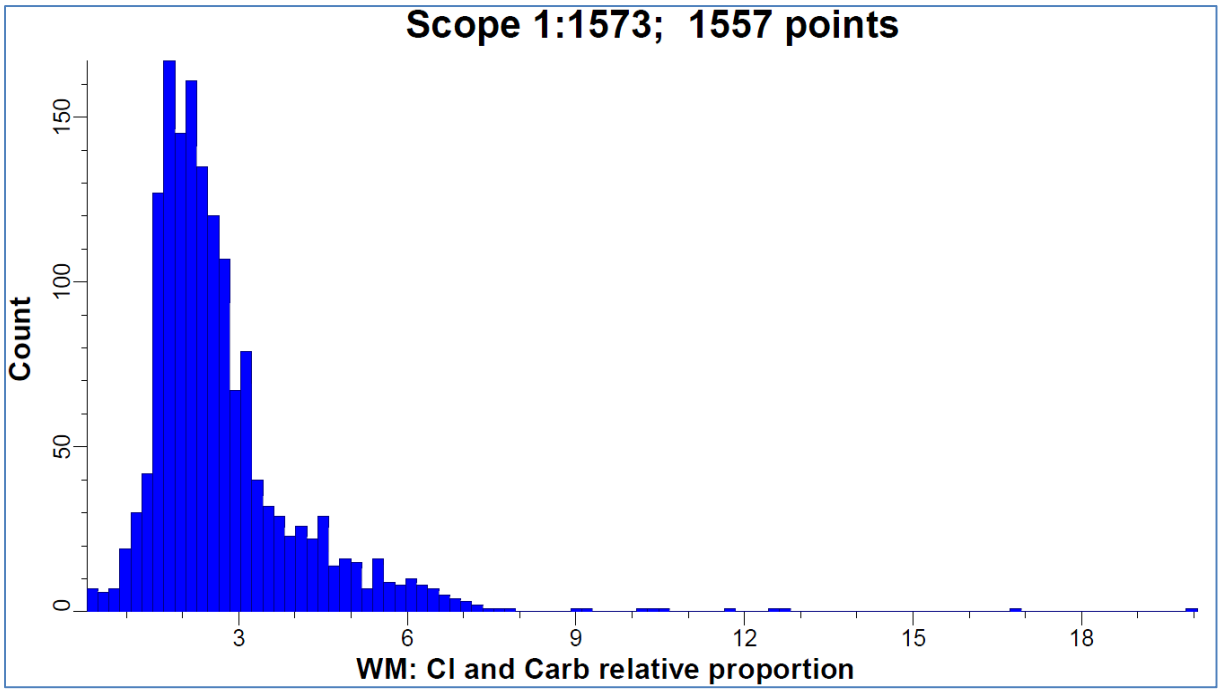

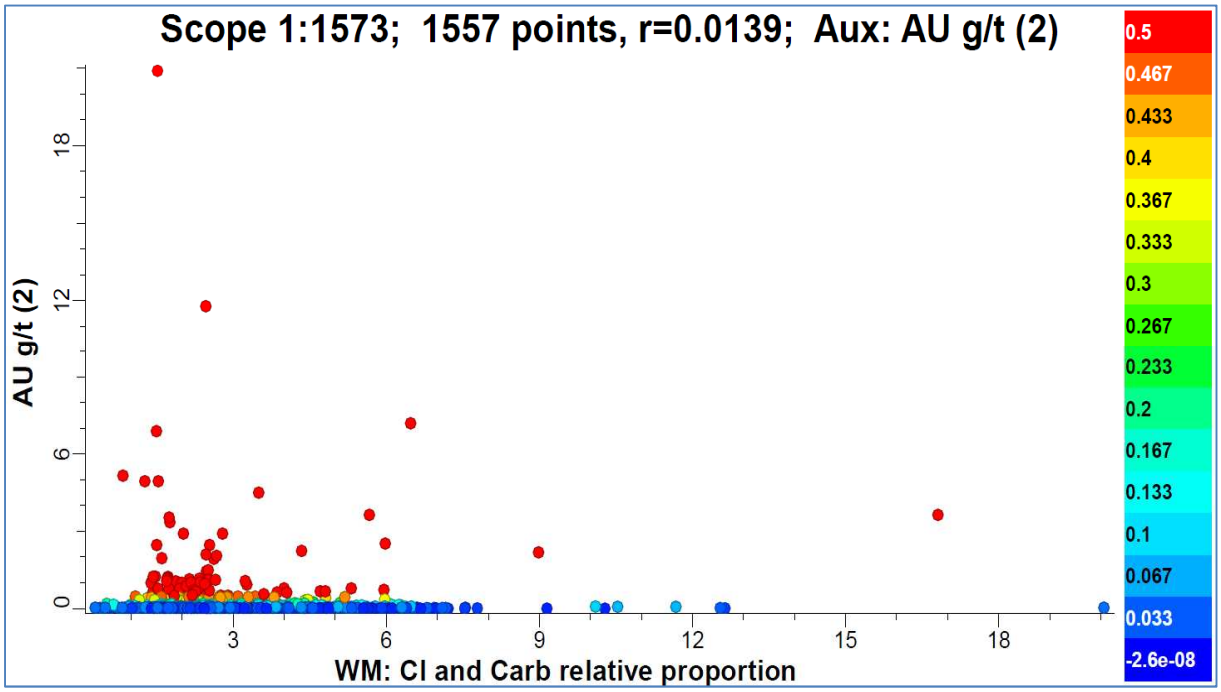

Figure 10-28, relative proportion of white mica against Chlorie and Carbonate. Values <1 imply that the MgOH-Ca mineral is dominant. Values >1 imply that the white mica is dominant (gold grade g/t scale is indicated on the right).

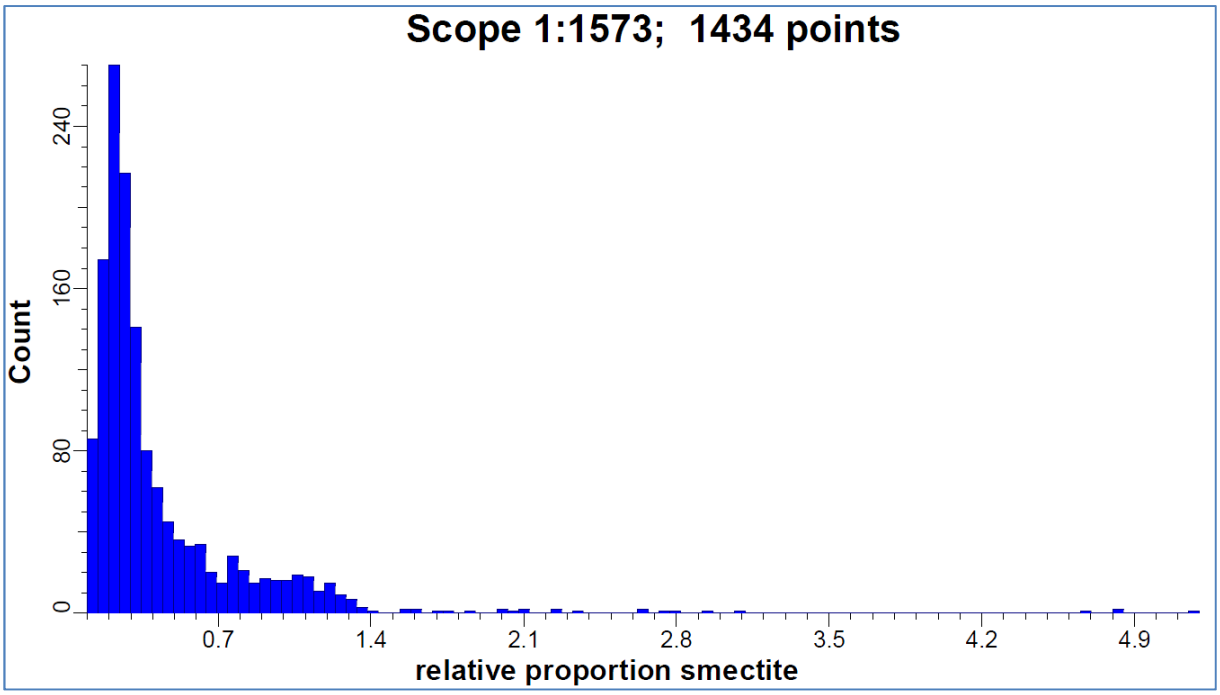

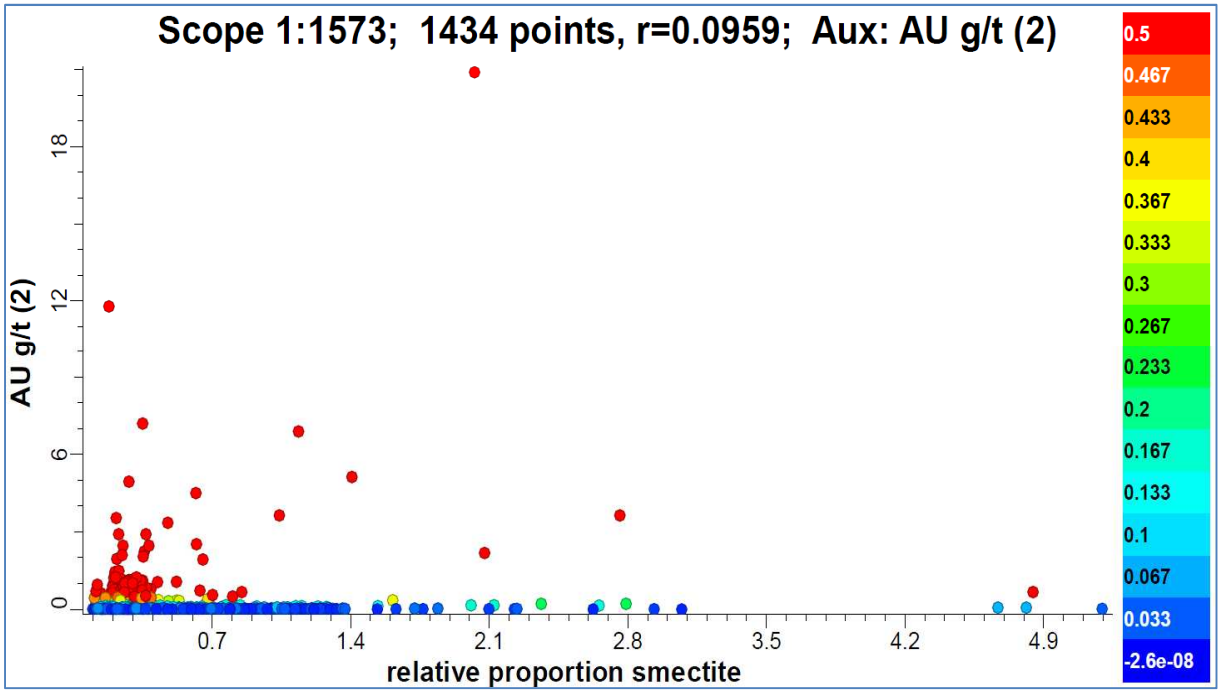

Figure 10-29, relative proportion of smectite. values <1 imply that hte smectite is subordinate to other minerals. values >1 imply that hte smectite is more dominant (gold grade g/t scale is indicated on the right).

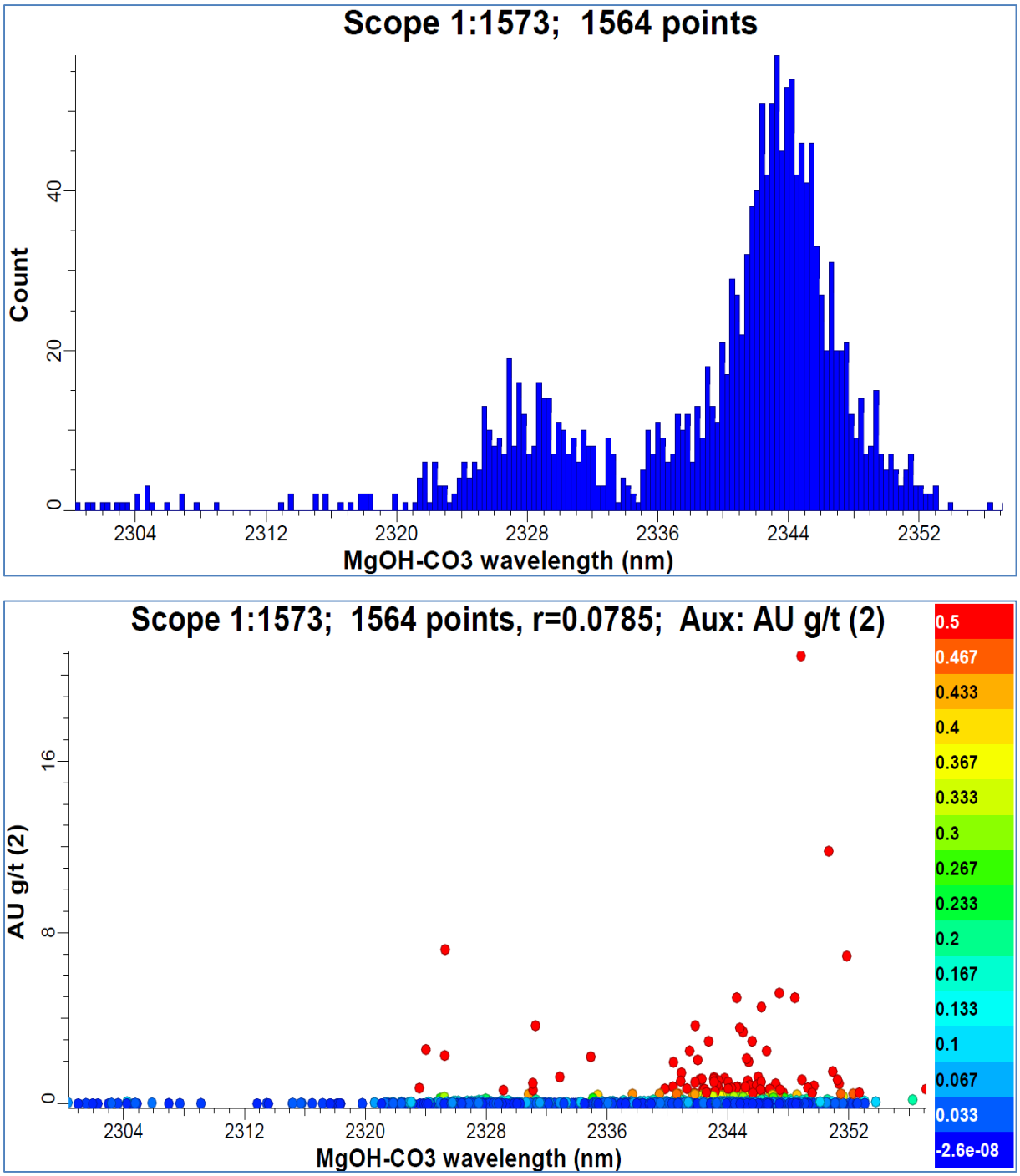

Figure 10-30, wavelength position of the MgOH-CO3 absorption feature that may be used to charactirize the carbonate composition. In this case the signal is likely to be overshadowed by the presence of white mica and chlorite (gold grade g/t scale is indicated on the right).

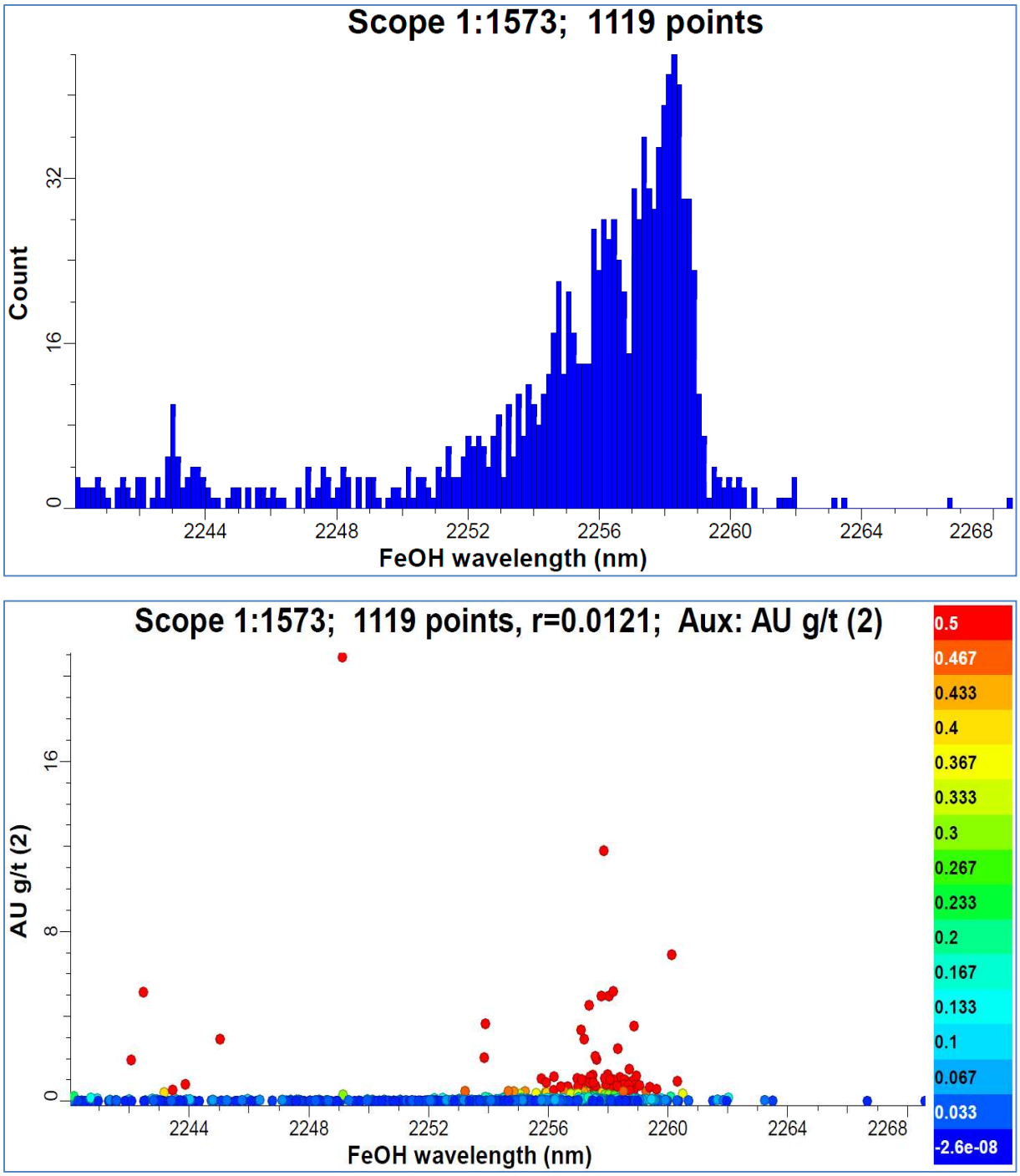

Figure 10-31, wavelength position of the FeOH absorption feature reflecting the chemical composition of chlorite (gold grade g/t scale is indicated on the right).

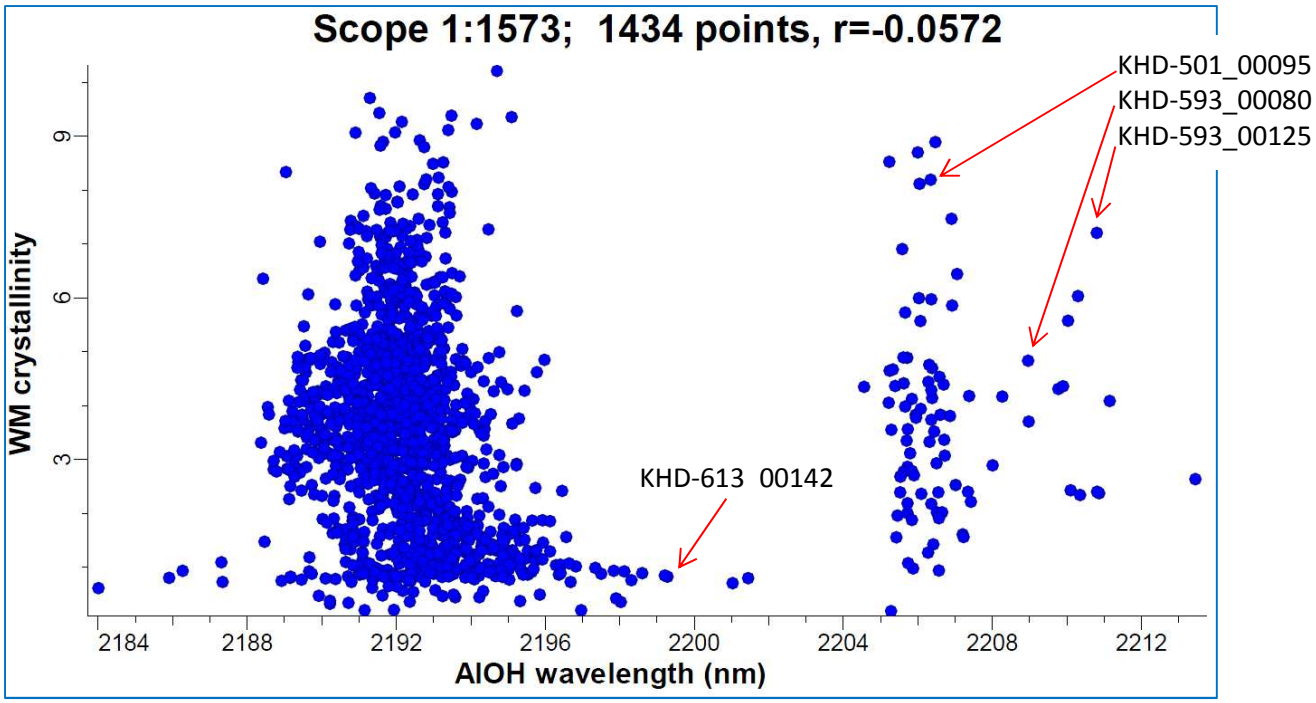

Figure 10-32, White mica crystallinity versus the AlOH wavelength of absorption. The majority of the crystallinity values of aproximatly 1 are the result of poor spectra.

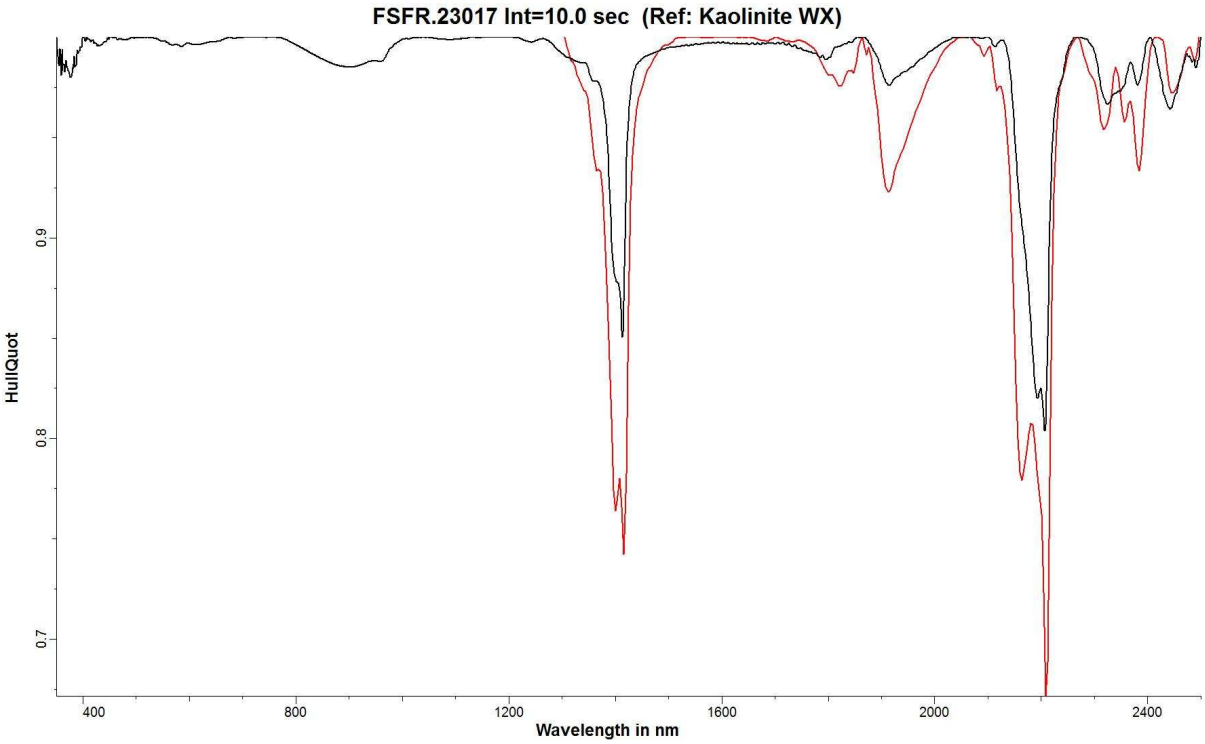

Figure 10-33, Spectrum KHD-613_142 in black and the reference spectrum of kaolinte WX in red.

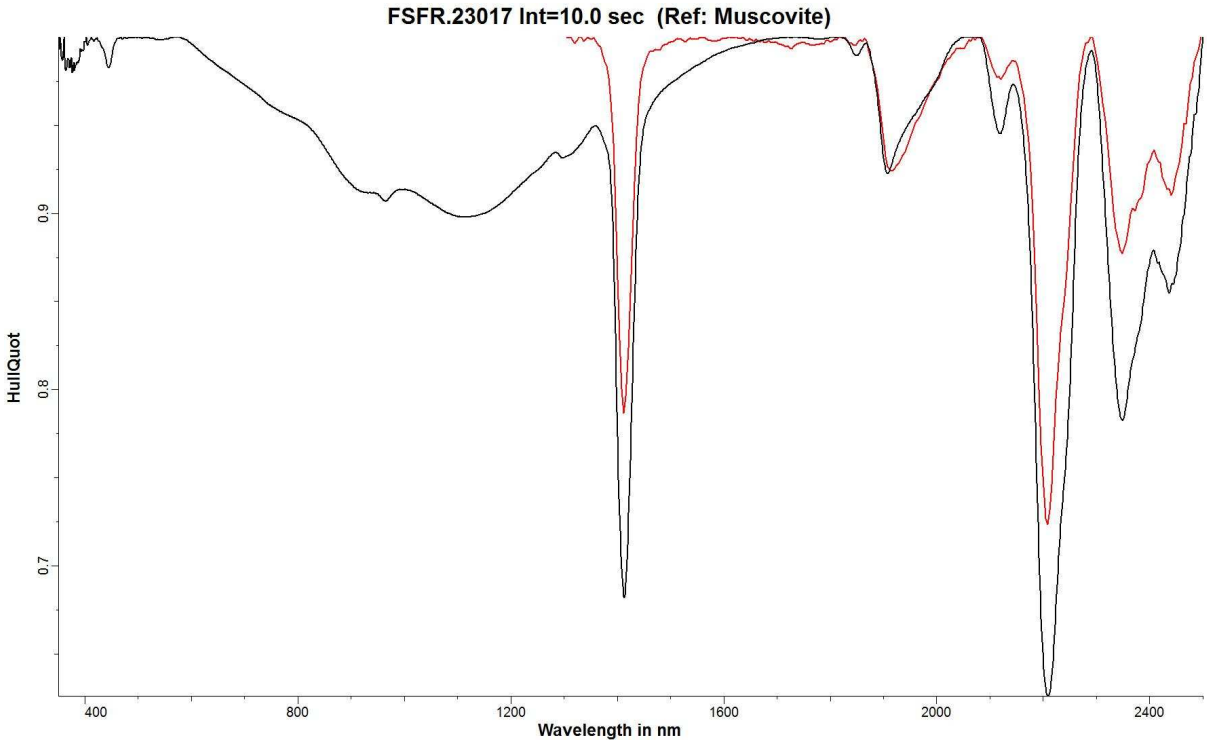

Figure 10-34, Spectrum KHD-593_00080 in black and the reference spectrum for muscovite in red.

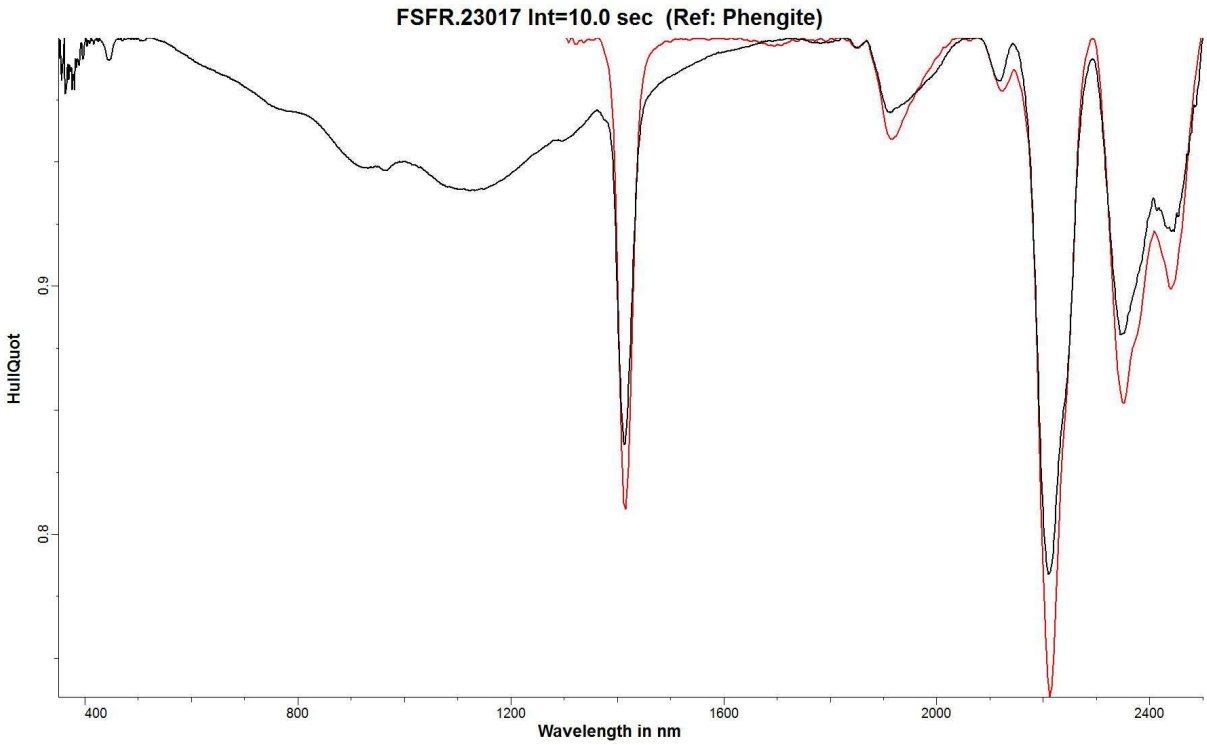

Figure 10-35, Spectrum KHD-593_00124 in black and the reference spectrum for phengite in red.

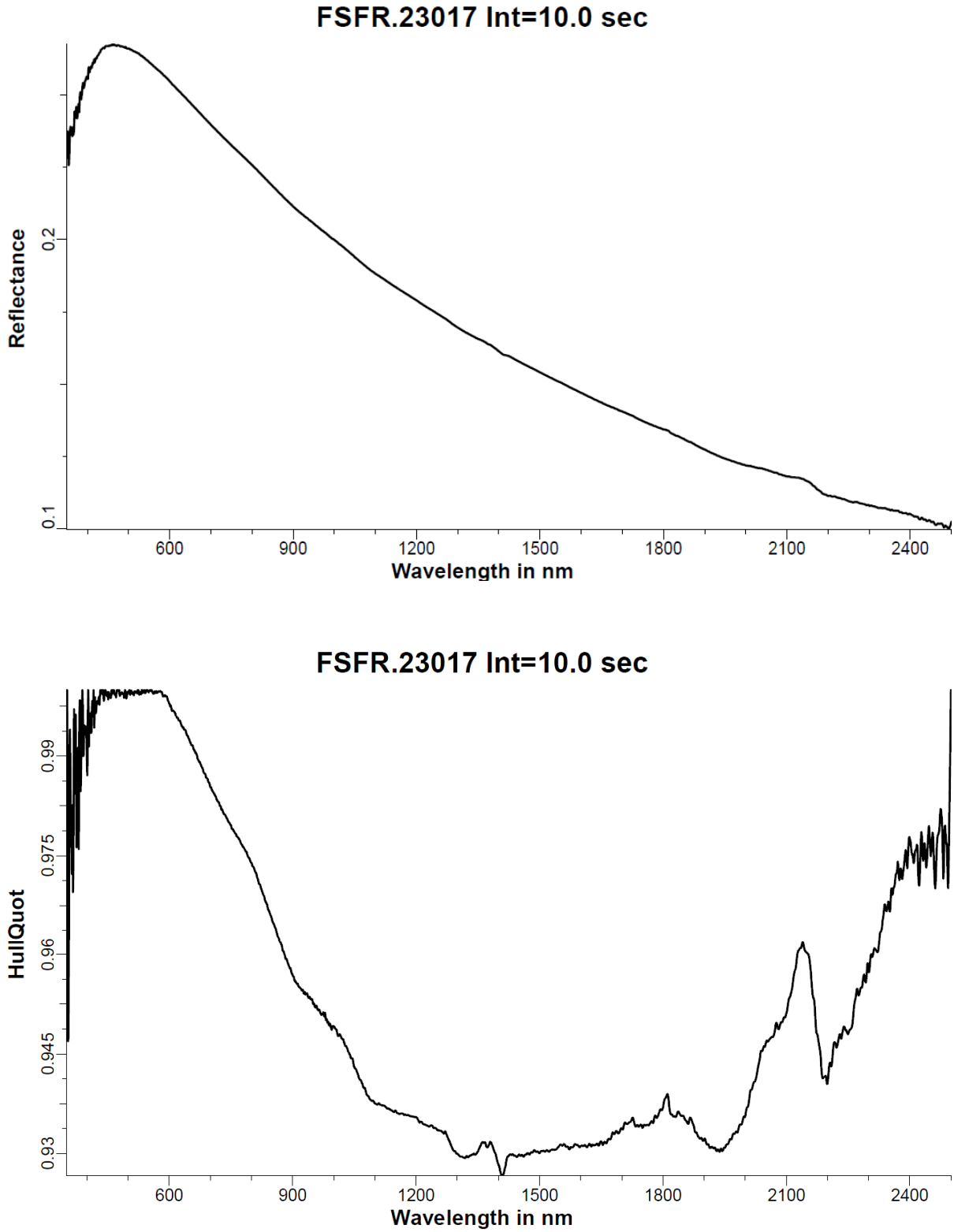

Figure 10-36, two spectra belonging to KHD-613_00142. Top spectra displays reflectance, botom spectra is after hull quotient correction has been applied.